SUPERCRITICAL WATER GASIFICATION

A conceptual study of a novel biorefinery based on SCWG of wet biomass residues from farming and food production practices

Avishek Goel
MSc. Thesis – Mechanical Engineering
August 2020

TUDelft

A CONCEPTUAL STUDY OF A NOVEL BIOREFINERY BASED ON SUPERCRITICAL WATER GASIFICATION OF WET BIOMASS RESIDUES FROM FARMING AND FOOD PRODUCTION PRACTICES

A thesis submitted to the Delft University of Technology in partial fulfillment
of the requirements for the degree of

Master of Science in Mechanical Engineering

by

Avishek Goel

August 2020

A Conceptual Study of a Novel Biorefinery based on Supercritical Water Gasification of Wet Biomass Residues from Farming and Food Production Practices (August 2020)

The work in this thesis was made in the:

Large Scale Energy Storage
Department of Process & Energy
Faculty of Mechanical, Maritime & Materials Engineering
Delft University of Technology

Delft University of Technology

Name:	Avishek Goel
Student number:	4797442
Supervisors:	Prof. dr. ir. Wiebren de Jong
	Dr. ir. Elyas M. Moghaddam
Thesis committee:	Prof. dr. ir. Wiebren de Jong
	Prof. dr. Dirk J.E.M. Roekaerts
	Prof. dr. ir. Johan T. Padding
	Dr. ir. Elyas M. Moghaddam

SYNOPSIS

Due to growing awareness and rising concern over the climate change impact, the demand for renewable energy has been increasing. In the coming decades, biomass is expected to play a crucial role as it is one of the most plentiful and well-utilized renewable resources in the world. Biomass can be sustainably converted to solid/liquid/gaseous biofuels which in turn can be used to produce both, power and heat. Among the many thermochemical conversion technologies, conventional gasification technology is one of the widely used conversion routes. However, the use of conventional gasifiers for the conversion of biomass feedstocks with more than 70% MC is not suitable without their pretreatment. Having the advantage of avoiding energy- and cost-intensive drying process, Supercritical Water Gasification (SCWG), offers a promising approach in converting these biogenic residues into valuable biofuels.

SCWG is an alternate thermochemical conversion route and is suitable for the conversion of wet biomass feedstocks having very high moisture content. The thermochemical conversion takes place in Supercritical Water (SCW) having temperatures and pressures higher than 374.29 °C and 221 bar, respectively. At such conditions, the thermo-physical properties of water change in a way that causes water to act as a solvent and catalyst at the same time. With the use of SCWG, large amounts of wet biomass wastes such as cattle manure, fruit/vegetable waste, and cheese whey residual streams which get disposed from farming and food processing industries globally, can be sustainably treated. Since an in-depth investigation of SCWG of the noted real wet biomass wastes is still at an early stage, in this study, we have therefore concentrated on the SCWG of these specific classes of waste.

To this end, different modelling scenarios, including global, constrained, and quasi-thermal thermodynamic equilibria models have been pursued so as to effectively predict system behavior. We used Factsage^{TM} and MATLAB modelling tools to develop and analyze these models. We observed reasonable agreements between experimental results and predictions from constrained and quasi-thermal equilibrium models, effectively emanating from conceptual improvements due to experimental data. The results showed that the superimposition of carbon conversion efficiency together with the use of a constant molar amount of specific compounds can improve the accuracy of the global equilibrium model. For example, deviation of CO_2 yield from experimental data significantly improved from 55% to 0.3% for fruit/vegetable residue gasification using a constrained equilibrium model. Furthermore, comparisons revealed the advantage of using a quasi-thermal equilibrium model which uses the "approach temperature" concept over the constrained equilibrium model. Results for fruit/vegetable waste showed an approach temperature between 60 and 80 °C for H_2 yield. Overall, the quasi-thermal equilibrium approach has its advantages of lumping all the additional constraints to be used in constrained equilibrium model into an effective approach temperature, offering a much better prediction of the compositions with an error margin of maximum 0.001%.

Furthermore, the results of this effort assisted us in designing a conceptual bio-refinery model based on the SCWG process. Using the ASPEN modelling tool, we were able to optimize and analyze the entire process for its chemical and thermal behavior. Using the results, the SCWG process was found to be self-sustaining for the assessed reactor conditions. However, with the reactor conditions; temperature (600 and 650 °C), pressure (240 bar), and fruit/vegetable waste feed concentration (11wt%), the process was assessed to be practically infeasible as larger part of the produced gas stream (i.e. 70% and above) was getting recycled back to the system. Finally, we compared the process modelling results based on global and constrained modelling scenarios and the use of GTE modelling for process designing was found to have its limitations. Overall the result of this thesis shows the great potential of using SCWG for thermochemically upgrading wet biomass feedstocks. Comparing the results from different modelling scenarios gave an insight into the process and the reactions taking place inside an SCW gasifier, thereby assisting in better reactor designing.

ACKNOWLEDGEMENTS

CONTENTS

LIST OF FIGURES

LIST OF TABLES

NOMENCLATURE

Abbreviations

$a.r.$	As received
$ASTM.$	American Society for Testing and Materials
BOD	Biochemical Oxygen Demand
BTW	Biomass to Water
CGE	Carbon Gasification Efficiency
$d.b.$	Dry basis
EoS	Equation of State
EU	European Union
FAO	Food and Agricultural Organization
GHG	Greenhouse Gas
GTE	Global Thermodynamic Equilibrium
HEX	Heat Exchanger
HP	High Pressure
IEA	International Energy Agency
IL	Ionic Liquids
LHV	Lower Heating Value
LP	Low Pressure
MC	Moisture Content
$MDEA$	methyldiethanolamine
$PRKS$	Predictive Redlich Kwong Soave
$PR-BM$	Peng Robinson-Boston Mathias
$PR-MHV2$	Peng Robinson-MHV2
$PR-WS$	Peng Robinson-Wong Sandler
PSA	Pressure Swing Adsorption
$RKS-BM$	Redlich Kwong Soave-Boston Mathias
$RKS-MHV2$	Redlich Kwong Soave-MHV2
$RKS-WS$	Redlich Kwong Soave-Wong Sandler
SCW	Supercritical Water
$SCWG$	Supercritical Water Gasification
$SILMs$	Supported Ionic Liquid Membranes
TGA	Thermogravimetric Analysis
$TPES$	Total Primary Energy Supply
$VTSD$	Variable-Temperature Stepwise Desorption
WBA	World Bioenergy Association

Symbols

a	Carbon atoms per molecule (-)
A	Fixed experimental value of the compound (mol/kg of d.b.)
g	Gas phase (-)
g^0	Standard molar Gibbs free energy (kJ/mol)
m	Number of carbon atoms (-)
$\dot{m}$	Mass or molar flow rate (kg/h or mol/h)
n	Mole (-)
p	Partial pressure (bar)
P	Power (kW)
R	Universal gas constant (J/mol-K)
s_p	Solution phase (-)
T	Temperature (K)
x	Mole fraction (-)

Greek Symbols

γ	Activity coefficient (-)
η	Process efficiency (-)

Subscripts

$feed$	Biomass feed
i	Compound i
ig	Ideal gas
pcp	Pure condensed phase
p	Pump
pg	Product gas
stu	Slurry thickening Unit
t	Turbine

1 | INTRODUCTION

This chapter gives an overview of the renewable energy sector with a special emphasis on biomass-based energy. It also discusses the state of the art of supercritical water gasification including thermo-physical properties of supercritical water, followed by the effect of different parameters on the reactor design and the prevailing challenges faced by the technology. Furthermore, it gives a detailed survey on current status of research in SCWG area. Finally, the chapter discusses research question and scope of this report which was formulated based on the literature survey.

The contents of this chapter has been adapted from:
Moghaddam, E. M., Goel, A., Siedlecki, M., Michalska, K., Yakaboylu, O., and De Jong, W. (2020). Supercritical water gasification of wet biomass residues from farming and food production practices: lab-scale experiments and comparison of different modelling approaches. Sustainable Energy and Fuels. **(Submitted)**

1.1 GLOBAL ENERGY OVERVIEW

Global energy systems still depend on fossil fuels. According to the IEA (2019), natural gas, coal, and oil constitute 81% of the world's TPES . TPES is defined as energy source production including import, export, and storage of the sources in the fuel bunkers. Since the beginning of this decade, renewable energy sources have registered a growth of approximately 1% percent in the TPES share, reaching 14% in the year 2017 (shown in Figure 1.1). Even though renewable energy has been increasing since 2000, TPES has also registered a similar growth (shown in Figure 1.1). IEA (2019) suggested that global energy demand will increase by 34% by the year 2040 as compared with 2018 levels under the current policy scenario .

Although the major sources of energy conversion; fossil fuels face the challenge of getting depleted. More importantly, IEA (2019) advocated that the use of fossil fuels will pose a major environmental threat with CO_2 emissions having increased from 23.1 to 33.2 gigatonnes within the period 2000-2018. It is expected that by the year 2040, the emissions will reach 41.3 gigatonnes under the current policies scenario, as mentioned by IEA (2019) in their Global Energy Outlook report 2019. The depletion of fossil fuel reserves combined with increasing energy demands and emissions necessitates the transition to a renewable-based economy.

Globally, biomass energy forms the largest renewable energy source with TPES from biomass being 56.5 EJ in 2016, thus constituting a 70% share among all the renewable energy sources, as implied by WBA (2018). Bioenergy is derived from different resources ranging from wood, crop residues, forestry residues, municipal and industrial wastes, energy crops, algae, and animal manure to name a few. To better understand the diversity of biomass, it becomes imperative to categorize it. First-generation biomass includes food crops such as wheat, corn, sugarcane, and pose challenges related to food vs fuel competition. The second generation was developed to overcome such challenges and include biomass such as wood, grass, food crop waste including straw, organic waste, etc. Third generation biomass mainly includes algae which are especially engineering energy crops and mitigates land-use competition. Among them, both industrial and municipal waste which form part of the second generation biomass are gaining importance as over the last decade it has become an increasingly recognized environmental issue across the world.

1.2 BIOENERGY – WASTE

WBA (2018) in their report highlighted the importance of both industrial and municipal waste form as important sources for energy production while contributing around 3% to the total biomass supply.
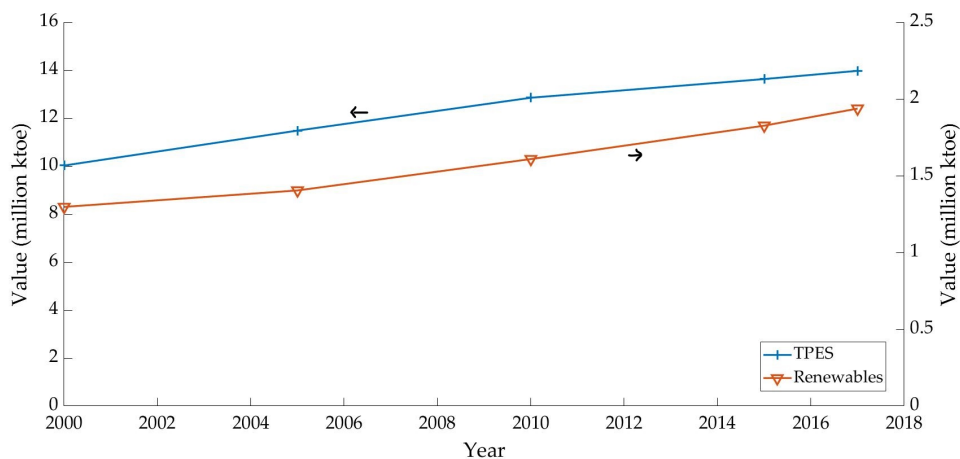
Figure 1.1: Global growth of TPES and renewable energy over the years. Extracted from IEA (2019).
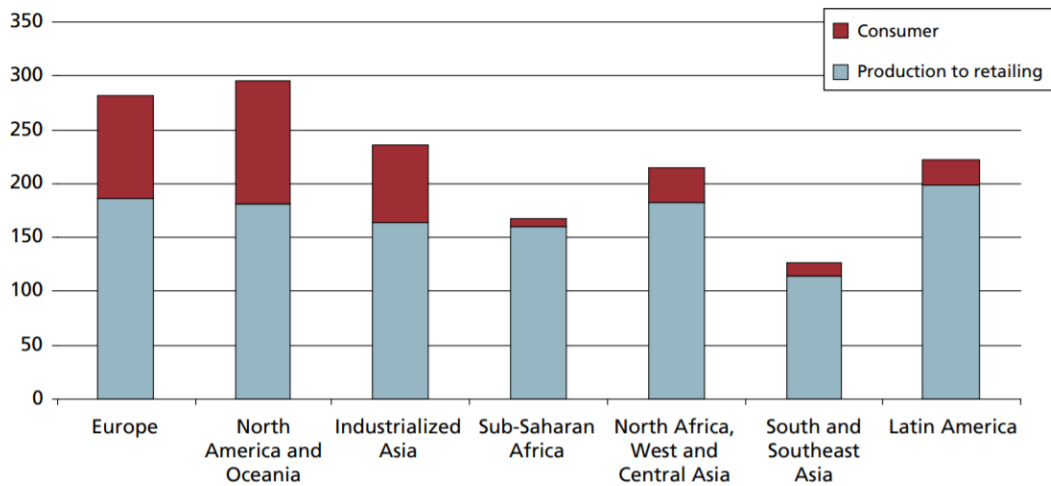
Figure 1.2: Average per capita food losses and waste (kg/year-person) for different regions around the world. Reprinted from Gustavsson et al. (2011).

The waste energy sector contributed 2.17 EJ of energy globally in the year 2015, as reported by WBA (2018). Few of the wet waste streams such as fruit and vegetable waste, cheese whey, and cattle manure from the second-generation biomass are gaining importance as they are present in huge quantities and energy recovery from these solves both environmental and energy problems. These residues have been selected in a European 'FACCE-SURPLUS Supervalue' project and this thesis work is being performed under its framework.

1.2.1 Fruit and vegetable waste

Gustavsson et al. (2011) and Chainey (2015) reported that according to the FAO, every year, nearly one-third of all the food produced (approximately 1.3 billion tons) for human consumption gets wasted around the world, which includes 45wt% fruits and vegetables . In addition to wasting of resources such as water, energy, and nutrients which are needed to produce the food being wasted, poor management of food waste affects our environment upon its decomposition, contamination of land and water resources. This not only creates a burden on our health in the form of diseases but also cause GHG emissions. FAO (2015) reported that the carbon footprint for such quantities of food wastage is around 4.4 Gt CO_2 equivalent per year, including land-use change. Furthermore, in their report FAO (2014) mentioned that globally, the environmental, economic, and social costs of food wastage lie in the order of about \$2.6 trillion annually. Due to wasteful food distribution and consumption patterns in high-income countries, per capita, food wastage carbon footprint is more than double than that of low-income countries. Figure 1.2 shows the average per capita food losses waste for different regions around the world. As seen from the figure, food loss per capita in the regions of Europe and North-America is around 280-300 kg/year while that of Subsaharan Africa and South/Southeast Asia is 120-170 kg/year. Research has proven that such carbohydrate-rich biomass can serve as a potential substrate for energy generation as the lower heating value of fruit and vegetable waste lies within a range of 8-17 MJ/kg (a.r. basis), as mentioned by Tanai (2017). These wastes sums upto an energy potential of 10.4 - 22.1 EJ (a.r. basis) and can be sustainably treated for biofuel production.

1.2.2 Cattle Manure

Over the past few decades, livestock production has undergone an industrial revolution which has resulted in large scale generation of manure. Though manure has numerous valuable applications due to the presence of valuable nutrients and can be used as an alternative to chemical fertilizers, still it requires proper treatment for agricultural land. If improperly treated it can pollute our rivers, soil, and underground water. Poor management of animal feces can expose humans to pathogens,
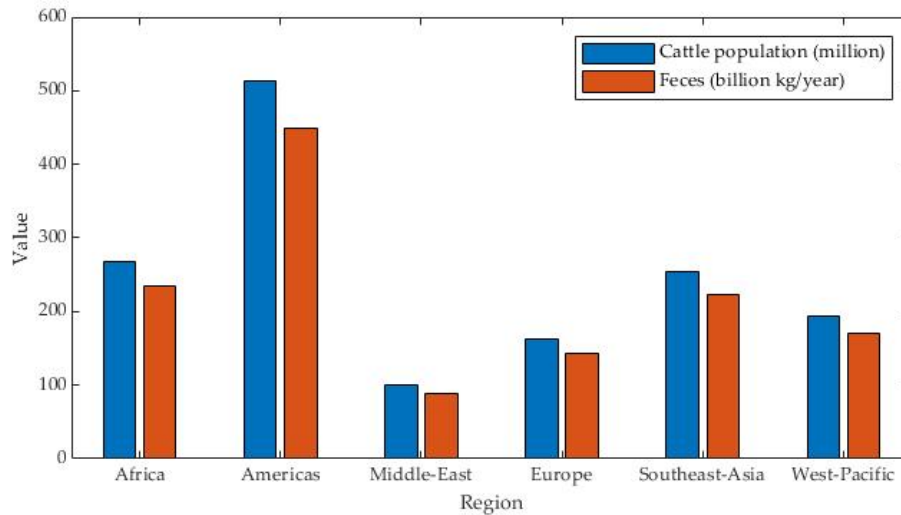
Figure 1.3: Estimates of regional cattle population and its feces production. Extracted from Berendes et al. (2018).

particularly in areas where humans live near animals. Such exposure has adversely affected human health in the form of soil-transmitted helminth infections, diarrhea, environmental enteric dysfunction, trachoma, and growth faltering. According to the World Health Organization, globally, 29.7 billion livestock animals produce an estimated 3.1 trillion kgs of feces every year, as presented by Berendes et al. (2018). Of which cattle were among the largest animal population (1.5 billion) producing an average of 1.3 trillion kg feces. Figure 1.3 shows the estimates of the regional cattle population along with feces produced. Across the globe, farms produce much more livestock manure than can be used for their land, especially the case of the Netherlands where nearly 80% of the dairy farms produce more livestock manure. Animal feces pose a persistent threat to global human health while at the same time offering opportunities for recovery of its energy resources as cattle manure holds a lower heating value of 13.5 MJ/kg (dry basis), as suggested by Font-Palma (2019). Globally, the energy content potential of cattle manure sums upto around 17.55 EJ (dry basis).

1.2.3 Cheese Whey

Cheese whey is a liquid by-product obtained after the precipitation of milk during the cheese production process. Nearly 90% of the volume used for cheese production gets converted to whey. Lopes et al. (2019) mentions that globally, 24 million tons of cheese is being produced every year which results in 21.6 million tons of cheese whey being produced. The largest proportion of nutrient found in cheese is lactose (39-60 kg/m^3), followed by protein (6-8 kg/m^3), lipids (4-5 kg/m^3), and dry extracts (8-10%), thus making cheese whey a valuable product, as suggested by Lopes et al. (2019). High concentrations of organic load such as lactose and hardly biodegradable proteins result in high chemical and biological oxidation demand, thus making cheese whey a major pollutant. It is estimated to be 100 times more polluting than domestic sewage. Lappa et al. (2019) researched that concentrations of COD and BOD in cheese can vary between 50,000 to 80,000 mg/L and 40,000 to 60,000 mg/L resulting in soil depletion potential upon disposal. Soil depletion may be caused by the rapid consumption of oxygen in the soil due to the breakdown of sugars and proteins, leading to high oxygen demand. This presents a major disposal issue. Several advanced technologies such as ultrafiltration and nanofiltration techniques have already been developed for the conversion of this by-product to a range of valuable components or beverages. Even with the implementation of such techniques, the deproteinized form of cheese whey still consists of a lactose rich-fraction having a BOD of over 30 kg/m^3, therefore requiring further treatment of this organic pollutant, as advised by Lappa et al. (2019). Dairy industries are still looking for alternatives for the correct disposal of cheese whey to comply with the environmental legislation. The lower heating value of cheese is approximately 14.47 MJ/ kg (dry basis) aggregating to a global energy potential of 0.31 EJ (dry basis).

Table 1.1: Properties of supercritical and subcritical water extracted from Basu (2010).

Property	Supercritical Water	Subcritical Water
Temperature (°C)	400	25
Pressure (MPa)	30	0.1
Density, kg/m^3	358	997
Dynamic Viscosity (kg/m.s)	43.83 x 10^{-6}	890.8 x 10^{-6}
Dielectric Constant (-)	5.91	78.46
Thermal Conductivity (W/m.k)	330 x 10^{-3}	607 x 10^{-3}
Diffusivity of particles (m^2/s)	1 x 10^{-8}	1 x 10^{-9}

Generally, biomass has a higher MC than that of fossil fuels like coal. Basu (2010) mentions that with wet waste streams such as fruit/vegetable waste, cattle manure, and cheese whey, the water content is even higher, with its content exceeding 90wt% . Higher MC results in the negative impact on gasification efficiencies as extra energy (approximately 2242 KJ/kg-moisture) gets consumed in evaporation, as reported by Basu (2010). Furthermore, experimental studies show that the total efficiency[1] from thermal gasification is inversely proportional to water content, as the total efficiency diminishes from 61% to 27% when the water content in the feed augments from 5% to 75%, as researched by Yoshida et al. (2003). While the case of anaerobic digestion in which organic waste is broken down in the absence of oxygen to produce biogas and biofertilizer. Basu (2010) mentions that anaerobic digestion is a time-consuming process with residence time in the order of a few days .

An alternate option to conventional biomass gasification and anaerobic digestion is the SCWG. Among others, SCWG offers a major advantage as it does not require energy to dry the biomass and has much shorter residence times ranging from a few seconds to a few minutes, as proposed by Matsumura and Minowa (2004). SCWG takes place in a liquid medium and at the supercritical water condition, i.e. with temperature and pressure above 374.29 °C and 221 bar, respectively. In the following section, we will elaborate on the state of the art in applications of SCWG and will discuss the opportunities and challenges towards the practical implementation of SCWG technology.

1.3 SUPERCRITICAL WATER GASIFICATION: AN OVERVIEW

1.3.1 Supercritical Water

Water is in its supercritical state when its temperature and pressure exceed 374.29 °C and 221 bar, respectively. Water when in its supercritical state has liquid-like density and gas-like diffusivity. A comparison of supercritical and subcritical water properties has been listed in Table 1.1. Above the critical point, there is a significant change in the thermophysical properties of water. Specific heat sharply increases near the critical point followed by a similar drop (Figure 1.4). The dielectric constant drastically decreases which changes the property of water from a highly polar solvent to a non-polar one (Figure 1.4). This results in poor solubility of inorganics and high miscibility of different hydrocarbons and gases. Some of the property changes which could be potentially relevant in the case of gasification have been listed below.

1. Practically, the non-polar nature of SCW makes it a good solvent for organic compounds and gaseous products due to their increased miscibility. This allows the intermediates to undergo single-phase reactions while enhancing mass transfer rates.
2. Ionic compounds such as inorganic salts are mostly insoluble in SCW. This encourages the easy separation of salts and gases from the product mixture.
3. SCW forms an ideal medium as gases such as O_2 and CO_2 are highly miscible in SCW, thus promoting homogenous single-phase reactions with organic compounds for gasification.
4. SCW has excellent transport properties thus allowing it to easily enter biomass pores and carry fast and affective reactions. Density is lower than that of subcritical water (997 kg/m^3) and

---

1 Total efficiency = (Mechanical + electrical + useful thermal energy)/(Lower heating value of input fuel x mass flow rate)
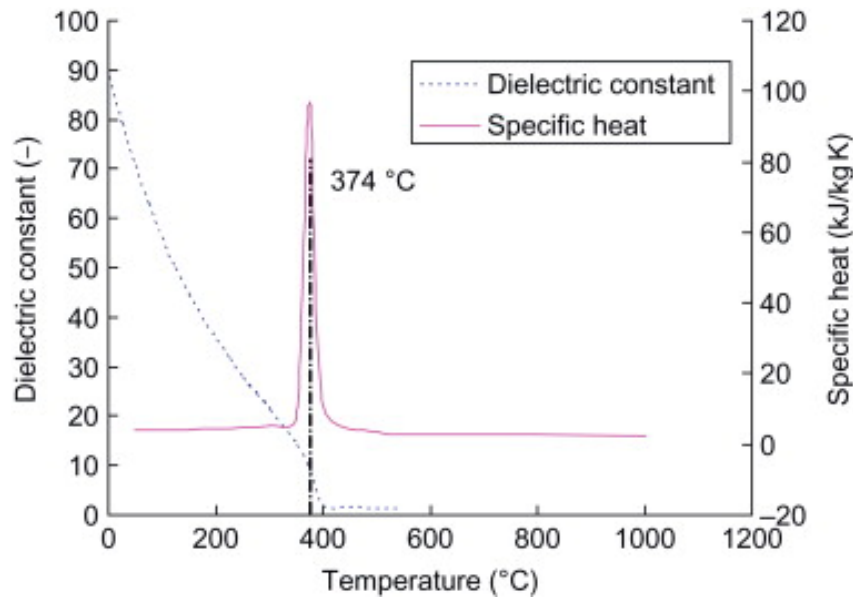
Figure 1.4: Dielectric constant and specific heat of water above and below its critical point. Reprinted from Basu (2010).

much higher than that of subcritical steam (+0.52 kg/m^3), low viscosity (Refer Table 1.1), low surface tension (0.07 N/m at 373°C reported by Basu (2010)) and high diffusivity (Refer Table 1.1) contribute to SCW's transportability.

1.3.2 SCWG technology

Supercritical gasification biomass can be divided into three temperature ranges
1. High temperatures (above 500 °C) without the use of catalysts and targets production of H_2-rich gas
2. Near critical temperatures (375-500 °C) with the use of catalyst and targets production of CH_4-rich gas and 350-500 °Cin the presence of a catalyst.
3. Sub-critical temperatures (below 375 °C) with essential use of catalysts and targets the production of smaller organic molecules and other gases.

During the process of gasification, biomass gets converted to intermediate products such as tar, char, and gas, which further gets reformed to form CO, CH_4, CO_2 and H_2. Overall, the gasification of biomass takes place according to the following reaction (Refer Equation 1.1).

$$aC_6H_12O_6 + bH_2O \rightarrow cH_2 + dCH_4 + eCO_2 + gCO \qquad (1.1)$$

SCWG offers various advantages over other conventional biomass conversion technologies, especially when the biomass has high MC i.e. over 30% MC. Some of the advantages proposed by Basu (2010) and Lu et al. (2012) are listed below:
- Due to the formation of char and tar, conventional thermal gasification techniques face significant problems as char residues are responsible for operational difficulties and energy loss. Tars can condense during downstream processing or polymerize to form complex structures, thus blocking the process equipment such as engines or burners. Char and tar production are low in the case of SCWG. The tar intermediates such as phenols get dissolved in SCW and get efficiently reformed during the gasification
- Dealing with very wet biomass (more than 70% MC) in conventional thermal gasifiers poses a major economical challenge as drying of wet biomass becomes economically unviable. Energy consumed while evaporating moisture from the fuel is about 2257 kJ/kg, which potentially goes unrecovered thus affecting the efficiency.
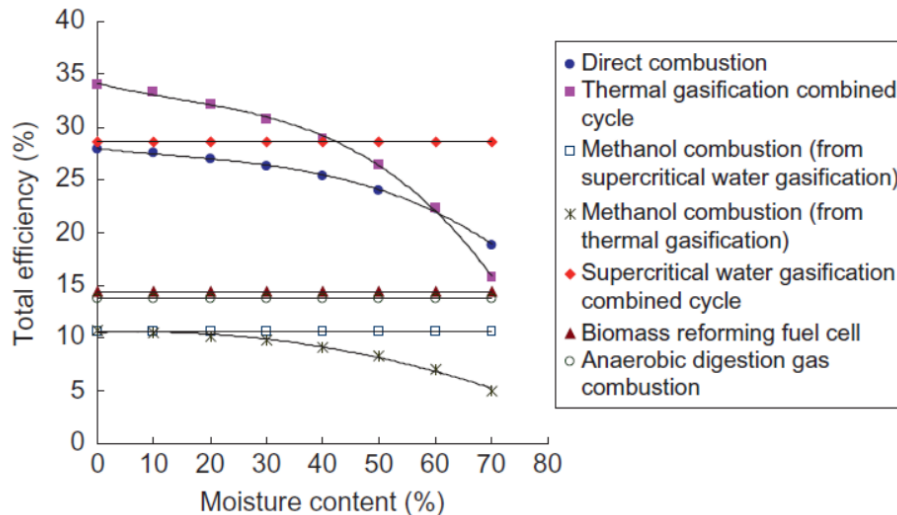
Figure 1.5: Total heat utilization efficiency of different thermal conversion technologies against biomass MC. Reprinted from Yoshida et al. (2003).

- In terms of efficiencies, SCWG is more efficient than conventional thermal conversion techniques or anaerobic digestion, particularly when the MC of biomass goes above 30%. Figure 1.5 shows the total heat utilization efficiency comparison of different thermal conversion techniques against the MC of biomass. It can be observed that the efficiency of the SCWG process remains constant with an increase in MC and SCWG is the most efficient process for MC above 40%.
- Comparing SCWG with conventional gasification systems, it does not require expensive gas cleaning techniques as inorganic impurities and heteroatoms like N, S and other halogens can be easily separated from the gas because they are insoluble in SCW.
- The ionic products (H^+ and OH^-) formed during the SCW state are several orders high as compared to water in the liquid state at ambient conditions, thus forming an effective medium for acid- and base-catalyzed reactions.

1.3.3 SCWG plant

A typical SCWG plant for wet biomasses consists of the following equipment. A schematic of a typical SCWG plant is shown in Figure 1.6.
- Pumping system for biomass feed
- Pre-heater system
- Gasification reactor
- Heat exchanger for waste heat recovery
- Gas-liquid separator

Before feeding, the biomass is converted to a slurry and pumped to reach the required supercritical pressure. Alternatively, the two processes can be carried out separately, pressuring the water, and then feeding biomass to it. The mixture thus formed is heated to the desired inlet temperature of the gasifier. The inlet temperature of the gasifier must be well above the gasification temperature as the enthalpy of water is required to provide the heat for carrying out endothermic reactions. The heat from the gasification products formed gets partially recovered in the heat exchangers which is used for partially heating the biomass feed. For completely heating the feed, either an externally fired heater or heat produced from burning a part of product gas could be utilized.

After cooling the gasification products, the products are sent to a gas/liquid separator. The solubility of CH_4 and H_2 in water is lower at low temperature and high pressure, so they get separated during cooling. CO_2 having high solubility remains in the liquid phase with water. CO_2 can then be separated
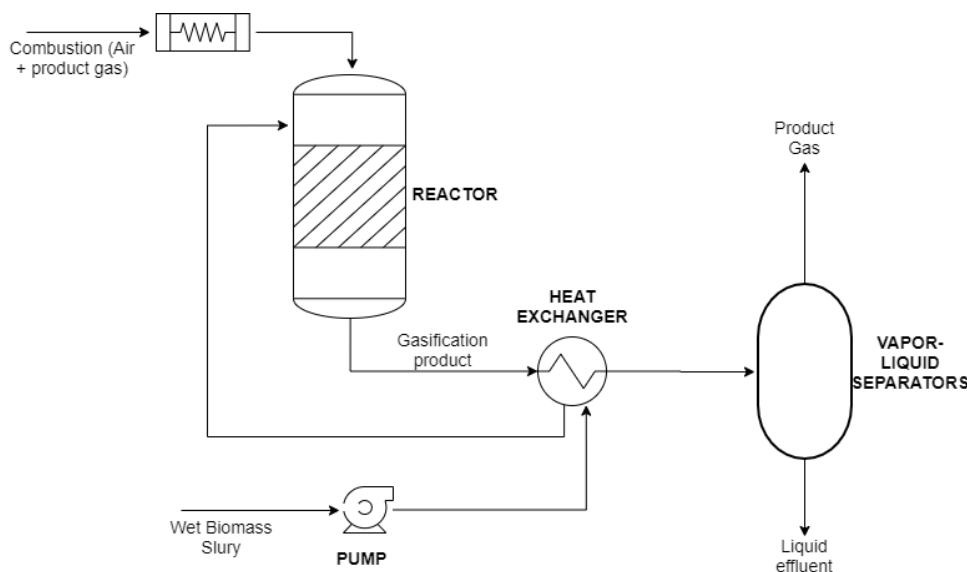
Figure 1.6: Schematic layout of a typical SCWG plant. Extracted from Basu (2010).

from the liquid and unconverted salts by depressurizing to atmospheric pressure. CH_4 and H_2 can be separated using pressure swing adsorption or membrane separation methods.

1.3.4 Parameters affecting SCWG

The yield and composition of gasification products depend on the gasifier design and several operating parameters. Below listed are the important parameters which play an important role in the efficient design and operation of SCWG.

Gasifier temperature – Energy efficiency and product composition depend a lot on the gasifier temperature. With the increase in temperature, overall Carbon Gasification Efficiency (CGE)[2] increases. Figure 1.7(A) shows the yield of gasification products (CO, CO_2, CH_4 and H_2) as a function of temperature when 0.6 mol/l of glucose is treated for 30s residence time at a pressure of 280 bar. The results are reprinted from Lee et al. (2002). With the increase in temperature, H_2 yield exponentially increases while CO_2 and CH_4 (lower than CO_2) shows a gentle increase. Above 650 °C, CO shows a gentle decrease due to beginning of water gas shift, methanation and hydrogenation reactions.

Gasification efficiency is usually measured in terms of carbon or hydrogen conversion i.e. ratio of the amount of carbon or hydrogen produced in gas to that present in biomass feed. As shown in Figure 1.7(B), (0.6 mol/l of glucose treated for 30 s residence time at a pressure of 280 bar), CGE increases with an increase in temperature and reaches about 100% above 700 °C and then gradually starts decreasing. While hydrogen conversion efficiency continually increases with temperature and reaches almost 140% at about 725 °C thus indicating the formation of H_2 from water. This shows that SCW indeed acts as a reactant in the gasification process.

Gasification pressure – It does not have a significant effect on the carbon conversion or gasifier product composition. The same has been suggested by Kruse (2008) when conducted experiments at 500 °C between 300-500 bars in a stirred tank reactor. Van Swaaij et al. (2003) in their experiments with a microreactor at 710°C between 280-345 bars and Lu et al. (2006) in their experiments using a plug-flow reactor at 625 °C between 180-300 bars displayed similar results.

Residence time – Longer residence time is favorable for SCWG as it gives a better yield of gasification products. Experiments conducted by Basu et al. (2009) using 2wt% rice husk at 650 °C and 300 bars in

---

2 CGE = (Carbon content present in the product gases including CO, CO_2, CH_4, C_xH_y)/(Carbon content present in the biomass feed)
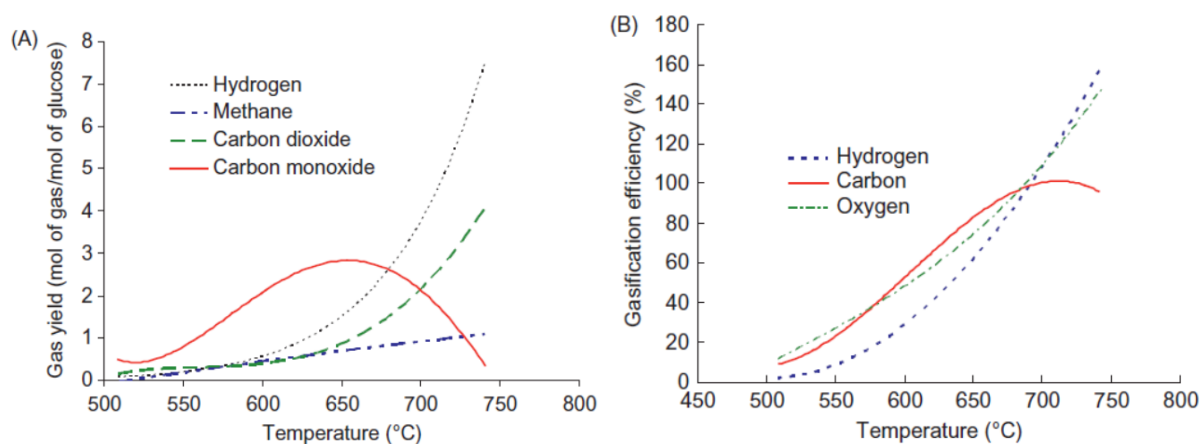
Figure 1.7: Effect of temperature on (A) gas yield and (B) gasification efficiencies for SCWG of 0.6 mol/l glucose at 280 bar for 30s of residence time. Reprinted from Lee et al. (2002).
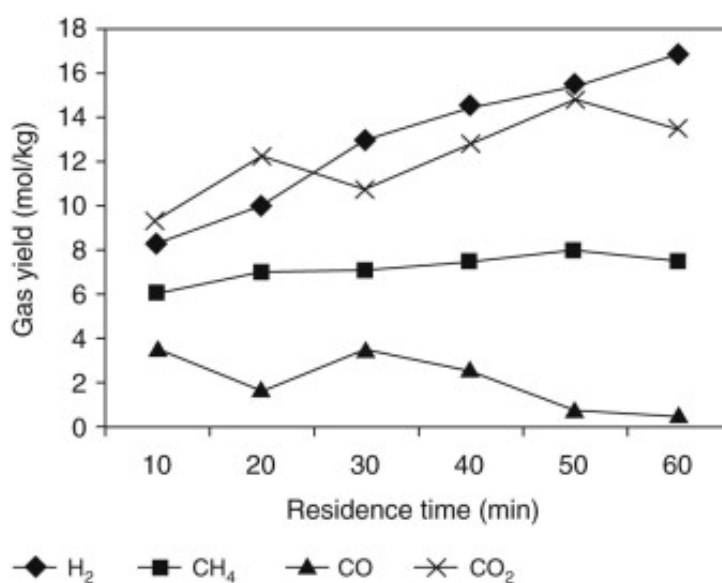
Figure 1.8: Effect of residence time on SCWG of 2 wt% rice husk in a batch reactor at 650°C and 25MPa. Reprinted from Basu et al. (2009).

a batch reactor suggested an increase in hydrogen and methane when the residence time was increased by three and six times, respectively (Figure 1.8). Although H_2 yield increases with an increase in residence time but only up to a certain extent, thereafter no significant change is observed, as suggested by Reddy et al. (2014). Reddy et al. (2014) proposed that an increase in residence time in the order of seconds increases gasification efficiency and vice versa.

Catalyst – For SCWG, higher conversion efficiency results at higher temperatures ($\geq$ 600 °C), especially for the production of hydrogen, but a lower gasification temperature is desired for high thermodynamic efficiency. The presence of catalysts helps in gasifying the biomass at lower temperatures, thereby retaining high thermal and high conversion efficiencies. Catalysts can be divided into three principal categories for SCWG.

- Alkali metal - Guo et al. (2010) mentions that use of alkali metal catalysts such as $KHCO_3$, Na_2CO_3, K_2CO_3, NaOH and KOH catalyzes the WGS reaction and improve H_2 yields. Experiments conducted by Minowa et al. (1998) reported a significant reduction in unconverted char when Na2CO3 was used while gasifying cellulose at 380 °C. Xu et al. (1996) reported a high gasification efficiency of 98% and 95.8% when gasifying glycerol and glycerine at 380-500 °C and 25MPa in the presence of Na_2CO_3 catalyst. Alkali metal catalysts are homogenous catalyst and

get dissolved in supercritical water which makes it difficult to recover them, as suggested by Basu (2010) and Guo et al. (2010). Guo et al. (2010) presented other issues encountered while using such catalysts include corrosion, reactor plugging, and fouling.

- Transition metals – Use of such catalysts such as Ni, Ru, Cu, and Co are found to be more effective for SCWG. A study by Furusawa et al. (2007) demonstrated the highest CGE of 30% when lignin was gasified at 600 °C in the presence of Ni/MgO catalyst. Byrd et al. (2007) observed a high H_2 yield (12 mol/mol of glucose) which was close to its theoretical value when glucose was gasified at 700 °C and 248 bar in the presence of Ru/Al_2O_3 catalyst. Generally, transition metals are heterogeneous catalysts and can be easily recovered from the effluent. They offer high recyclability, selectivity, and high catalytic activity but they also have severe corrosion effect when used at high temperatures needed for high hydrogen yield, as suggested by Basu (2010). Elliott (2008) observed that the formation of char during SCWG affects the activity of transition metal catalysts.

- Activated Carbon – Such catalysts include e.g. macadamia shell charcoal, spruce wood charcoal, coal, and coconut shell activated carbon and they offer high gas yield, enhanced CGE with very low tar formation. Reddy et al. (2014) highlighted that during gasification, the activity of AC decreases as this is prone to chemisorption which leads to a decrease in their surface area. Activated carbon is also not easy to recover as it is generally washed with HCl at room temperature followed by filtration.

Biomass to water ratio – It plays an important role in defining the SCWG efficiency. Using thermodynamic calculations Prins et al. (2005) suggested that carbon conversion significantly declines when biomass content in the liquid feed exceeds 50%. When experimentally tested, the decline in efficiency is observed at even a lower concentration. Experiments conducted by Basu et al. (2009) and Schmieder et al. (2000) showed that gasification efficiency starts to decline even when biomass concentration in fluid feed exceeds 2%. Similarly, results by Nanda et al. (2016) suggested a higher total gas yield and high LHV with a lower concentration (1:10 BTW ratio) as compared to 1:15 BTW ratio when orange peel was gasified at 600 °C.

Biomass feed size – Though there is no significant research conducted on the effect of biomass feed size, with the limited data available, Lu et al. (2006) observed an improvement in H_2 yield and increased gasification efficiency with smaller particles. The researchers based their results on the experiments conducted with feedstock such as rice straw (2wt%) + sodium carboxymethylcellulose (2wt%) at a temperature of 650 °C and pressure of 250 bar with a residence time of 30 s.

1.3.5 Challenges to SCWG technology

Supercritical water gasification is a promising technology that still faces commercialization issues due to some of the technical impediments listed below.

- Basu (2010) suggests that a large heat input is required for the endothermic reactions during SCWG . The heat input affects the thermal energy efficiency unless most of the sensible heat is recovered from the products. For recovery, the need for highly efficient heat exchangers requires high capital investment thus affecting the viability of SCWG.
- Similarly, feeding large quantities of wet biomass is a challenge as it is often fibrous and heterogeneous in nature, as discussed by Basu (2010) and Davis (2001). A high capacity pump which involves high capital cost is required to feed the slurry into high-pressure reactors.
- Reddy et al. (2014) mentions that stability of catalyst at such high temperatures and pressures also poses a major challenge as catalyst poisoning and deactivation increases the regeneration and processing costs .
- Basu (2010), Calzavara et al. (2005), and Guo et al. (2007) highlighted that pre-heating of biomass in the HEX promotes reactor plugging, char and tar formation . The low solubility of salts in the SCW leads to precipitation of salts which then combine with char resulting in reactor plugging, as observed by Bermejo and Cocero (2006) and Kruse (2008).
- Another issue is the corrosion of reactor walls which was mentioned by Basu (2010), Nanda et al. (2016), and Kritzer (2004) in the research works. Biomass such as fruit and vegetable waste

contains a significant amount of organic acids which upon reaction with alkali metal catalysts leads to salt formation thus corroding the reactor walls.

1.3.6 An overview of the literature

Back in the 1970's supercritical water was first explored as a gasifying medium with organic material being gasified under supercritical conditions. Modell et al. (1978, 1982) submitted a patent to report the gasification of organic materials including, maple sawdust, glucose, and sewage sludge to name a few. Since then, SCWG of high MC biomass feedstocks has been the subject of numerous analytical and experimental researches by the following research groups such as Modell et al. (1978); Modell (1982); Matsumura et al. (1997); Kabyemela et al. (1999); Antal Jr et al. (2000); Mizuno et al. (2000); Yoshida et al. (2003); Kruse (2008); Guo et al. (2007); Nanda et al. (2015), and Yakaboylu et al. (2018). Relevant research works on SCWG are discussed below.

Experimental overview

Nanda et al. (2015,2016) conducted experimental studies on supercritical water gasification of several agricultural residues and fruit wastes including banana, orange, pineapple, and lemon peel, coconut shell, sugarcane bagasse, and aloe vera rind in a tubular batch reactor. The authors investigated the influences of different parameters such as temperature (400-600 °C), pressure (230-250 bar), reaction time (15-45 min), and catalyst (NaOH and K_2CO_3). In case of orange peel as the feed, the optimal condition for total gas and hydrogen yield was found at 600 °C (temperature), 230-250 bar (pressure), 45 min (residence time), 1:10 (BTW) which gave an LHV of 722 kJ/Nm^3 for syngas produced. Furthermore, the researchers assessed the use of fructose as a model compound for fruit/vegetable waste using different parameters. In case of fructose as feedstock the optimal conditions for total gas yield, hydrogen yield, and carbon gasification was found to be 700 °C (temperature), 250 bar (pressure), 4wt% (feed), 60 s (residence time), and highest LHV for syngas production was 3630 kJ/m^3 when using 0.8wt% KOH as a catalyst. The authors concluded that temperature plays an essential role in the gasification of food wastes. With an increase in temperature, the gas yield (H_2, CH_4, and CO_2) and carbon gasification efficiency increases.

Amrullah and Matsumura (2018) investigated phosphorous recovery and gas generation from sewage sludge in a continuous supercritical water gasification tubular reactor. Experiments were conducted in a temperature range of 500-600 °C with a pressure of 250 bar, a feedstock flow rate of 1.3-15 ml/min and a residence time of 5-60 s. The authors developed a first-order reaction kinetics model and were found to fit well with the experimental results. The authors observed that during the reaction, the organic phosphorous quickly got converted to inorganic phosphorous within a residence time of 10 s. The authors even observed a high CGE of 73% at a temperature of around 600 °C.

Molino et al. (2017) studied the supercritical water gasification of municipal waste leachate followed by catalytic gas upgradation. The gasification was conducted in a continuous tubular reactor having a flow rate between 10-40 ml/min and process time of 20-60 min, with temperature and pressure of 550 °C and 250 bar respectively. The syngas produced was upgraded to increase the methane fraction in synthetic natural gas using Ni catalyst. The authors concluded that a 2-stage process involving SCWG of waste followed by a product gas catalytic upgrading produced a syngas with a calorific value of 15-17 MJ/kg. It was observed that Methane concentration in the syngas increased by 50v/v% when using Ni catalyst. Table C.13 gives an overview of the experiments conducted in the recent past using real biomass feedstocks.

Thermodynamic equilibrium modelling overview

The thermodynamic equilibrium modelling approach was first used by Antal Jr et al. (2000) on biomass feedstocks such as potato waste, potato, corn starch gel, and wood saw in a cornstarch gel. The researchers conducted experiments at temperatures and pressures above 650 °C and 220 bar, respectively. The experiment results were then compared with the equilibrium concentrations predicted using STANJAN and HYSIM. STANJAN used the ideal gas law as an EoS and PR EoS was used for

HYSIM. The authors concluded that there were no tar products and the liquid effluent had low COD (49-54 mg/l) and TOC (0.3-0.5 wt% of carbon content in feed) values with a pH between 3-8.

Tang and Kitagawa (2005) developed a thermodynamic model based on Gibbs free energy minimization for estimation of product gas composition for supercritical gasification of biomass. The authors used PR EoS to conduct their studies on methanol, glucose, cellulose, starch, and sawdust. One of their interesting observation was a very limited effect of pressure on the yield of gases.

Yanagida et al. (2008) used a thermodynamic equilibrium modelling approach for SCWG of poultry manure. The authors used HSC Chemistry 6.12 software to predict the equilibrium composition of both organic and inorganic elements including carbon, hydrogen, oxygen, calcium, sodium, potassium, chlorine, silicon, sulfur, and phosphorous. The equilibrium compositions were compared with the experimental results conducted at 600 °C and 320 bar along with activated carbon as a catalyst. The authors observed that most of the silicon, calcium and phosphorous were found in the solid phase whereas almost all of chlorine, sodium and potassium were found in the liquid phase during SCWG of the biomass.

Yakaboylu et al. (2014; 2015a; 2015b; 2018) used different approaches to model the thermochemical conversion in supercritical water gasifier. The authors developed unconstrained and constrained equilibrium models to assess the behaviors of gaseous products together with the distribution of elements at different gasification conditions for different feedstock including cattle manure and wheat starch. It was observed that with the use of constrained equilibrium modelling the accuracy of models can be increased. Furthermore, the authors concluded that CGE is the most important additional constraint. Table 1.3 gives an overview and presents some main results of the GTE modelling approaches for SCWG of biomass studied in the past.

Table 1.2: Overview of experiments conducted in the past using real biomass feedstocks.

Author(s), Year	Biomass type	Reactor type	Temperature (°C)	Pressure (bar)	Res. time (s)	Feed conc. (wt%)	Flow rate (ml/min)	CGE (%)	H_2	CO_2	CH_4	CO
									Operating conditions		Yield	
Nanda et al. (2016)	Fructose	Continuous flow	700	250	60	4	-NA-	88	3.3 mol/mol feed	3.2 mol/mol feed	1.2 mol/mol feed	0.2 mol/mol feed
Nanda et al. (2015)	Orange peel	Batch type	600	230-250	2700	10	-NA-	14.8	1.6 mmol/g feed	3.3 mmol/g feed	1.4 mmol/g feed	0.25 mmol/g feed
Amrullah and Matsumura (2018)	Sewage Sludge	Continuous flow	600	250	60	-NA-	1.3-15	73	20 vol%	25 vol%	40 vol%	-NA-
Molino et al. (2017)	Municipal waste leachate	Continuous flow	550	250	1200	-NA-	40	6	25 vol%	45 vol%	18 vol%	12 vol%

Table 1.3: Overview of research conducted using GTE modelling approaches for SCWG of biomass feedstocks.

Author(s), Year	Biomass type	EoS/software used	Phases considered
Antal Jr et al. (2000)	Potato waste, potato and corn starch gel & wood saw in a cornstarch gel	Ideal gas law and Peng-Robinson	Gas phase
Tang and Kitagawa (2005)	Methanol, glucose, cellulose, starch and sawdust	Peng-Robinson	Gas phase
Yanagida et al. (2008)	Poultry manure	HSC Chemistry 6.12	Multiphase
Yakaboylu et al. (2013; 2015b)	Pig-cow manure	FactSage 5.4.1 and SimuSage 1.12 Multiphase	Multiphase

1.4 RESEARCH QUESTION

SCWG is an alternative process to both anaerobic digestion and conventional biomass gasification. It offers good potential in processing wet waste as it does not require drying of biomass and the gasification process gets completed in much shorter residence time. Surveying the literature, it was found that multiplicities of the relevant subject need to be duly addressed to be able to put this technology into practice. These include the inadequacy of the models to replicate the localized physio-chemical phenomena in the SCW gasifier and the availability of studies for a narrow range of biomass wastes that need further deliberation and investigation. Also, SCWG technology has unresolved process challenges, such as energy integration, low biomass conversion in SCWG reactor, high-pressure filtration, the mechanisms of char and tar formation together with the clogging problems due to salts depositions in a highly non-ideal slurry system which needs further essential efforts. Many research groups have already conducted quality research ranging from theoretical models to practical experiments. However, there is still a need for a thorough analysis of SCWG for real wet biomass wastes such as manure, fruit/vegetable residues, and cheese whey.

1.5 SCOPE OF THESIS

The main aim of this study is to conduct a thorough analysis of SCWG of the real wet waste streams. In particular, the study is aimed at:

1. A detailed thermal equilibrium model will be developed based on the data from the SCWG experiments conducted on the three wet waste streams. The design will be focused on the different feedstock compositions i.e. cattle manure, fruit/vegetable waste, and cheese whey. The model will work towards the optimization of different process design parameters including but not limited to temperature, pressure, and biomass-to-water ratio that all could directly influence the total gas yields, carbon gasification efficiency, and syngas composition.

2. We will study and analyze different thermodynamic modelling scenarios such as global thermodynamic equilibrium, constrained thermodynamic equilibrium, and quasi-thermal equilibrium which are based on Gibbs free energy minimization method to predict the system behavior. The reactor will be modeled using FactSage^{TM} 7.2 software and the constrained equilibrium model after the work of Yakaboylu et al. (2015b). A novel thermal equilibrium model will be proposed based on the concept of approach temperature. All the three scenarios will be measured against the supplementary experimental results conducted using samples from the partner industries.

3. Apart from this, optimization of downstream processing will be carried out including effluent, H_2S, and CO_2 rich streams. The results from the reactor modelling will be then fed to the ASPEN Plus software which will further optimize the entire biorefinery model in terms of energy/work process integration.

4. The study will further explore the technologies available to process the downstream and sustainable integration with the reactor system.

1.6 OUTLINE OF THESIS

The study is divided into 6 chapters and arranged in the following manner.

Chapter 2 'Experiments and Biomass Waste Characterization' presents the experimental results conducted on the three wet biomass residues; Cattle manure, Fruit/vegetable waste, and Cheese whey.

Chapter 3 'Thermodynamic Equilibrium Modelling', concerns with the modelling of the SCWG reactor using Factsage^{TM} software. Furthermore, it discusses the equilibrium gas and elements behavior results based on SCWG reactor modelling.

In **Chapter 4, 'Advanced Thermodynamic Equilibrium Modelling'**, we present the gas behavior results using two advanced modelling techniques such as constrained thermodynamic and quasi-thermal equilibrium modelling. Furthermore, these results are compared with the global thermodynamic equilibrium results discussed in chapter 3.

In **Chapter 5, 'Thermodynamic Process Modelling and Analysis'**, we present a design of the process model for a conceptual bio-refinery based on SCWG of wet biomass waste. Following which, we investigated the gas and thermal behavior results from the process model simulation.

Lastly, **Chapter 6, 'Concluding Remarks'**, summarizes the main conclusions and provide suggestions for future work.

2 | EXPERIMENTS AND BIOMASS WASTES CHARACTERIZATION

This chapter illustrates the experimental setup used for SCWG of the wet waste. Experiments were conducted at the University of Groningen, the Netherlands at the green chemical reaction engineering lab using a 7ml stainless steel batch type reactor. The chapter also discusses characteristic properties such as proximate, ultimate and major element analysis for the considered biomass feedstocks.

2.1   EXPERIMENTAL SETUP

The experiments are conducted under a non-catalytic environment in a custom-built high-pressure stainless-steel (304L) batch reactor with an internal volume of 7 ml. Figure 1 represents the schematics of the reactor assembly. The main seal of the reactor is coated with a silver metal ring to prevent any leakage. A K-type thermocouple connected to a data logger (USB-501-TC-LCD) is used to measure the internal temperature. The pressure is monitored using a manometer ranging from 0-450 bar. A glass insert made from borosilicate 3.3 glass is used to feed samples in the reactor. The reactor assembly is placed in a custom-built oven set to 530-600°C.

Tests are designed in a way that: i) all reactor parts weighed empty including the glass insert before the start of each experiment. ii) Glass insert loaded with approximately 4.5 g of wet biomass. iii) Post assembly of the reactor weighed and transferred for high-pressure operation. iv) The reactor was flushed three times with nitrogen and was pressurized with nitrogen to 50 bar so as to perform a 15 min leak test. v) Having carried out a successful leak test, the pressure is released just above the atmospheric pressure, and the entire reactor assembly was finally weighed again. vi) The reactor was then placed in a pre-heated oven at 530-600 °C and pressure and temperature values are recorded at an interval of 1 min. vii) After 45 mins of operation, the reactor assembly was removed from the oven and cooled down to room temperature using an air fan. viii) Having cooled the reactor, it was weighed again, and the produced gases were collected using a 50 ml syringe so as to measure the volume of gaseous products. ix) The collected gases were weighed and transferred to a gas chromatograph (HP 5890 series II dual column) for further analysis. The gas chromatograph employed is equipped with one Varian Capillary Column CP-PoraBond Q (L=50 m, ID=0.53 mm, 10 μm) and one Agilent Technologies HP-Molsieve (L=30m, ID= 0.53mm, 50 m) column wherein Helium was used as the carrier gas.
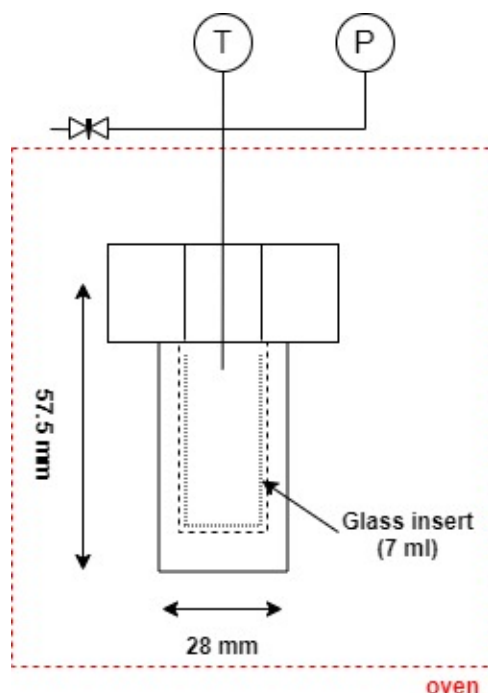
Figure 2.1: Schematics of the experimental setup.

2.2 FEED CHARACTERIZATION

For the SCWG experiments, three different biomass wastes such as cattle manure, fruit/vegetable waste, and cheese whey are chosen (Figure 2.2). Cattle manure is obtained from Agri farm Janusz Paweta, Krokocice Kolonia, while fruit/vegetable waste and cheese whey are provided by our partner FRESH and Jogo Dairy Cooperative, Łódź, respectively. Analyses are carried out to enable determining the influence of composition and different process parameters on the SCW gasification conversion. Standard ASTM test procedures were used to conduct the proximate and ultimate analysis using TGA and CHNS analyzer. Moreover, an optical spectrometer with excitation in inductively coupled plasma ICP-OES SpectroBlue (Polish standard PN-EN-ISO-11885-2009E) was used for the elemental characterization of the biomass. The proximate, ultimate, and major element analysis for the considered feedstocks has been shown in Table 2.1.

Table 2.1: Proximate, ultimate and major element analysis of the biomass wastes.

Parameters	Cattle manure	Fruit & vegetable waste	Cheese whey
Proximate analysis			
M [% w/w a.r.]	82.9	89.0	97.0
V [% w/w d.b.]	66.0	72.4	62.1
FC [% w/w d.b.]	15.3	20.4	19.0
A [% w/w d.b.]	18.7	7.2	18.9
Ultimate analysis			
C [% w/w d.b.]	43.5	46.3	38.9
H [% w/w d.b.]	5.3	5.6	5.2
N tot/NH_4^+ [mg/l]	3320 / 2.9	628 / 1.1	131 / 0.4
TOC [g/l]	8.9	27.9	16.8
COD [g/l]	27.7	91.1	45.7
HHV/ LHV [MJ/kg (d.b.)]	19.2 / 18.1	19.8 / 18.6	15.6 / 14.5
Major element analysis (mg/kg of biomass) (a.r.)			
K	3191.0	1863.0	1417.0
Ca	3202.0	317.0	995.0
P	891.0	192.0	586.0
Mg	1604.0	152.0	130.0
Fe	289.0	-	-
S	420.0	94.8	51.4
Na	548.0	32.2	420.0
Sr	-	5.4	-
Zn	-	2.4	3.7
B	-	4.3	1.9
Al	81.7	-	0.7
Si	80.6	-	-

(a) Cow manure

(b) Fruit/vegetable waste

(c) Cheese whey

Figure 2.2: Biomass waste samples

3 THERMODYNAMIC EQUILIBRIUM MODELLING

This chapter deals with the multiphase model based on Gibbs free energy minimization using FACTSAGE^{TM} software to perform extensive analysis on the wet biomass wastes. The thermodynamic equilibrium model is used to predict the behavior of product gases for a wide temperature range between 100-700°C and a reaction pressure of 240 bar. Apart from the study on product gas composition, the investigation also focuses on the partitioning of elements such as phosphorous, silicon, sulphur, magnesium, potassium, sodium, bromine, etc. which are present in the considered biomass wastes.

3.1 INTRODUCTION

Despite the complexity of the thermochemistry of biomass conversion in supercritical water, modelling is always an important tool for a better understanding of such complex system behavior. Three thermodynamic modelling approaches have been proposed to study the SCWG optimization: (i) GTE which simply uses Gibbs free energy minimization technique, (ii) Constrained thermodynamic equilibrium model which is based on GTE along with additional constraints, and (iii) Quasi-thermal equilibrium model based on the concept of the approach temperature.

Simulations for each of the three different biomass wastes have been considered based on 100 kg waste as input with temperature and pressure ranging from 100-700 °C and 230-260 bar, respectively. Molar inputs for the simulations were calculated based on proximate, ultimate, and major element analysis of the biomass wastes and are presented in Table 3.1.

3.2 MODEL DEVELOPMENT

Here, FactSage^{TM} is the modelling software that is used to assess the gasification behavior of the different biomass. FactSage^{TM} is a thermochemical equilibrium software consisting of different calculation modules and databases. The 'equilib' tool uses Gibbs free energy minimization for computing multi-component equilibria, multiphase conditions with a large possible range of natural constraints. The Gibbs free energy minimization is based on the ChemApp algorithm, as reported by Eriksson et al. (1997). Gibbs free energy of the system is minimized for a combination of composition, temperature, and pressure and has been shown in equation 3.1.

$$
\begin{aligned}
G = &\sum_{ig} n_i \left(g_i^o + RT \ln P_i \right) + \sum_{pcp} n_i g_i^o \\
&+ \sum_{s_p-1} n_i \left(g_i^o + RT \ln x_i + RT \ln \gamma_i \right) \\
&+ \sum_{s_p=2}^{s_p-1} n_i \left(g_i^o + RT \ln x_i + RT \ln \gamma_i \right) + \ldots + \ldots
\end{aligned}
\tag{3.1}
$$

where, ig, pcp, and s refer to the ideal gas, pure condensed, and solution phase. n_i, p_i, x_i, γ_i, and g_i^0 refer to the number of moles, partial pressure, mole fraction, activity coefficient, and standard molar Gibbs free energy for the ith compound. R and T are the universal gas constant and temperature, respectively.

Calculations are separately performed for two distinct regions i.e. the subcritical regime with temperatures ranging from 100 – 375 °C and the supercritical regime with temperatures ranging from 400 – 700 °C. The two regions are divided based on the fact that for a selected reactor pressure of 240 bar, the pseudo-critical point of water is expected to lie between 385-390 °C, as mentioned by Yakaboylu (2016). Hodes et al. (2004) indicates that pseudo-critical point refers to the temperature where the phase transition of water is completed and the isobaric heat capacity is at its maximum . Under subcritical reaction conditions, for the selection of compounds and solutions, three different modules, FactPS, FTsalt, and FThelg have been employed. For the supercritical region, three modules are selected, namely FactPS, FTsalt, and FToxid. FactPS is used, providing inclusive databases for over 500 compounds. Data for the gaseous phase will generally be found in FactPS. FTsalt module consists of data from pure salts and salt solutions and under this module, the database considered are FTsalt-CSOB, FTsalt-SALTF, FTsalt-ALKN, FTsalt-ALOH, FTsalt-SCSO, and FTsalt-SSUL. FThelg module consists of infinite dilution properties of aqueous solute species based on the Helgeson equation of state which is considered for handling non-ideal fluid systems. Coupled with the FThelq module, the FTHelg-AQDD database is considered. The FToxid module consists of data from all pure oxides and oxide solutions (both liquid and solid) and the databases considered are FToxid-SlagD, FToxid-C3Pa, and FToxid-C3Pr. It is noteworthy that the selection of modules and databases was adapted from the work of Yakaboylu (2016) which is based on the activity and fugacity of compounds.

Table 3.1: Molar input for all the feedstocks considering 100 kg of biomass waste input.

Component	Input (mole/100 kg of d.b.)		
Feed type	Manure	Fruit pulp	Cheese whey
C	3625.8	3854.2	3237.5
H	5250.0	5560.0	5146.0
S	7.7	2.7	5.4
P	16.9	5.6	63.0
N	195.6	2.9	0.6
O	2652.5	2857.9	2748.6
K	48.1	43.4	121.1
Ca	47.1	7.2	82.9
Mg	38.8	5.7	17.8
Fe	3.1	-	-
Na	14.0	1.3	60.9
Sr	-	0.1	-
Zn	-	0.03	0.19
B	-	0.4	0.6
Al	1.78	-	0.003
Si	1.7	-	-
H_2O	27124.2	44949.5	179629.6

3.3 RESULTS AND DISCUSSIONS

3.3.1 Validation

This section aims to assess the validity of different modelling approaches by comparing the simulation results to that of experiments. To this end, validation of the models is investigated for all three feedstock cases at 'as received' condition for specific SCW gasifier temperature and pressure. It is worth mentioning that due to the purging of nitrogen and using different amounts of feedstocks in the tests, pressure levels varied from 230 to 260 bar. Further, pressure does not have much effect on SCWG. Figures 3.1a, 3.1b, and 3.1c illustrate the comparative results for manure, fruit/vegetable waste, and cheese whey, respectively, where the gas yield for the main gaseous products is benchmarked against test results. Overall, the bar plots show a reasonable agreement between the test results and those of FactSage^{TM} simulations.

The observed deviation of the predicted gas yield from the experimental data can be explained by the fact that GTE predicts gas compositions at the global minima of Gibbs free energy whilst in real reactor environment local equilibrium occurs. Thus, GTE does not take into account the role of limited carbon conversion observed in practice. Therefore, it is anticipated that the results of thermal equilibrium modelling can be improved by imposing additional constraints to cover carbon gasification efficiency. This will be addressed in more detail in the upcoming sections.

3.3.2 Gas behavior

Simulations for the different biomass (manure, fruit/vegetable waste, sewage, and cheese whey) have been conducted using Factsage^{TM} at a pressure of 240 bar and a temperature range of 100-700 °C and the emanated results are presented in Figures 3.2, 3.3, and 3.4. The product gas is mainly composed of CO_2, CO, H_2, and CH_4 while CO, H_2S, and other species such as N_2, NH_3 (not shown in the figures) are produced in small quantities. Overall, results show that total gas yield significantly increases above 300 °C, which is ascribed to the drastic decrease of solid carbon in this range of temperature. Similar behavior is reported by other research groups such as Kabyemela et al. (1999), Nanda et al. (2015), Yakaboylu et al. (2013, 2015b), and Yan et al. (2006). Furthermore, several research groups, e.g. Guo et al. (2010), Promdej et al. (2010), and Nanda et al. (2016) have reported that the density of water

(a)

(b)

(c)
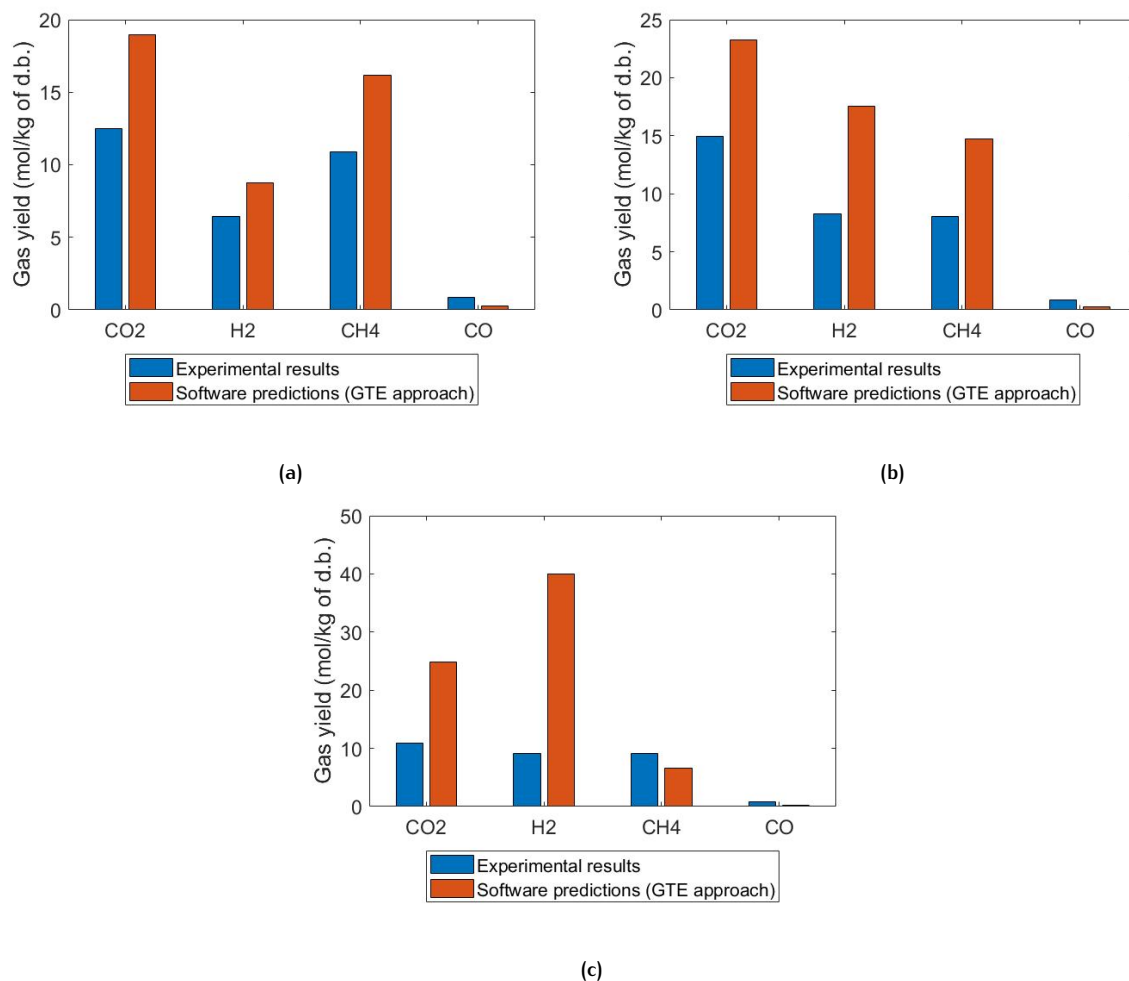
Figure 3.1: Comparison between experimental results and FactSage^{TM} predictions for (a) manure (17wt% feed concentration) at 552°C and 260 bar (b) fruit/vegetable waste (11wt% feed concentration) at 560°C and 240 bar (c) cheese whey (3wt% feed concentration) at 539°C and 235 bar.

decreases above its critical point, resulting in the disruption of ionic products formation. In fact, the decreased formation of ionic products enhances free radical mechanisms and, thus, leading to a higher yield of gases.

Methane gas yield for all the three types of biomasses demonstrative of a decline at temperatures higher than 400 °C, whilst that of CO and H−2 reveals an increasing trend. This can be explained by the backward methanation reaction which consumes methane and water to form hydrogen and carbon monoxide (methanation reaction, Equation 3.2). High hydrogen yields are complemented as the water gas shift reaction (Equation 3.3) is enhanced at higher temperatures and possible hydrogen formation routes due to thermal decomposition of intermediates, as suggested by Acelas et al. (2014). The increase in carbon dioxide yields at higher temperatures is attributed to the enhanced forward water gas shift reaction in a higher temperature range (Equation 3.3). The overall trend and behavior of the main gaseous products for all the three biomasses show a good agreement with literature findings reported by Acelas et al. (2014), Wilkinson et al. (2012), Nanda et al. (2016), Guo et al. (2010), Cao et al. (2016), and Yakaboylu (2016).

$$CO + 3H_2 \leftrightarrow CH_4 + H_2O \tag{3.2}$$
$$CO + H_2O \leftrightarrow CO_2 + H_2 \tag{3.3}$$
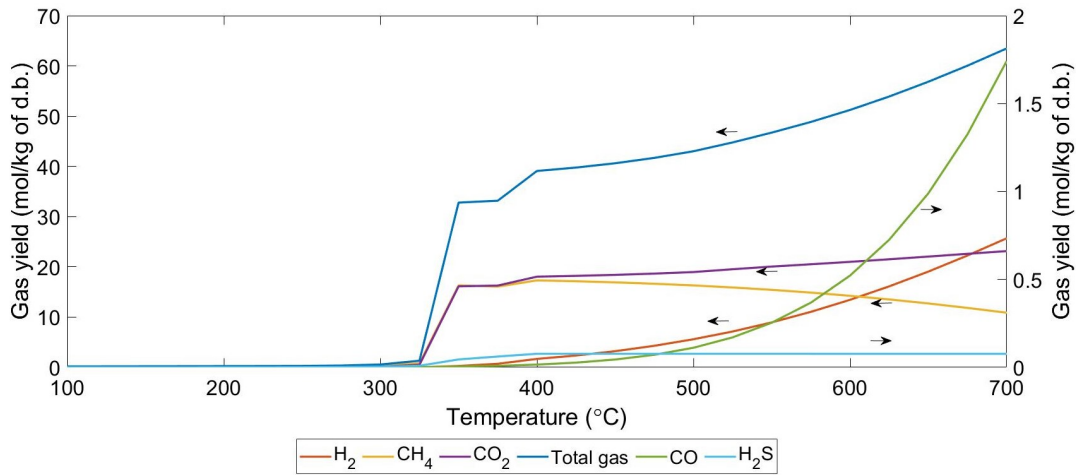
Figure 3.2: Behavior of different gases released during SCWG of manure with a feed concentration of 17% at 240 bar and temperature range of 100-700 °C. Results based on GTE approach using FactSage^{TM} simulations.
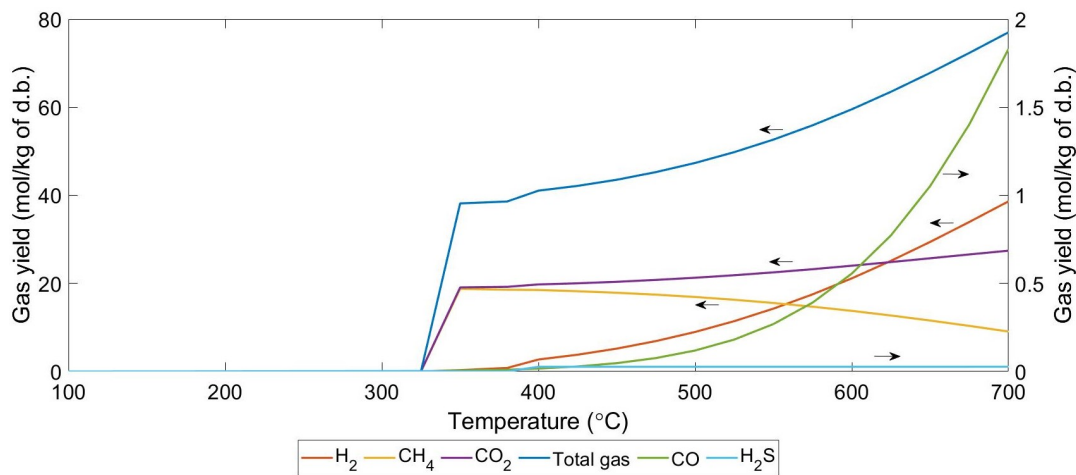
Figure 3.3: Behavior of different gases released during SCWG of fruit/vegetable waste with a feed concentration of 11% at 240 bar and temperature range of 100-700 °C. Results based on GTE approach using FactSage^{TM} simulations.
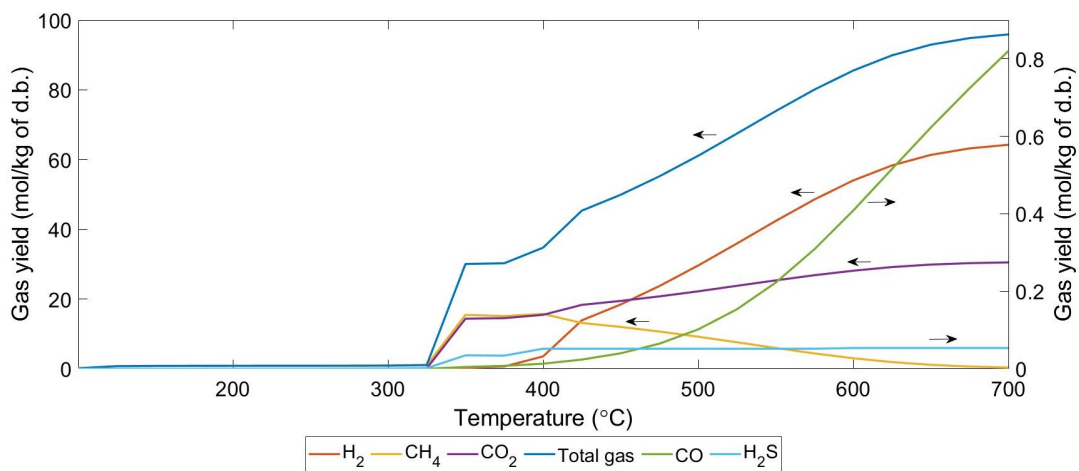
Figure 3.4: Behavior of different gases released during SCWG of cheese whey with a feed concentration of 3% at 240 bar and temperature range of 100-700 °C. Results based on GTE approach using FactSage^{TM} simulations.

3.3.3 Element behavior

The distribution of elements such as carbon, sodium, magnesium, calcium, phosphorous along other inorganic elements is addressed and discussed in this section. The basis of the partitioning assessment is the GTE approach. Such information is of high interest as it assists in the evaluation of ash and slags formation and their predicted compositions. Furthermore, such results can assist in a better quantification of the operating parameters for the SCW reactor, and, in principle, for potential reduction of the number of solid residues to be further processed or disposed of. The elemental partitioning behavior results for fruit/vegetable waste are presented and discussed below. The partitioning behavior for manure and cheese whey are discussed in Appendix A for the sake of brevity. The results are based on SCWG for fruit/vegetable waste at 240 bar and a temperature range of 100-700 °C. For this, Factsage^{TM} simulations were performed under subcritical conditions for a temperature range of 100-375 °C, whilst 400-700 °C temperature range was considered for supercritical conditions.

Partitioning behavior of carbon is shown in Figure 3.5. As presented in the figure, the first region which lies between 100-325 °C is dominated by solid carbon in the form of graphite along with small amounts of Mg(butanoate)$_2$. While the second region lying between 350 – 700 °C shows the dominance of gas products such as CO_2, CH_4, CO followed by the appearance of other compounds such as $K_2Ca_2(CO_3)_2$, and HCO_3^- present in smaller quantities. The trend can be explained as at temperatures higher than 350 °C, solid carbon decomposes to form CO_2 and CH_4. Furthermore, CH_4 starts decomposing around 400 °C and gets converted into CO_2, CO, and H_2.

Partitioning behavior of sulfur is shown in 3.6. Around 100 °C, an approximate of 20% molar fraction of K2SO4 in the solid form gets formed. Between 100-325 °C, the region is mainly dominated by KSO_4^- and HS^- followed by SO_4^{2-}, aqueous H_2S, and ZnS(s) present in smaller quantities. KSO_4^- decreases with an increase in temperature while HS^- increases. The region between 375 °C and 700 °C is dominated by the gaseous form of H_2S.

As shown in Figure 3.7, phosphorous compounds are only present in solid form in the entire gasification temperature range. At temperatures lower than 375 °C, phosphorus is present majorly in two forms, $Ca_5HO_{13}P_3$ and $Na_2CaP_2O_7$ with an average of 70% and 20% respectively. The region also contains smaller quantities of $HP_2O_7^{3-}$ HPO_4^{2-}, $P_2O_7^{2-}$, and $H_2PO_4^-$. Between 400 °C and 450 °C, the region is dominated by $Mg_3P_2O_8$ with an average of 50% molar fraction, while $NaMgPO_4$ and $Ca_5HO_{13}P_3$ present in small quantities (average of 25% each). At temperatures exceeding 475°C is dominated by $Ca_5HO_{13}P_3$.

Partitioning behavior of nitrogen is shown in Figure 3.8. At temperatures below 325°C, the region is dominated by N_2 in its aqueous form while containing smaller quantities of N_2 in its gaseous form and NH_3 in its aqueous form. Nitrogen in the form of N_2 gas is the most stable compound present between 350 °C and 400 °C along with smaller quantities of NH_3(g). At temperatures higher than 400 °C, the only stable compound present is NH_3(g). Such a finding has previously been reported by Yakaboylu (2016) and Klingler et al. (2007). Yakaboylu (2016) highlighted that nitrogen is only released in the form of NH_3 during the gasification of biomass. Klingler et al. (2007) mentioned that under hydrothermal conditions when amino acids react with water, NH_3 is formed. Therefore, N_2 was deselected for the supercritical condition in the FACTPS module.

Partitioning behavior of potassium is shown in Figure 3.9. In the subcritical region, KOH in its aqueous form and K^+ ions are majorly formed, with K^+ ions decreases with an increase in temperature while KOH(aq) increases. The supercritical region only consists of solid compounds of potassium in the form of $K_2Ca_2(CO_3)_3$ present at temperatures below 450 °C along with K_2CO_3. At temperatures exceeding 450 °C K_2CO_3 is the only stable compound present.

Partitioning behavior of calcium is shown in Figure 3.10. The analysis suggests that calcium is only present in its solid form in the entire temperature range of 100-700 °C. $Ca_5HO_{13}P_3$ is majorly present in the subcritical region along with smaller quantities of $Na_2CaP_2O_7$. In the supercritical region between

400-450 °C, $Ca_5HO_{13}P_3$ along with $K_2Ca(CO_3)_2$ and $CaCO_3$ are present. Furthermore, at temperatures higher than 475 °C, the region is dominated by $Ca_5HO_{13}P_3$ along with small quantities of $CaCO_3$.

Partitioning behavior of magnesium is shown in Figure 3.11. In the subcritical region, the only stable form of magnesium is $Mg(butanoate)_2$, wherein it is present in its aqueous form. Only solid forms of magnesium compounds are present in the supercritical region including $NaMgPO_4$, MgO, $Mg_3P_2O_8$, $Mg_3B_2O_6$, and $Mg(OH)_2$. $Mg(OH)_2$ can be found only between 475 °C and 500 °C.

Partitioning behavior of sodium is shown in Figure 3.12. The results suggest that at temperatures lower than 375 °C, $Na_2CaP_2O_7$ is the most stable form present with Na^+ ions found only around 375 °C. At temperatures higher than 400 °C, the region is dominated by $NaMgPO_4$ with small quantities (average of 35% molar fraction) of Na_2CO_3 present between 600 °C and 700 °C.
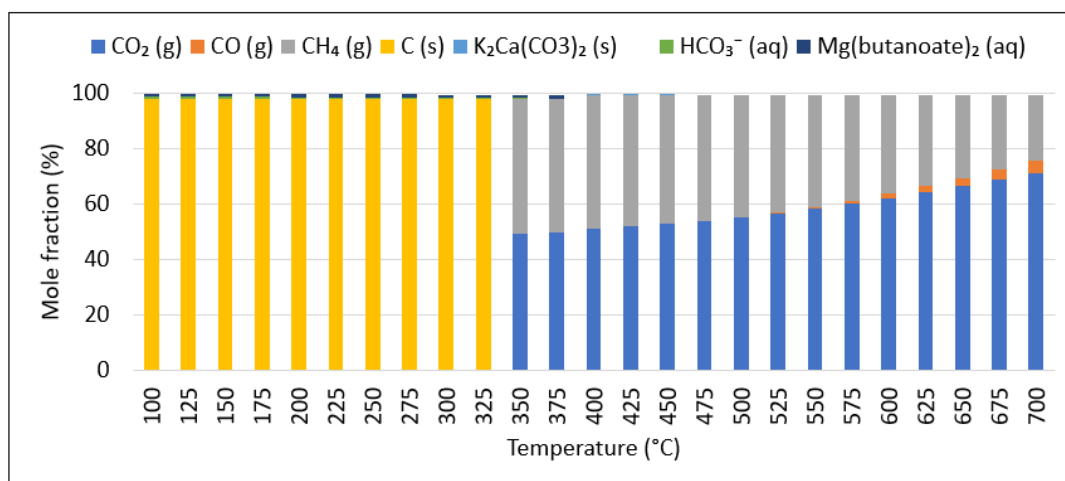
Figure 3.5: Partitioning behavior of carbon compounds during supercritical water gasification of fruit/vegetable waste for a temperature range of 100-700°C at 240bar having a concentration of 11wt%.
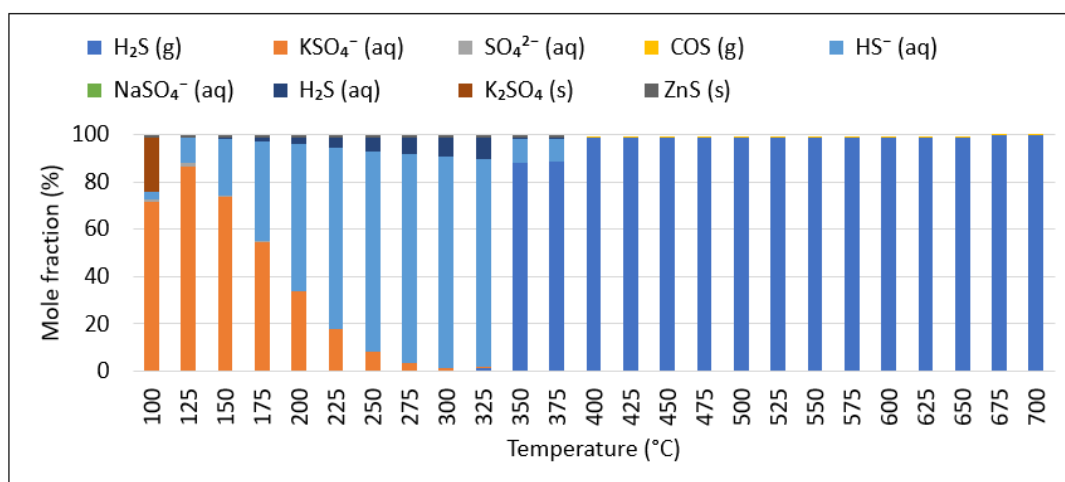
Figure 3.6: Partitioning behavior of sulphur compounds during supercritical water gasification of fruit/vegetable waste for a temperature range of 100-700°C at 240bar having a concentration of 11wt%.
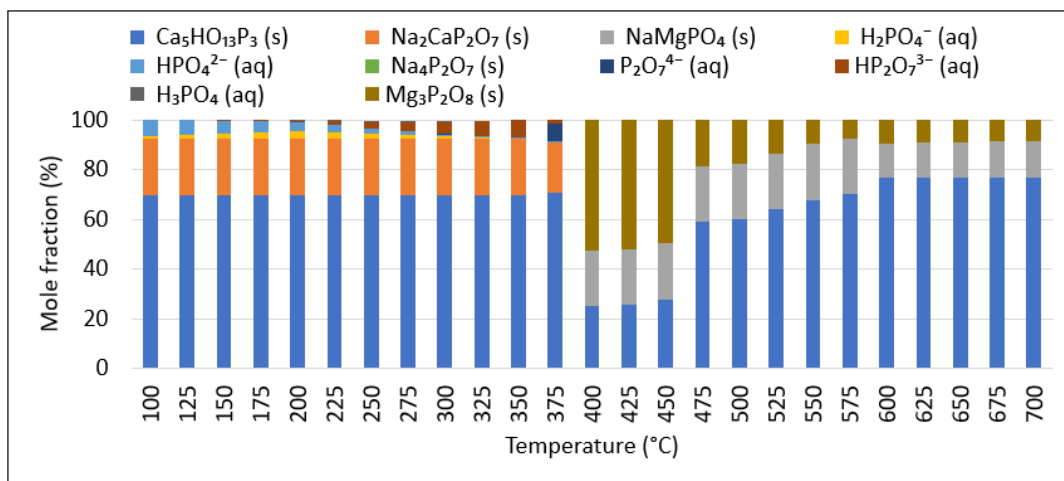
Figure 3.7: Partitioning behavior of phosphorous compounds during supercritical water gasification of fruit/vegetable waste for a temperature range of 100-700°C at 240bar having a concentration of 11wt%.
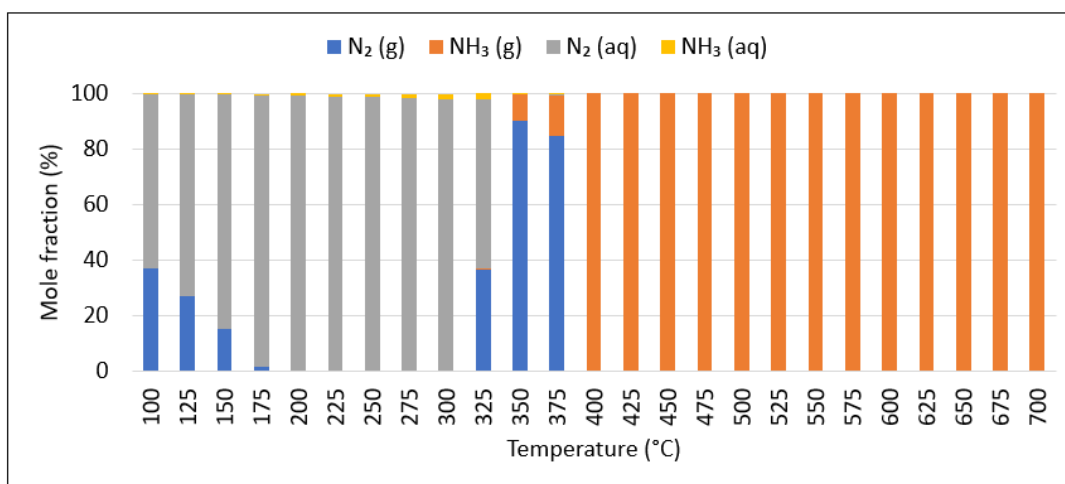
Figure 3.8: Partitioning behavior of nitrogen compounds during supercritical water gasification of fruit/vegetable waste for a temperature range of 100-700°C at 240bar having a concentration of 11wt%.
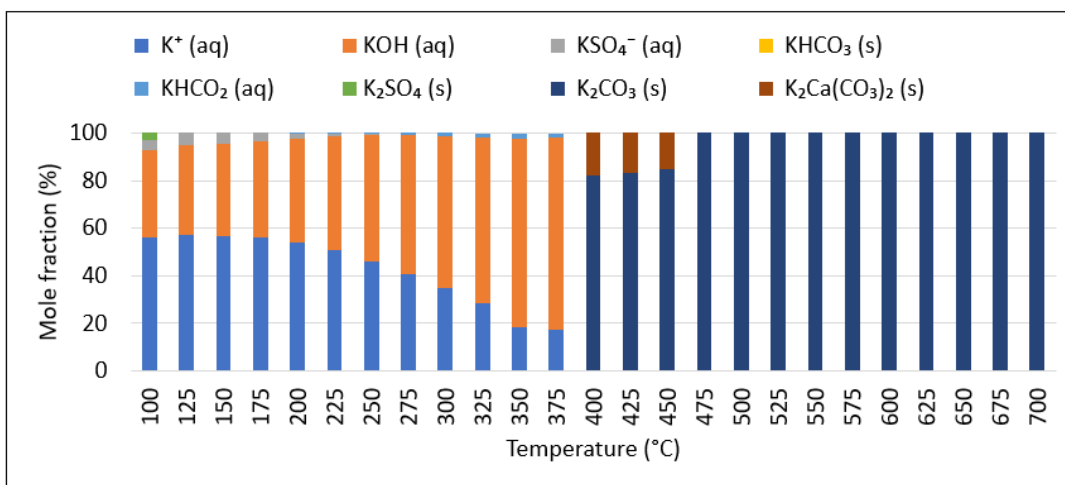
Figure 3.9: Partitioning behavior of potassium compounds during supercritical water gasification of fruit/vegetable waste for a temperature range of 100-700°C at 240bar having a concentration of 11wt%.
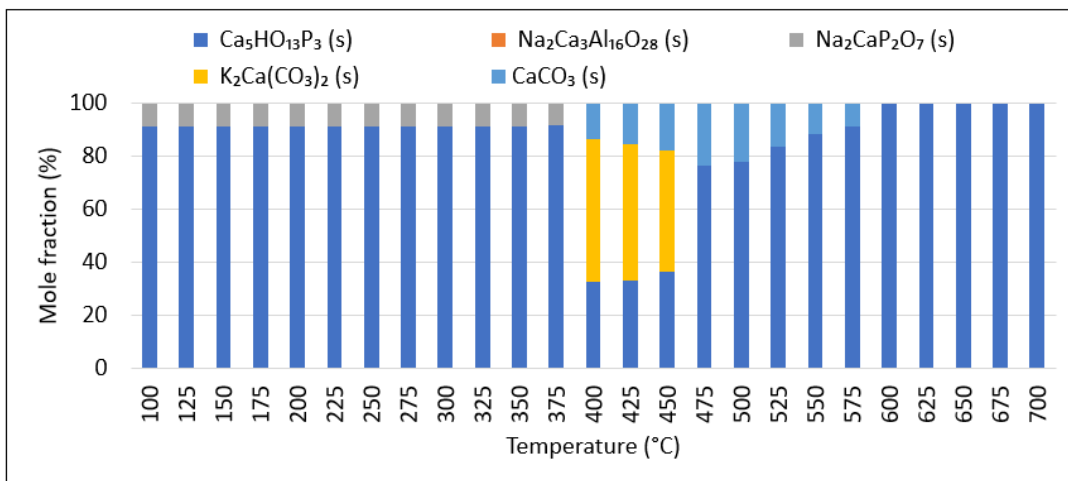
Figure 3.10: Partitioning behavior of calcium compounds during supercritical water gasification of fruit/vegetable waste for a temperature range of 100-700°C at 240bar having a concentration of 11wt%.
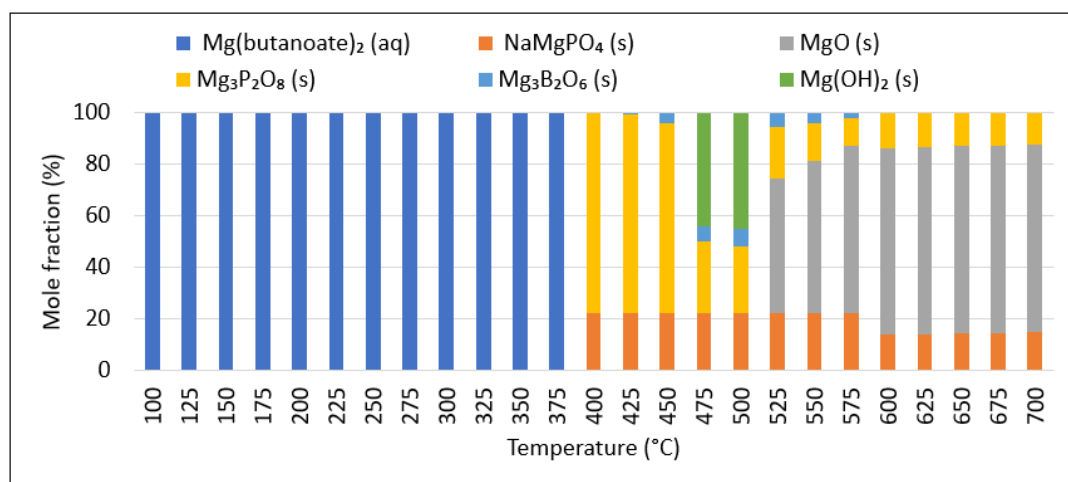
Figure 3.11: Partitioning behavior of magnesium compounds during supercritical water gasification of fruit/vegetable waste for a temperature range of 100-700°C at 240bar having a concentration of 11wt%.
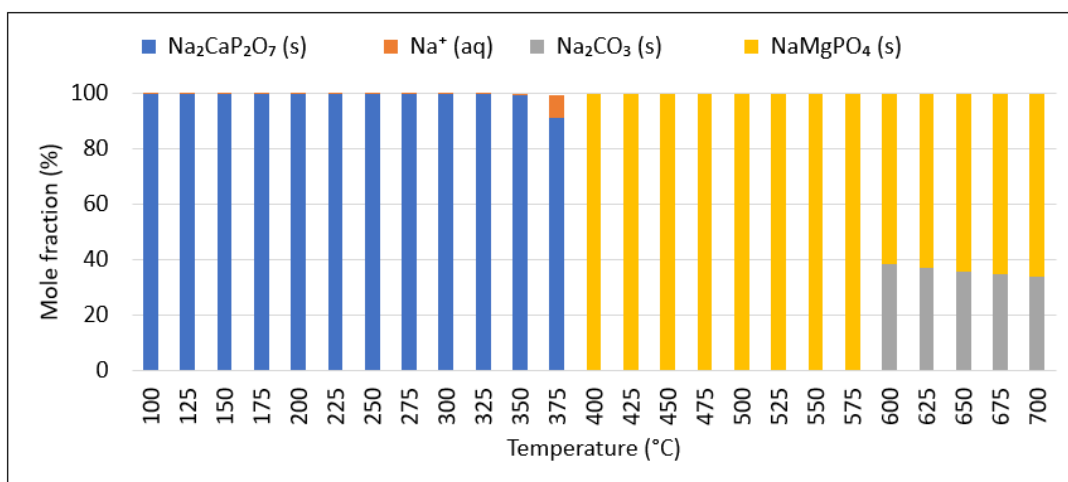
Figure 3.12: Partitioning behavior of sodium compounds during supercritical water gasification of fruit/vegetable waste for a temperature range of 100-700°C at 240bar having a concentration of 11wt%.

3.4 CONCLUSIONS

A detailed multiphase-thermodynamic equilibrium model of SCWG for different-sourced biomass wastes including cattle manure, fruit/vegetable waste, and cheese whey predicting chemical equilibrium was developed. The conceptual model is based on Gibbs free energy minimization and uses Factsage^{TM} for the simulations. The GTE model gives a general insight into the SCW gasification of wet biomass wastes while predicting the reasonable equilibrium composition of main product gases as compared with the experimental results. The main inadequacy of this approach is the inability to account for the carbon gasification efficiency. However, the limitations of the GTE model can be overcome using advanced thermal equilibrium models, discussed in chapter 4.

This effort also shed some light on the elemental partitioning regarding all feedstock cases. The results can provide a better understanding of how and to what extent the different elements in biomass are distributed in different compounds during the gasification process. It can further assist in evaluating ash and slag formation along with its composition and expected solid residue amounts which would require further processing.

4 | ADVANCED THERMODYNAMIC EQUILIBRIUM MODELLING

In this chapter, advanced thermal equilibrium modelling techniques including constrained thermodynamic equilibrium model and quasi-thermal equilibrium model have been developed and assessed against the experimental results. Advanced thermal equilibrium modelling techniques are an upgrade to the GTE modelling to better predict the product compounds. Use of additional constraints and approach temperature concept have also been reported in this chapter.

4.1 INTRODUCTION

The GTE model is simply based on the use of Gibbs free energy minimization to predict the compositions. The model assumes that reactions have reached chemical equilibrium which is not the case with a real reactor. Yan et al. (2006), Puig Arnavat et al. (2011), and Yakaboylu et al. (2015b) suggested that a real gasification system deviates from its ideal system as the GTE model either over- or underestimates the gas yields . This may impact the predictive capability regarding the gasifier including over-prediction of carbon conversion and serious disagreements with compositions. For such reasons, the GTE model needs to be modified using more advanced approaches to potentially predict the local equilibrium state with better precision. More advanced modelling techniques such as constrained thermodynamic equilibrium and quasi-thermal equilibrium models are discussed in the following sections.

4.2 CONSTRAINED THERMODYNAMIC EQUILIBRIUM MODEL

The constrained thermodynamic equilibrium method is an adaptation of the Gibbs free energy minimization by the addition of new constraints to the already existing natural constraint such as the charge conservation and mole balances for the elements, and non-negativity of all the species amounts. In general, the new additional constraints can be defined in terms of different methods including carbon and hydrogen gasification efficiencies, dissolved carbon conversion, selected constant species yield values based on direct experimental measurements, and multi-faceted mechanistic models. Additional constraints used for modelling are discussed below.

1. Carbon gasification efficiency – This gives an appropriate indication of how far is the system from its global equilibrium. Due to kinetic limitations, the effective carbon content participating in the reaction is less than actually present in the biomass feed. Carbon gasification efficiency can be defined as the ratio of the total number of moles of carbon in the product including CO_2, CH_4, CO, C_xH_y to the total number of carbon moles in biomass feedstock. Equation 4.1 shows how the carbon gasification efficiency, as an equal constraint, is superimposed to the model.

$$CGE \times n_{\text{feed}} = \sum_{i=1}^{g} a_{i,\text{ gas}} \, m_{i,gas} \qquad (4.1)$$

where, g refers to the gas phase. n_{feed} refers to the no. of moles of feed. a and m_i refers to the number of carbon atoms per molecule and moles of ith gas including CO_2, CH_4, CO, C_xH_y.

2. Experimental limits on specific compounds – Due to kinetic limitations, some reactions are possibly slower than others and are termed as rate-limiting reactions. Due to different reaction rates, the formation of products is over- or underestimated. In the case of SCWG, at lower temperatures formation of CH_4 is favored whilst H_2 is a favorable product at a higher temperature. This can be taken into account by considering a fixed yield of that specific compound in the model. A fixed value of the compound can be computed by conducting simple laboratory-scale experiments. Equation 4.2 shows how this constraint is introduced into the model.

$$n_i = A \qquad (4.2)$$

where, n_i and A moles of the ith compound and the fixed experimental value of the same compound.

Constrained equilibrium mathematical model using Gibbs free minimization technique has been adapted and developed by Yakaboylu et al. (2015b). The authors developed a MATLAB code using the *fmincon*[1] optimization routine. The code uses Gibbs free energy minimization equations for gases, aqueous

---

1 fmincon is an optimization routine that finds minimum of a constrained nonlinear multivariable function starting at an initial estimate.

species, and solids phase species while taking into account the effect of mentioned additional constraints.

4.3 QUASI–THERMAL EQUILIBRIUM MODEL

The basic philosophy behind the quasi-thermal equilibrium model is the estimation of carbon gasification efficiency by representing kinetic limitations through the concept of the "approach temperature" and improve the predictions of the GTE model. Other than carbon, there is no systematic way to handle the incomplete conversion of elements, as suggested by Yan et al. (2006). Therefore, using a quasi-thermal equilibrium model, it is inevitably assumed complete conversion of all the elements. The concept behind the approach temperature is to counterbalance the carbon conversion obtained from experimental data by considering a temperature difference between the SCW gasifier temperature and the temperature associated with the same gas composition from the GTE model. This difference between the two temperatures is termed as approach temperature.

Gumz (1950) investigated similar approaches for fluidized bed and downdraft gasifiers. In his study, the author found that the average bed temperatures could be potentially considered as the process temperatures for fluidized beds while the exit temperature at the throat of a downdraft gasifier could be a good estimate for the process temperature. Li et al. (2001), who focused on coal gasification, established that the carbon conversion obtained experimentally at 1020-1150 K was similar to the equilibrium predictions at 800-900 K. The working principle behind the model is described in the flow chart, shown in 4.1. The biomass waste is divided into two process streams. The first process stream includes lab-scale experiments to compute real product compositions. The second process stream includes biomass analysis using proximate and ultimate analyses. The results from such analyses are further processed and molar quantities of the elements are fed into the GTE model using Factsage^{TM} software. The equilibrium product compositions and the compositions obtained using experiments are compared for each individual component for a maximum relative error of 0.001% to calculate the approach temperature. Finally, a relation is determined between the actual temperature, approach temperature, and the carbon gasification efficiency calculated using experimental results. Using this correlation, one can estimate the carbon gasification and reliably predict product composition by simply using the results from the GTE model generated based on Factsage^{TM} simulations.
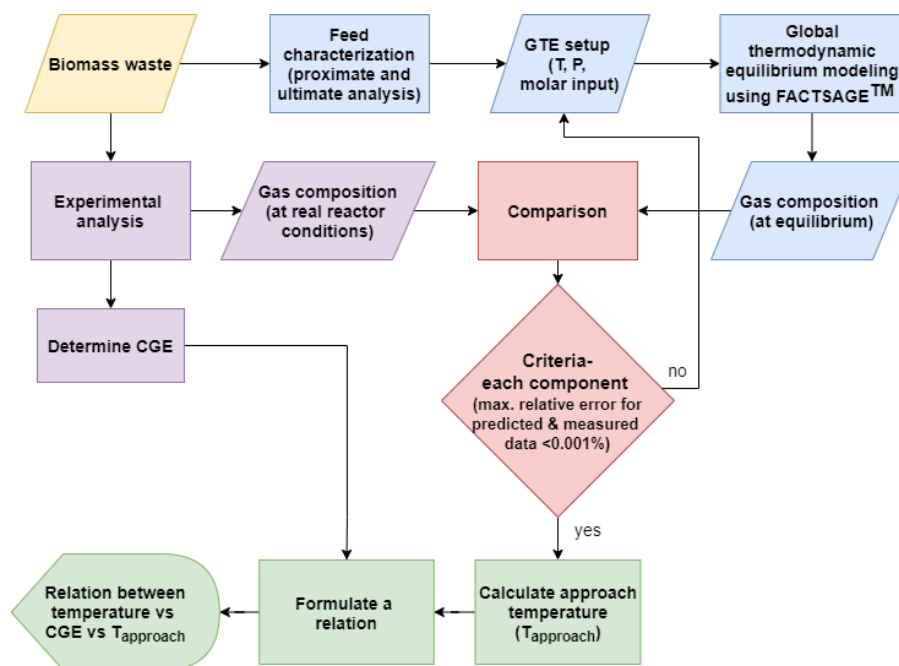
Figure 4.1: Flow chart depicting the working principle behind quasi-thermal equilibrium model.

4.4 RESULTS AND DISCUSSIONS

4.4.1 Constrained thermodynamic equilibrium

Figures 4.2, 4.3, and 4.4 show comparison results for the main gaseous product behavior predicted by constrained and unconstrained (FactSage^{TM} Simulations) models and the experimental data for all the biomasses. The comparison study for each biomass type has been conducted at specific temperatures and pressures, and additional results for other range of temperature and pressure are addressed in Appendix B for the sake of brevity. Our analyses include case studies, for each biomass Case A involves no additional constraints, and gas compositions are based on the GTE approach. Case B uses carbon gasification efficiency as the only additional constraint. Case C uses carbon gasification efficiency along with a specific amount of CH_4, obtained from experiments as additional constraints. Case D uses carbon gasification efficiency together with specific amounts of CH_4 and H_2, obtained from experiments as additional constraints. It is worth noting that carbon gasification efficiencies are determined using experimental data. The overall view of the data to be used for the constraint equilibrium model is presented in Table 4.1.

Table 4.1: Additional constraint values used for modelling.

Biomass feed	Experimental conditions (T (°C) / P (bar))	Carbon gasification efficiency (%)	CH_4 amount (mol/kg of d.b.)	H_2 amount (mol/kg of d.b.)
Manure	552 / 260	86.0	6.4	10.9
Fruit/vegetable waste	560 / 240	83.3	8.1	8.3
Cheese whey	539 / 235	83.9	9.1	9.2
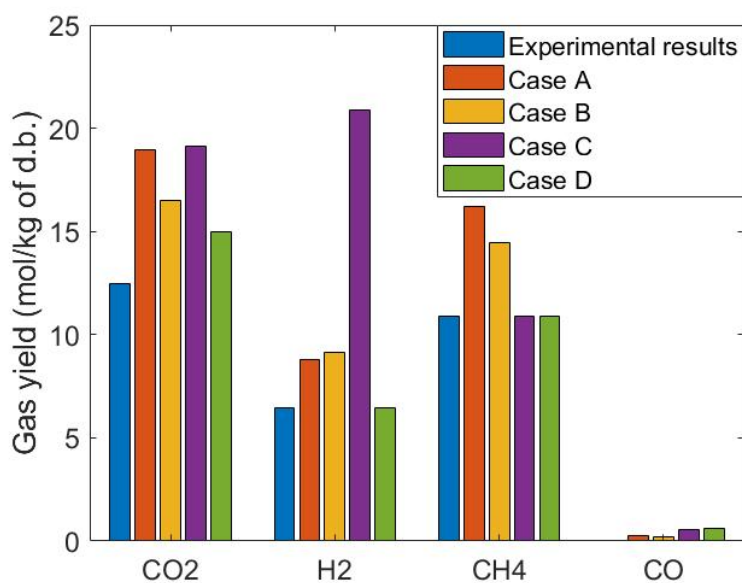
Figure 4.2: Comparisons between different modelling approaches and the experimental values for manure at 552°C and 260 bar with a feed concentration of 17%. Case A includes only GTE values, case B includes CGE as constraint, case C includes CGE + constant amount of CH_4 as constraints, case D includes CGE + constant amount of CH_4 and H_2 as constraints.
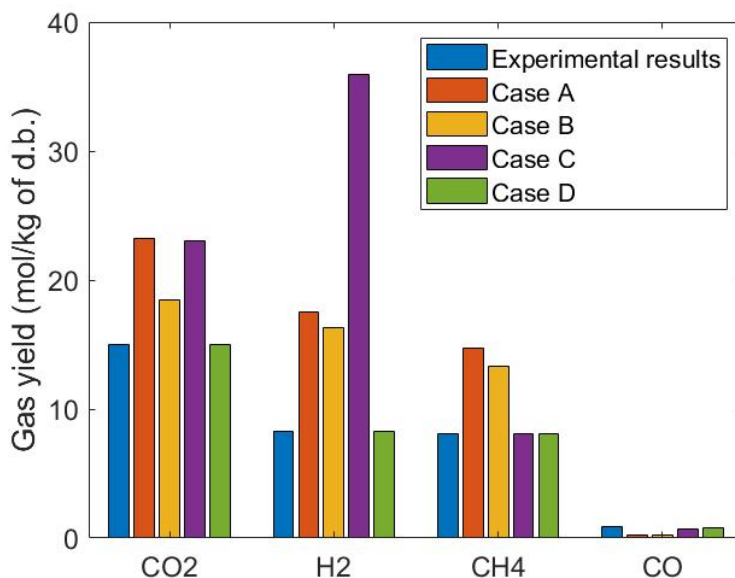
Figure 4.3: Comparisons between different modelling approaches and the experimental values for fruit/vegetable waste at 560°C and 240 bar with a feed concentration of 11%. Case A includes only GTE values, case B includes CGE as constraint, case C includes CGE + constant amount of CH_4 as constraints, case D includes CGE + constant amount of CH_4 and H_2 as constraints.
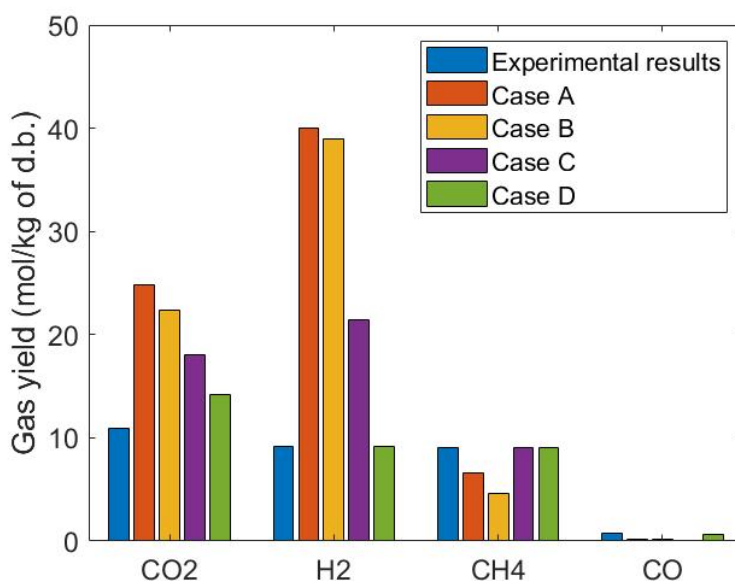
Figure 4.4: Comparisons between different modelling approaches and the experimental values for cheese whey at 539°C and 235 bar with a feed concentration of 3%. Case A includes only GTE values, case B includes CGE as constraint, case C includes CGE + constant amount of CH_4 as constraints, case D includes CGE + constant amount of CH_4 and H_2 as constraints.

As evident in Figures 4.2, 4.3, and 4.4, GTE approach (Case A) does not show a satisfactory agreement with the experimental gas compositions for all the biomass feeds. It can also be realized that cases B and C are even not in good agreement with the experimental data. However, Case D, which includes three constraints, shows a very good agreement with the experimental values. Results of Case D substantiate that imposing values of CGE and experimental values of CH_4 and H_2 into the model would result in an accurate prediction of the product gas (see Table 4.2). Similar findings have been reported

Table 4.2: Deviations based on the product gas concentrations for the three biomass wastes with all the four different cases. Case A includes only GTE values, case B includes CGE as constraint, case C includes CGE + constant amount of CH_4 as constraints, case D includes CGE + constant amount of CH_4 and H_2 as constraints.

	Deviations from experimental results (%)			
Product gas	Case A	Case B	Case C	Case D
Manure				
CO_2	52.0	32.3	53.1	19.9
H_2	36.5	42.1	224.9	0.0
CH_4	48.4	32.5	0.0	0.0
CO	-70.0	-73.8	-28.8	-23.8
Fruit pulp				
CO_2	55.0	23.1	53.9	0.3
H_2	111.5	97.1	333.6	0.0
CH_4	82.7	65.0	0.0	0.0
CO	-69.0	-70.3	-17.2	-6.9
Cheese whey				
CO_2	126.0	103.9	64.3	29.2
H_2	336.6	325.3	133.6	0.0
CH_4	-27.8	-48.7	0.0	0.0
CO	-75.6	-79.5	-91.0	-23.1

by Yakaboylu et al. (2015b). From Table 4.2 which shows deviations of product gas compositions from experimental values, it is observed that accuracy of predictions improved significantly in Case of D as compared with Cases A, B, and C. It can be concluded that carbon gasification efficiency forms one of the most important additional constraints and the accuracy of the model can be improved by an increase in the number of additional constraints using experimental values.

4.4.2 Quasi–thermal equilibrium

To understand the concept of the "approach temperature", experimental gas compositions along with carbon gasification efficiencies are studied. Results from experimental gas compositions and calculated carbon gasification efficiencies shown in Figure 4.5 are fitted to temperature-dependent function using simple curve fitting techniques. For the analysis, four experimental data sets for fruit/vegetable waste are considered and are shown in Figure 4.5. Based on the nature of the data, exponential and logarithmic curve fitting functions have been utilized having an R-squared (R^2) value of at least 0.75. The carbon gasification efficiency and gas composition results, illustrated in Figure 4.5, show a very good agreement with the experimental data of Nanda et al. (2015; 2016). In their research, the authors gasified fruit/vegetable waste and fructose as a model compound representing fruit/vegetable waste under critical conditions. The authors also acknowledged that carbon gasification efficiency increases with increasing temperature.

While comparing the composition results, gas compositions obtained from experiments are found to be comparable with the GTE compositions obtained using FactSage^{TM} simulations with a temperature deviation of up to ±180 °C. This temperature deviation is termed as "approach temperature". Taking the particular case for SCWG of fruit/vegetable waste, it is observed that H_2 composition (mol/kg of d.b.) computed using the GTE model (based on FactSage^{TM} simulation) at 525 °C is similar to the experimental H_2 composition (mol/kg of d.b.) at 600 °C. From Figure 4.6, the absolute approach temperature is 75 °C. In the case of H_2, the temperature deviations are negative, therefore, the approach temperature becomes -75°C.

Based on this comparative analysis, a relation has been derived among the carbon gasification efficiencies, approach temperatures, and reactor temperatures, which are shown in Figure 4.6. The figure illustrates the absolute approach temperature values for CH_4, CO, and H_2 along with carbon gasifi-
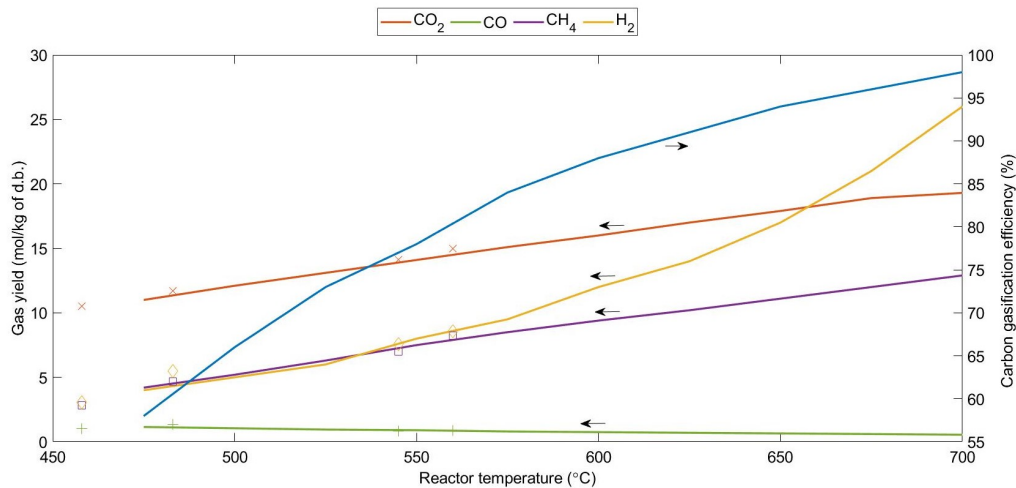
Figure 4.5: Carbon gasification efficiency and measured gas composition as a function of reactor temperature for fruit/vegetable waste at 24MPa having a feed concentration of 11%. The experimental data values for CO_2, CO, CH_4 and H_2 are also presented.

cation efficiencies as a function of reactor temperature. One can use the relation shown in Figure 4.6 in order to realize few of the most important parameters, such as carbon gasification efficiency and product gas compositions in the real reactor. Considering an example, if one decides to estimate the real reactor conditions at 600 °C, then one can use the relation to find the CGE value which comes around 90 %. Also, one can estimate the concentration of product gases, like for the case of CH_4, the absolute approach temperature is approximately 95 °C. Therefore, the composition (mol/kg of d.b.) of CH_4 will be equal to the GTE composition (mol/kg of d.b.) at 695 °C, which can be obtained from FactSage^{TM} results. A similar method can be employed to estimate the composition of other gases for the real reactor conditions. It is worth noting that in the case of CH_4, temperature deviations are positive(+) while for CO, H_2, the temperature deviations are negative(-). The deviation trend is due to the fact that methanation reaction, mainly responsible for the formation of CH_4, is an endothermic reaction while water gas shift reaction, which is mainly responsible for CO and H_2 product gases, is an exothermic reaction.

In general, quasi-thermal equilibrium approach provides advantages over the constrained thermodynamic model. In terms of accuracy, the quasi-thermal model can better predict product composition with a maximum relative error of 0.001% as compared to a constrained thermodynamic model whereby reaching error up-to 29%, even with the use of three additional constraints (see Table 4.2, deviation in CO_2 composition of cheese whey). Furthermore, the accuracy of the constrained thermal equilibrium model is highly pertinent to the number of constraints imposed on the model. Here it is noteworthy that the accuracy of both the models (quasi-thermal equilibrium and constrained thermodynamic equilibrium) largely depends on the number of experimental data points. The other advantage of quasi-thermal equilibrium approach is the ease of implementation. In fact, the model offers an effective approach temperature to lump all the constraints to be used in the constrained equilibrium model.
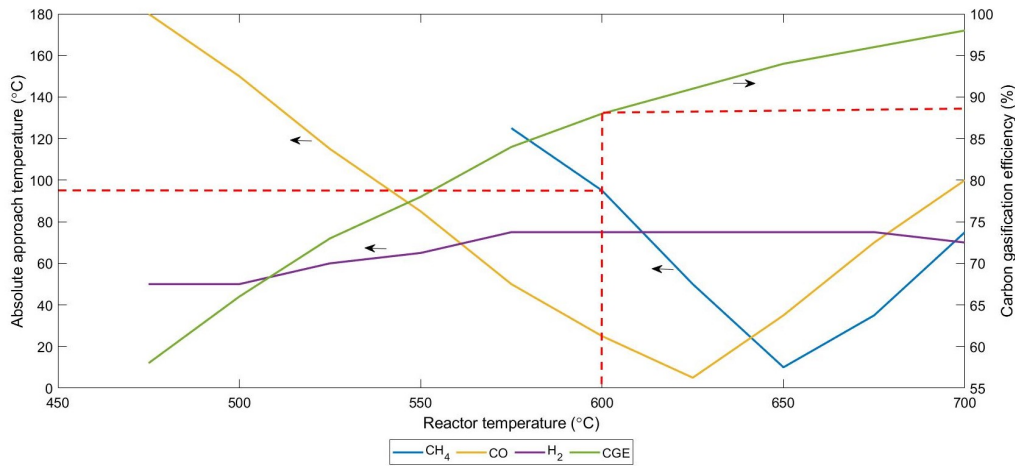
Figure 4.6: Absolute value of approach temperatures and carbon gasification efficiencies as a function of reactor temperature for fruit/vegetable waste at 24MPa having a feed concentration of 11%.

4.5 CONCLUSIONS

The GTE model based on Gibbs free energy minimization was further improved to account for the carbon conversion efficiency, resulting in two different methodologies including constrained thermodynamic equilibrium and quasi-thermodynamic equilibrium. Detailed comparisons were made with the results of autoclave batch experiments of the same biomass wastes. Overall, both theoretical and experimental analyses confirm the important roles of temperature on the final yield on the products and carbon gasification efficiency.

As discussed, the main adequacy of the GTE model can be overcome using advanced thermal equilibrium models. The constrained thermodynamic equilibrium model uses additional constraints based on simple experiments, offering a much precise prediction of compound compositions in the SCW gasifier. The post-processing of the results showed that carbon gasification efficiency is the most important constraint and also the prediction capabilities of the model can be further improved by imposing additional constraints into the model. However, the drawback of this approach is the dependency on the experimental data and the reliance on multiple constraints. Quasi-thermal equilibrium model uses the basis of approach temperature. It simply establishes a temperature correlation between equilibrium compositions of the conceptual model (GTE in this case) and the real reactor compositions, although the model still requires simple process-specific experimental results to determine the correlation. The model has its advantages of not using multiple additional constraints and will better predict the compositions with an error margin of a maximum 0.001%.

5 | THERMODYNAMIC PROCESS MODELLING AND ANALYSIS

This chapter deals with the process modelling of a conceptual bio-refinery founded on SCWG of wet biomass wastes using ASPEN software. The emphasis of this chapter is on detailed analysis of the influence of main process parameters along with the chemical and thermal behavior of the entire process. Furthermore, technologies available for separation of H_2S and CO_2 mixture stream have been discussed.

5.1 INTRODUCTION

In order to optimize the gas yield and maximize the biomass feed conversion, a study on the key parameters affecting the performance of the entire process was imperative. An in-depth study on the composition of each stream and efficiencies of different process equipment entails modelling the entire SCWG biorefinery system. To our knowledge, Feng et al. (2004) were among the first researchers to study and analyze phase- behavior, and equilibria in the reactors and separators. Furthermore, the researchers designed a heat exchanger network and conducted an exergy analysis of the entire process. The first detailed study about the design and optimization of a complete SCWG process was conducted by Ortiz et al. (2012). The authors used a water-glycerol mixture as feedstock for the SCWG reactor to produce synthesis gas and eventually combust the synthesis gas to provide the enthalpy for the reactor. The process model had turbines and heat exchangers along the streams for pressure and heat recovery. Along with Ortiz et al. (2012), several other research groups, such as Fiori et al. (2012), Withag et al. (2012), and Louw et al. (2014) have conducted research with the SCWG systems using biomass feeds such as glycerol, sewage sludge, chicken manure, glucose, leather waste, bituminous coal, etc. The mentioned researchers modelled the entire process including reactors and separators to study the energy and product composition performances across the process.

In this chapter, we introduce and investigate a bio-refinery conceptual design based on the SCWG of wet biomass waste with an aim to produce treated biogas having maximum lower heating value. To this end, we developed a process model using ASPEN software and integrated different process equipment such as slurry thickening unit, heat exchangers, turbines, gas/liquid separators, and reactors. For the setup of ASPEN model, we used the gas composition results from thermodynamic equilibrium modelling of fruit/vegetable waste as our input. The model was then employed for further sensitivity analyses wherein the influence of different process conditions including reactor temperature, pressure, and feed concentration were investigated. The gas and thermal behavior, and process efficiency results have been discussed in the coming sections. The chapter was completed by detailed description and comparison of the prevailing approaches for separating of CO_2 and H_2S from sour-gas mixture stream.

5.2 MODEL AND SIMULATION

5.2.1 Process description and modelling

The overall system involves the use of wet waste streams and feeding into the gasification reactor with temperatures and pressure above supercritical conditions, followed by the conditioning of the produced gas for feeding to the gas network. The conceptual process scheme shown in Figure 5.1 has been adapted from Yakaboylu et al. (2015a). The process is designed to be simple while at the same time self-sustainable and energetically convenient.

As presented in Figure 5.1, the 'as received' form of biomass slurry (stream 1) is fed to the sludge thickening unit in which part of the water is shed depending on the prescribed water content of biomass waste. The exit stream (stream 2) is then pumped to the desired reactor pressure, then is passed through the tube side of a multiside heat exchanger (heat-box) whereby pre-heating to 5-10° above supercritical water temperature. The hot gas stream (stream 4) then enter the SCWG reactor where it is gasified at the desired temperature and pressure. The gasified stream (stream 5) is passed through the multiside heat exchanger to cool it down. The heat extracted from this can be potentially used to pre-heat the inlet slurry stream before feeding to the reactor. The cold gas stream (stream 6) is further cooled down using heat exchanger (HEX-1), adjusting temperature to the optimum temperature of the gas modification unit located in the downstream of high-pressure gas/liquid separator. At the separator, the gas fraction of the stream gets separated from the liquid effluent (stream 8) which is then passed through a valve for throttling. Following this low pressure gas is fed to a low-pressure gas/liquid separator to knockout the liquid effluent. The gas stream coming from HP gas/liquid separator (stream 9) is then fed to a series of turbines to adjust and recover the pressure for HP membrane sepa-

rator. To prevent condensation in multistage pressure recovery unit, the outlet gas from every turbine stage is heated up to 10-20° above dew point in multiside heat exchanger. The adjusted gas stream at optimum temperature and pressure (stream 11) is then fed to the high-pressure polymeric membrane separator. Here the polyamide membranes were utilized to remove CO_2 and H_2S (stream 14) from produced gas leading to a modified gas stream which majorly include CO, CH_4, H_2, and H_2O (stream 12). This gas product stream (stream 12) is further split into two streams. One of the split streams (stream 13) consists of the final product gases is fed to the gas network for further downstream processing such as biofuel production. Having a HP gas membrane separator, the treated gas (stream 15) is passed through 2-stage turbine with intercooling to recover the pressure/work. The stream is then finally mixed with the combustible gas stream (stream 20) coming from the low-pressure gas-liquid separator. This mixed stream (stream 21) is fed back to the furnace to supply necessary heat for the SCWG reactions.

Process flow diagram shown in Figure 5.1 was adapted and modelled in the ASPEN plus software for simulation and analysis. Figure 5.2 exhibits a typical flowsheet model developed in ASPEN plus software which represents general setup for fruit/vegetable waste having feed concentration of 20wt% and reactor conditions of 600 °C and 240 bar. Detailed streamwise ASPEN simulation data for all the cases including fruit/vegetable waste, cattle manure, and cheese whey is presented in Appendix C. It is worth mentioning that the SCWG reactor was separately modelled using as a Gibbs free energy minimization routine in Factsage^{TM}. The product gas compositions result from global thermodynamic and constrained equilibrium modelling (section 4.4.1) were used for setting up ASPEN simulations. Setting up of process flowsheet involved the calculation of the pseudo critical point of the biomass slurry and heat requirements of pre-heater and furnace and was completed using Factsage^{TM} software.

Simulations were performed for various reactor conditions i.e. different temperatures ranging between 450 and 700 °C, 3 different pressures (230, 235 and 240 bars), and two different feed concentrations (11wt% and 20wt% with the rest being water). All the simulations performed and presented are on the basis of 100kg/h input (dry basis). The assumptions and modelling criteria that were used for carrying out simulations are listed below.

1. Pressure losses in the pipes were neglected.
2. Pre-heated slurry (stream 4) temperature was 390 °C for all the cases. The following has been chosen as it is above the critical temperature of the water and all the water is in the gaseous phase.
3. The temperature of the furnace for all the cases was kept approximately 1000 °C.
4. Filter (stream 5) was considered 100% efficient and assumed to separate all the precipitated salts.
5. Low-pressure gas/liquid separator was operated at a temperature and pressure of 20 °C and 2 bar, respectively.
6. High-pressure membrane for separation of CO_2 and H_2S from the produced gas was considered to work with 100% efficiency and operate at around 30 °C. The efficiency assumption is based on the research of Marzouk et al. (2010) and Luis et al. (2012) while the operating temperature was based on research works of Ma and Koros (2013), He et al. (2014), and Ahmad et al. (2014).
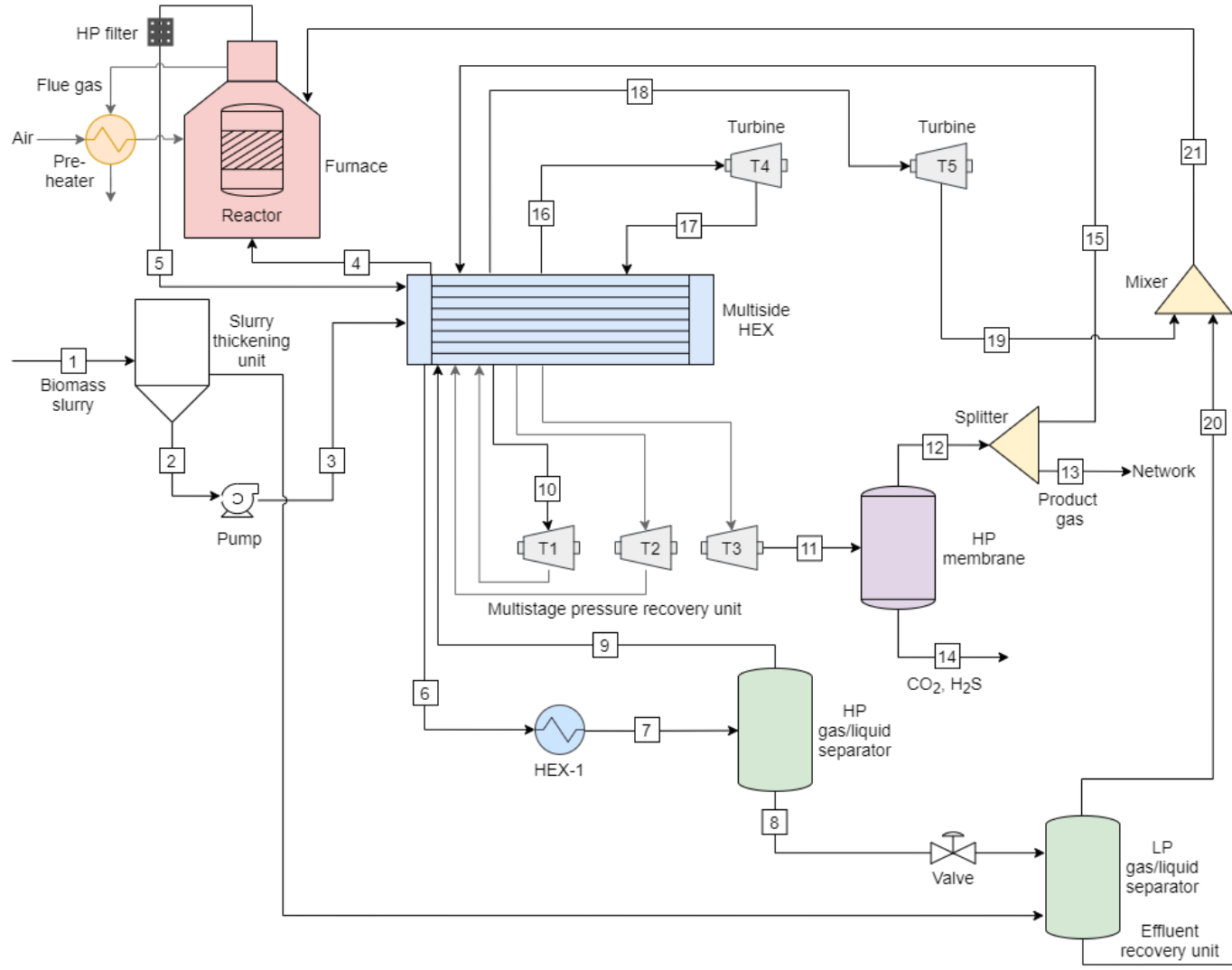
Figure 5.1: Conceptual process design of the bio-refinery for SCWG of wet biomass
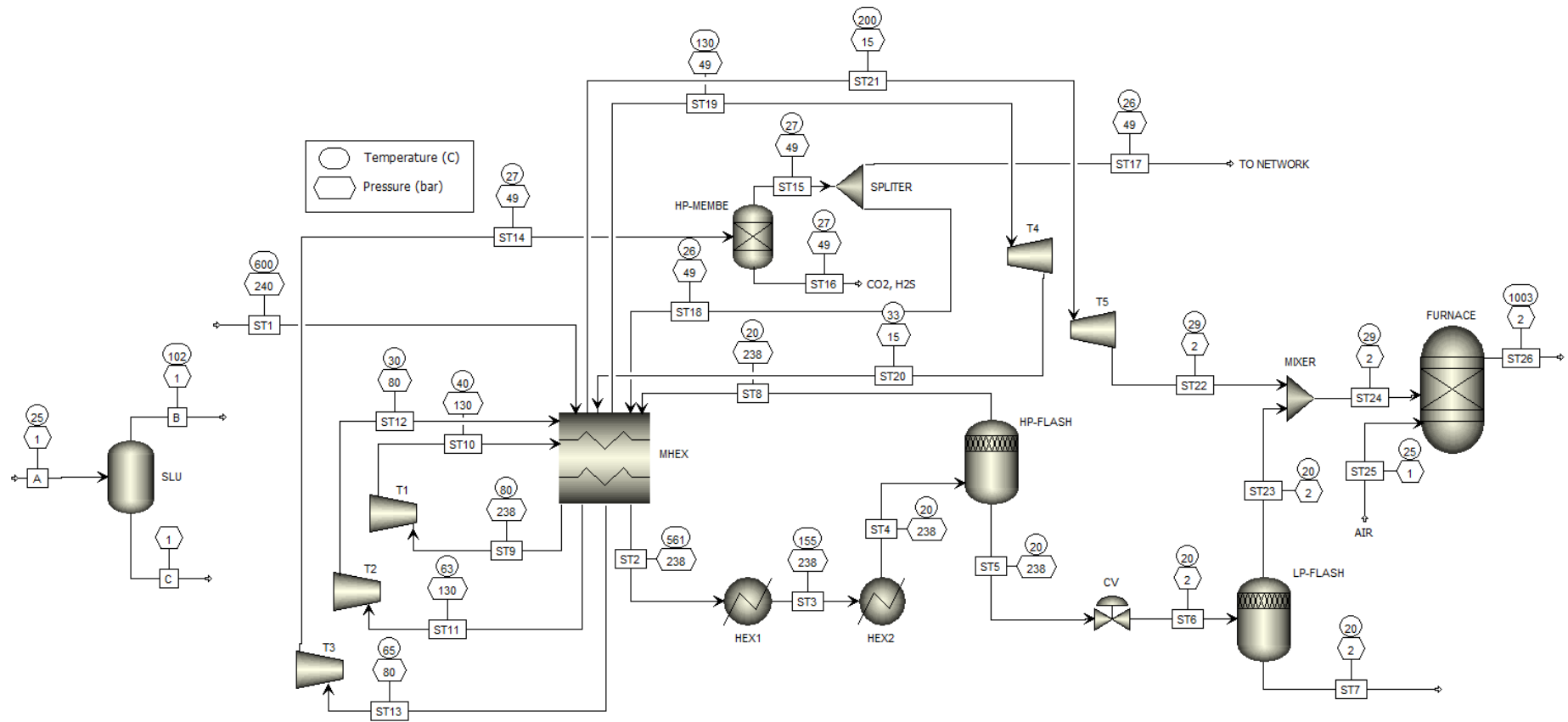
Figure 5.2: Schematic process flow sheet designed in ASPEN for SCWG of fruit/vegetable waste having a feed concentration of 20wt% and reactor conditions of 600 °C and 240 bars.
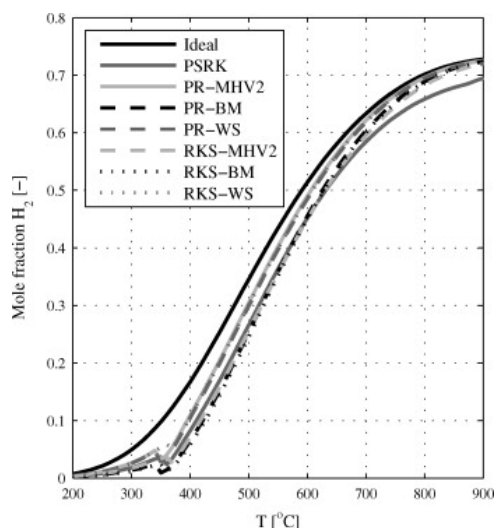
Figure 5.3: Comparison of different EoS methods for H_2 molar fraction. The experiments were performed using methanol (10wt% feed concentration) with a temperature range between 200-900 °C and a pressure of 300 bar. Reprinted from Withag et al. (2012).

5.2.2 Property method used

Property methods can strongly influence the thermodynamic properties of the systems, therefore it becomes imperative to choose the right property method. There are two main ways in which the thermodynamic properties can be calculated; EoS (Equation of state) and the activity coefficient method. One of the major advantages of using EoS over the activity coefficient is its robustness as the EoS method can work with a wide range of temperatures and pressures, as suggested by Ruya et al. (2020) and Withag et al. (2012).

As our model deals with both high-pressure reactors and separators, therefore it would be more reasonable to use the EoS method. Additionally, we will be looking into the most suitable EoS method for using with our process model. Withag et al. (2012) compared hydrogen production against increasing temperatures for different EoS methods. Methanol with a 10wt% feed was gasified at different temperatures and 300 bar pressure and the authors compared the H_2 production results for ideal, PRKS, PR-MHV2, PR-BM, PR-WS, RKS-MHV2, RKS-BM, and RKS-WS EoS. The comparison study is presented in Figure 5.3. Considering the temperature range of our interest i.e. between 373 °C and 700 °C, it is shown that the largest difference for H_2 molar fraction is observed with the ideal gas equation, particularly near the critical temperatures (373 °C approx.). H_2 molar fraction using all the property methods derived from Peng Robinson (PR) and Redlich-Kwong Soave (RKS) EoS was found to be within the bandwidth of 3.5%. Similarly, Louw et al. (2014) compared different EoS and concluded that PR, SRK-BM, and PR-BM all provided the closest predictions with the experimental results for SCWG of ethanol having a feed concentration (5-10%) with a temperature and pressure of 600-800 °C and 221 bar, respectively. Considering this, we have selected PR EoS for our process modelling.

5.3 RESULTS AND DISCUSSIONS

5.3.1 Gas behavior

Influence of reactor temperature on gas composition

The change in the gas composition (stream 11, Figure 5.1) with the reactor temperature for both 11wt% and 20wt% feed concentration cases is depicted in Figure 5.4. The figures show that for both cases the trend is similar with H_2 and CO molar fractions, increasing with the temperature as the molar fractions of CH_4 and CO decrease. This is attributed to endothermic reactions (Equations 5.1,5.2, 5.3,
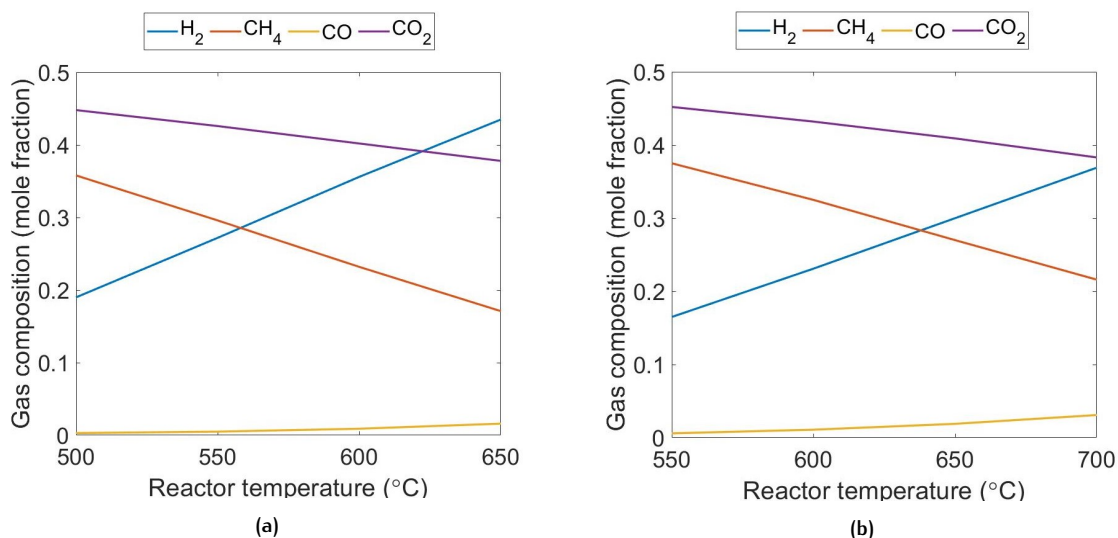
Figure 5.4: Gas composition behavior of the produced gases for SCWG of fruit/vegetable waste are presented for different process conditions such as temperatures (500 °C, 550 °C, 600 °C, 650 °C, and 700 °C) pressure (240 bar) and feed concentration ((a) 11 wt% and (b) 20 wt%)) concentration.

5.4) and reverse boudouard reaction (Equation 5.5) which are favoured at higher reactor temperatures. This results in increased formation CO and H_2 which was previously observed by Rahbari et al. (2018). While the exothermic reactions which includes decarboxylation reactions for the formation of CH_4 and CO are favoured at lower temperatures, as investigated by Rahbari et al. (2018). Experiments conducted by Byrd et al. (2007) and Chen et al. (2013) show that with increasing reactor temperature, H_2 yield increases while yield of CH_4 decreases. The decline in CH_4 yield could be attributed to the methane steam reforming and water gas shift reactions at elevated temperatures (refer Equation 5.4 and 5.6), as investigated by Behnia et al. (2016).

$$C_xH_yO_z + (2x - z)H_2O \rightarrow xCO_2 + \left(2x - z + \frac{y}{2}\right)H_2 \tag{5.1}$$

$$C_xH_yO_z + (x - z)H_2O \rightarrow xCO + \left(x - z + \frac{y}{2}\right)H_2 \tag{5.2}$$

$$CH_4 + H_2O \rightarrow CO + 3H_2 \tag{5.3}$$

$$CH_4 + 2H_2O \rightarrow CO_2 + 4H_2 \tag{5.4}$$

$$2CO_2 + C \rightarrow CO \tag{5.5}$$

$$CO + H_2O \leftrightarrow CO_2 + H_2 \tag{5.6}$$
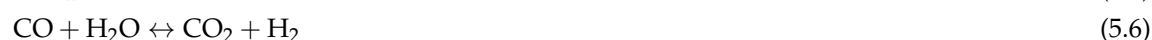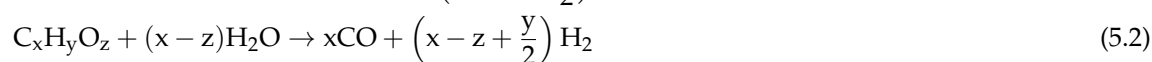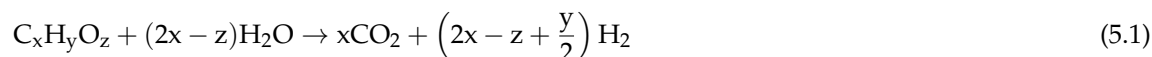
Influence of feed concentration on gas composition

The change in H_2 and CH_4 compositions (stream 11, Figure 5.1) with different feed concentration of fruit/vegetable waste for reactor temperatures of 550 °C, 600 °C, and 650 °C is presented in Figure 5.5. The results reveal that with increasing feed concentration (wt%), the CH_4 molar fraction in the gas composition increases while H_2 decreases. Considering reaction equations 5.3 and 5.4, it can be comprehended that methane dissociation reaction consumes water and forms H_2 as one of the product. Therefore, presence of higher feed concentration, which means lower water content favours CH_4 formation, as suggested by Withag et al. (2012) and Ruya et al. (2020).
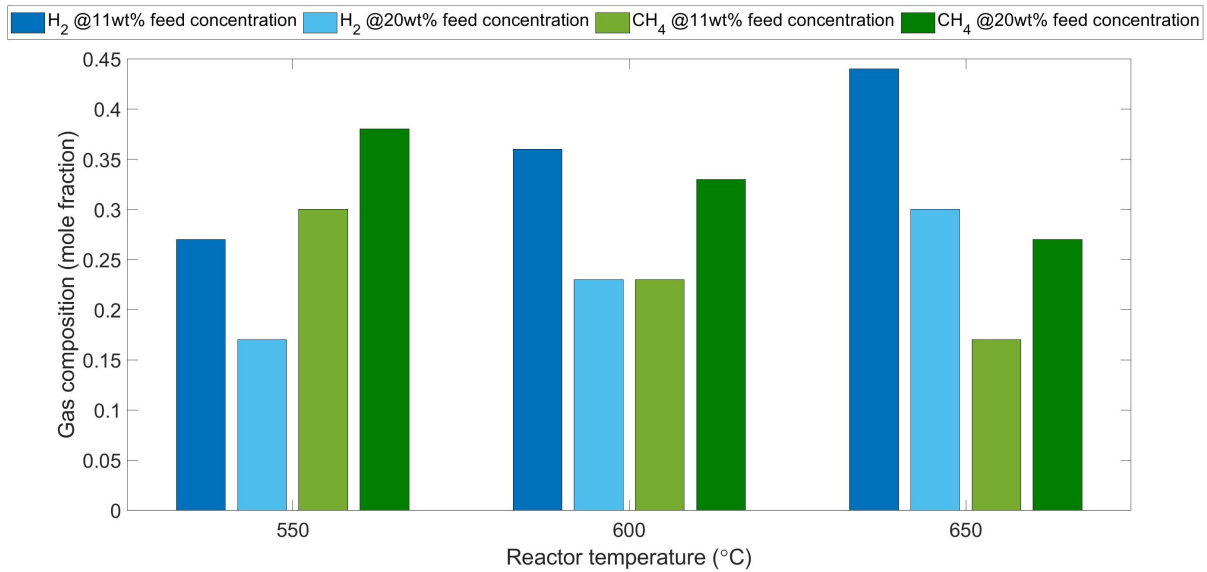
Figure 5.5: Change in H_2 and CH_4 compositions of produced gas mixture (stream 11, Figure 5.1) for different feed concentrations and reactor temperatures. The results are presented for fruit/vegetable waste as feedstock.

Gas composition at various units

The behavior of gases for different adopted reactor temperatures across different process units such as reactor, HP gas/liquid separator, and LP gas/liquid separator has been illustrated in Figure 5.6. Due to the similarity in results of different feed concentrations, the results for only 11wt% feed concentration have been shown. The results show that H_2, CH_4, and CO_2 are insoluble in water and leaves the HP gas/liquid separator in gas phase (stream 9, Figure 5.1), while 15% of H_2S and 100% NH_3 leave the HP liquid/gas separator in aqueous form. This is attributed to the solubility of H_2S and NH_3 in water and their presence in the ionic form such as HS^- and $NH4^+$, respectively.
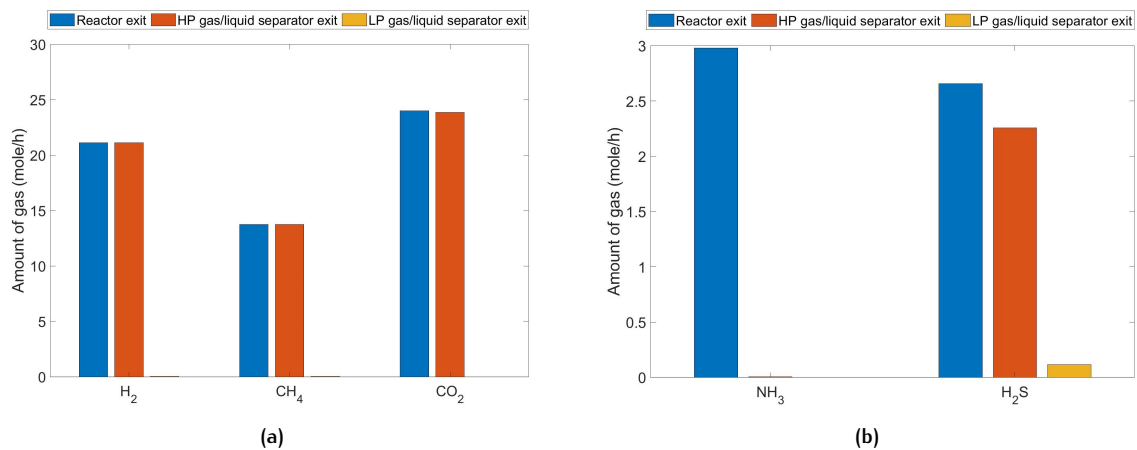
Figure 5.6: The amount of various gases that leave the different process equipment; Reactor, HP gas/liquid separator, and LP gas/liquid separator. The values are presented for SCWG of fruit/vegetable waste at 600 C, 240 bar and 11wt% feed concentration.
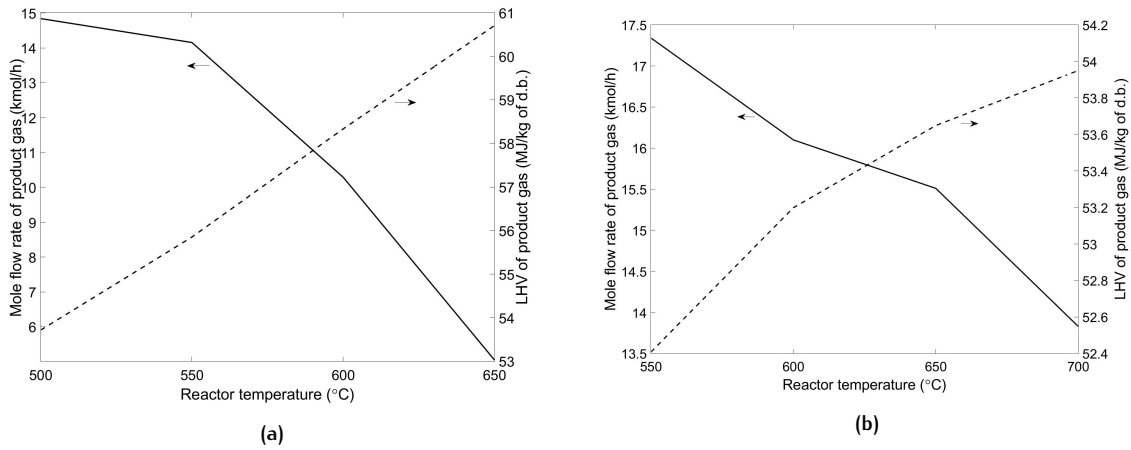
Figure 5.7: The molar flow rates and LHV of the product gas from SCWG of fruit/vegetable waste are presented for different process conditions such as temperatures (500 C, 550 C, 600 C, 650 C, and 700 C) pressure (240 bar) and feed concentration ((a) 11 wt% and (b) 20 wt%)) concentration.

5.3.2 Thermal behavior

Influence of temperature on LHV of product gas

The results of LHV and molar flow rates (stream 13, Figure 5.1) versus the reactor temperature for both feed concentrations (11wt% and 20wt%) are plotted in Figure 5.7. The results show that increasing the reactor temperature the LHV of product gas increases while the molar flow rate decreases. The trend of LHV and molar flow rate with the reactor temperatures are attributed to the increased energy supply for the reactor operation. Furthermore, recycle stream (stream 15, Figure 5.1) feed (mol/h) increased while decreasing the feed to network (stream 13, Figure 5.1) to compensate for the increased enthalpy requirement at the reactor. The lower heating values of all the three feedstock (fruit/vegetable waste, cattle manure, and cheese whey) have been presented and compared in Appendix C.

Process efficiency and feasibility

The efficiency of a process is a key factor in determining the feasibility of the entire system. Here, process efficiency is defined as the sum of energy contained in the product gas and the energy recovered from the pressure recovery units (see figure 5.1 - T1, T2, T3, T4, and T5) minus the energy required for the pumping and thickening the slurry, divided by the energy present in the feed. The relation is represented in the equation 5.7.

$$\eta = \frac{\dot{m}_{pg} \times LHV_{pg} + P_t - P_p - P_{stu}}{\dot{m}_{(feed)} \times LHV_{(feed)}} \tag{5.7}$$

where, η refers to process efficiency, $\dot{m}_{pg}$ and LHV_{pg} refers to molar flow rate and lower heating value of product gases, respectively. P_t, P_p, and P_{stu} power of turbines, pump and slurry thickening unit, respectively. $\dot{m}_{feed}$ and LHV_{feed} refers to the molar flow rate and lower heating value of feed, respectively.

It is worth noting that the results of this section are based on global thermodynamic modelling. The process efficiency behavior results for fruit/vegetable waste (with 11wt% and 20wt% feed concentration) versus the reactor temperatures are depicted in Figure 5.8. The results indicate that the process is thermally more efficient at higher feed concentrations and lower reactor temperatures. The process efficiency is the highest with an efficiency of 56.7% at 550 °C, 240 bar, and 20wt% feed concentration, among the analyzed cases. Such behavior is expected since at higher feed concentrations more product gas is formed for the same total feed amount. Furthermore, with lower reactor temperatures less enthalpies are required for heating the feed to the desired temperatures.
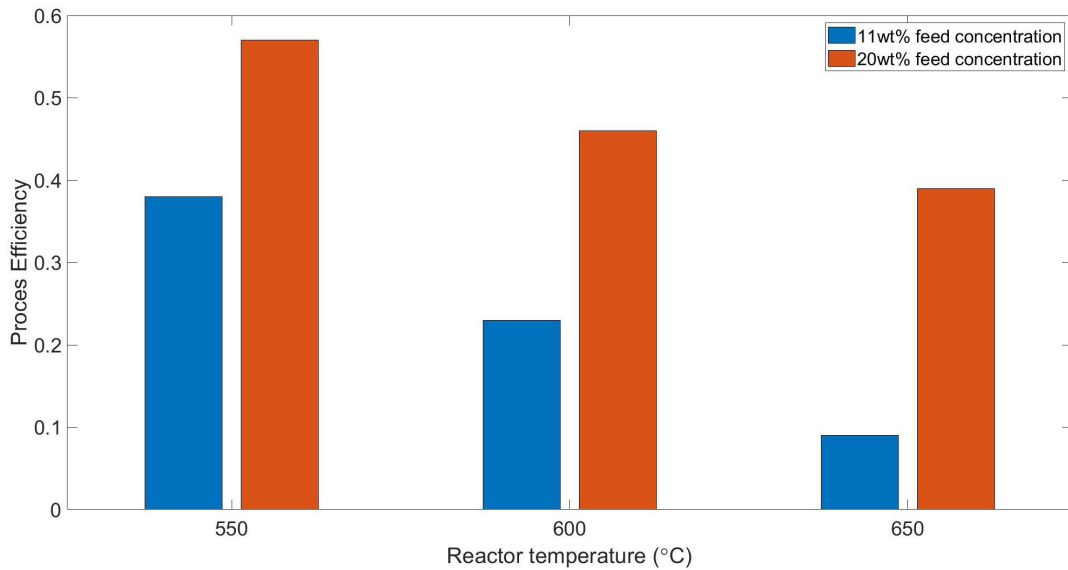
Figure 5.8: Process efficiency for SCWG of fruit/vegetable waste at different reactor temperatures, 240 bar pressure and 11wt% feed concentration.

The influence of reactor temperature and feed concentration on the required energy for furnace and the product split fraction is shown in Figure 5.9. Here, split fraction refers to the ratio of the recycle stream (stream 15, Figure 5.1) to the network stream (stream 13, Figure 5.1). The results show that for the investigated cases, process is thermally self-sufficient. However, as shown in Figure 5.9b, the process becomes practically infeasible for reactor temperatures of 600 °C and 650 °C at a feed concentration of 11wt% as the split fraction becomes higher than 0.7, which means a larger part of the produced gases getting recycled back to the system. In fact, a high value of split fraction can be anticipated when (i) SCW gasifier operates at higher temperature and (ii) higher water content in feedstock.
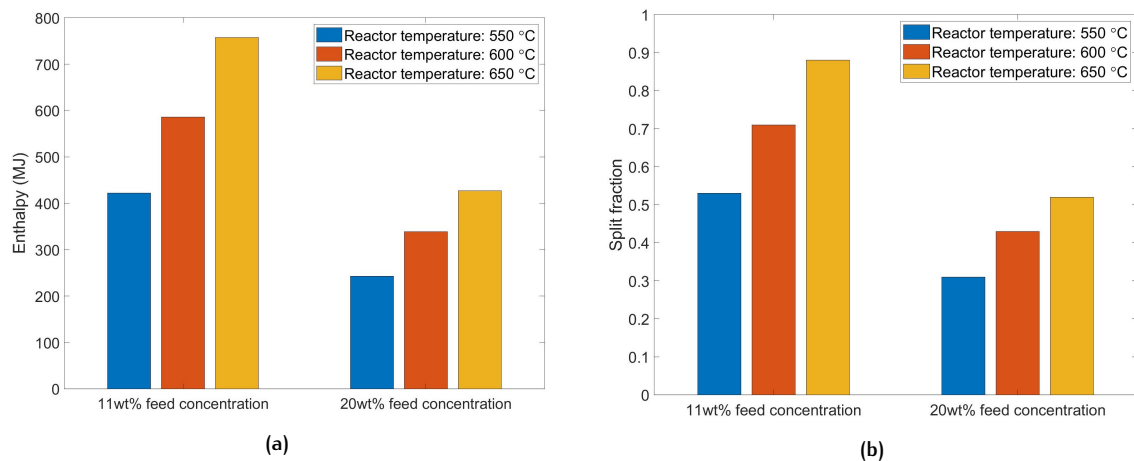
Figure 5.9: (a) Thermal energy requirements of furnace and (b) split fraction at splitter for SCWG of fruit/vegetable waste at different reactor temperatures and feed concentrations, and 240 bar pressure.

In a further attempt, we incorporated the gas composition results based on constrained thermodynamic equilibrium modelling of gasifier into ASPEN simulations. The ASPEN simulations were then conducted based on the gas composition results obtained from global and constrained thermodynamic equilibrium modelling of the gasifier. The simulations were setup for feed concentration (11wt%), reactor temperatures (Case A - 483 °C, Case B - 545 °C, and Case C - 560 °C) and pressure (Case A - 235 bar, Case B - 230 bar, and Case C - 240 bar). It is noteworthy that the results of chapter 4 showed a satisfactory agreement between the gas composition results obtained from constrained equilibrium

modelling and experimental values. Remarkably for all the above-mentioned cases (A, B, and C) using constrained modelling resulted in exceptionally high split fractions, say higher than 0.95, whilst the calculated split fractions for cases A, B, and C using GTE modelling results were 0.37, 0.55, and 0.6 respectively. Therefore, we can infer that the process model becomes practically infeasible when using more realistic figures or data based on constrained thermodynamic equilibrium modelling. The comparison results emphasize the inadequacy of using GTE approach for process modelling.

5.4 GAS MIXTURE CONDITIONING: SEPARATION OF CO$_2$ AND H$_2$S

CO$_2$ and H$_2$S are few of the major impurities of the effluent gaseous stream (refer stream 14, Figure 5.1) which gets formed during conditioning of raw synthesis gas. They both have similar physical and chemical properties and are acidic in nature. Both these gases have similar molecular kinetic diameters having values of 3.3 $\mathring{A}$ for CO$_2$ and 3.6 $\mathring{A}$ for H$_2$S. The presence of both these gases in the synthesis gas forms a major problem during its processing and usage. CO$_2$ is highly acidic in nature and causes equipment corrosion due to the formation of carbonic acid in the presence of water. The presence of CO$_2$ in the fuel gas reduces its calorific value and CO$_2$ is considered as one of the major contributors to climate change. While H$_2$S is a strongly corrosive and highly toxic acid gas. Faiz and Al-Marzouqi (2009) and Rezakazemi et al. (2011) proposed that H$_2$S combusts to form SO$_2$ which in turn can react with water in the atmosphere to produce acid rain. Furthermore, H$_2$S also forms a valuable chemical as it can be used to produce sulphuric acid and sulphur. It can be used in the chemical industries to produce leather, pharmaceuticals, dyes, and pesticides. H$_2$S also finds its application in the nuclear industry for the production of heavy water used by nuclear power plants. Therefore, it becomes imperative to remove and separate CO$_2$ and H$_2$S from industrial gases such as synthesis gas.

Various technologies such as absorption, adsorption, membrane technology, and cryogenic process are already present for capturing and separation of CO$_2$ and H$_2$S. Some of these technologies are discussed in the coming sections.

5.4.1 Pressure Swing Adsorption (PSA)

It is a well-established technology used for the separation of single gases from a gas mixture. It works on the principle of pressure differences as high pressures are favored for adsorption while desorption favors low pressures. The adsorbent material selected is based on the characteristics of the gas to be adsorbed and their affinity towards the adsorbent material. In the past, PSA technology has been a subject of interest among many researchers and has been studied both theoretically and experimentally for removal of trace amounts of H$_2$S from the industrial gases including synthesis gas and other mixtures containing CO$_2$, as researched by Truong and Abatzoglou (2005), Cosoli et al. (2008), and Hernández-Maldonado et al. (2003).

Kulvaranon et al. (1990) investigated the multicomponent-adsorption method using Variable Temperature Stepwise Desorption (VTSD) for separation of a gas mixture. A 13X molecular sieve (refer Table 5.1 for sieves specification) was used for separation of gases such as C$_3$H$_8$ (80vol%), CO$_2$ (10vol%) and H$_2$S (10vol%). The researchers were successfully able to remove H$_2$S from the adsorption output flow, thus obtaining over 50vol% concentration in the desorption step. Tomadakis et al. (2011) also studied the separation of CO$_2$ and H$_2$S mixture using PSA technology and with various molecular sieves such as 4A, 5A, and 13X. Specifications for all the three sieve types are mentioned in Table 5.1. The authors investigated the separation of gases for different pressures, flow rates, and H$_2$S molecular ratio (0.28-0.53) in the mixture. The author observed high H$_2$S/CO$_2$ selectivity[1] using all the three types of molecular sieves, with the highest selectivity of 11.9 when using a fresh 13X sieve with a pressure of 5.3 bars at adsorption and 1 bar at desorption step and temperature varying between 33-37 °C. Pure carbon dioxide was obtained during the adsorption stages with fresh 5A and 13X molecular sieves.

---

1 Selectivity of H$_2$S/CO$_2$ = (mole amount of H$_2$S removed or adsorbed)/(mole amount of CO$_2$ removed or adsorbed)

While the highest H$_2$S molar concentration of 80% was reported using 5A molecular sieve.

Table 5.1: Specification of different molecular sieves.

Particular	Sieve type		
	13X	4A	5A
Pore diameter	10 Å	4 Å	5 Å
Bulk density (g/ml)	0.55-0.65	0.60-065	0.60-0.65
Bed porosity	0.41	0.37	0.38
Heat capacity (KJ/kg-K)	0.96	0.96	0.96

5.4.2 Ionic liquid membrane separation

Ionic liquids (ILs) are organic salts having low melting points, close to ambient temperatures. ILs are unique in nature and offer properties such as good thermal stability, negligible volatility, and great solubility for acid gases, as proposed by Zhang et al. (2015). Use of ILs for separation of gas mixtures have been particularly interesting due to their ease in preparation and operation around atmospheric temperatures and pressures. Previously, ILs have been widely studied by researchers including Bates et al. (2002), Pomelli et al. (2007), Gurkan et al. (2010), Wang et al. (2011), and Wang et al. (2012). Zhang et al. (2017) investigated the permeability of CO$_2$, H$_2$S and CH$_4$ in various Supported Ionic Liquid Membranes (SILMs) prepared using neutrals ILs such as [bmim][PF6][2], [bmim][BF4],[bmim][TfO], and [bmim][Tf2n] and basic IL ([bmim][Ac]). The authors observed the highest H$_2$S selectivity over CO$_2$ of 11.9 and H$_2$S permeability of 5279 barrers using [bmim][Ac] membrane with a temperature of 30 °C and trans-membrane pressure of 0.1 bar. The authors also acknowledged the use of [bmim][Ac] as a potential membrane separation method for selective separation of H$_2$S from gas mixtures. Similarly, Handy et al. (2014) studied the use of ILs prepared using [bmim][Br] for separation of H$_2$S-CO$_2$ gas mixtures. The authors reported a H$_2$S/CO$_2$ selectivity of 3.48 with solubilities of H$_2$S and CO$_2$ of 0.0313 mol/mol and 0.00090 mol/mol respectively at 26 °C and 1 bar.

5.4.3 Hollow fiber membrane contractors

The use of membrane contracts for separation of gases is a hybrid process combining the membrane separation technique with the gas-liquid absorption method. In the absorption step, the two streams i.e. gas and liquid flow along the two sides of the membrane without making any direct contact, as suggested by Rongwong et al. (2012). Thus, the membrane acts as a physical barrier thereby offering no substantial effect on the process selectivity. Mirfendereski et al. (2019) carried out experiments with the polypropylene hollow fiber membrane contractors to separate the mixture of CO$_2$ and H$_2$S, with concentrations of H$_2$S upto 20vol% in the mixture. The experiments were conducted at 25 °C with a pressure of 0.5 bar for the feed gas. Furthermore, a 0.5 molar aqueous solution of methyldiethanolamine (MDEA) was used for chemical absorption at a pressure of 2 bar. The authors reported a high H$_2$S/CO$_2$ selectivity of 30 (approx.) for a feed flow rate of 2.5 lit/h having H$_2$S concentration of 5000ppm and a gas/liquid flow ratio of 200. Table 5.2 gives an overview and some main results of the selected research works for the separation of gas mixtures using different separation methods.

---

2 [bmim] refers to 1-butyl-3-methylimidazolium bromide

Table 5.2: Overview of the past research works for separation of H_2S and CO_2 mixtures.

Author(s), Year	Separation method	Operating temperature (°C)	Operating pressure (bar)	Selectivity of H_2S/CO_2
Tomadakis et al. (2011)	Pressure Swing Adsorption	33-37	Adsorption: 5.3 \newline Desorption: 1	11.9
Zhang et al. (2017)	Ionic liquid [bmim][Ac]	30	0.1	11.9
Handy et al. (2014)	Ionic liquid [bmim][Br]	26	1	3.48
Mirfendereski et al. (2019)	Hollow fiber-membrane contractors	25	0.5-2	∼30

5.5 CONCLUSIONS

A conceptual process design for SCWG of wet biomass waste was developed and investigated. The gas behavior results shows a decrease in concentration of CH_4 and CO_2 and an increase in concentration of H_2 and CO with increasing reactor temperature. Furthermore, the results illustrates that with increasing feed concentration (wt%), the CH_4 molar fraction in the gas composition increases while H_2 decreases. Considering the thermal behavior, the process becomes practically infeasible for SCWG of fruit/vegetable waste at reactor temperatures of 600 °C and 650 °C, pressure 240 bar and feed concentration of 11wt% as the split ratio becomes higher than 0.7 indicating a larger part of the produced gas getting recycled back to the system. The comparison results between global and constrained equilibrium modelling gas compositions for ASPEN simulations emphasizes the inadequacy of using GTE approach for process modelling. The recycle stream ratio for the same process conditions was computed to be higher than 0.95 using more realistic constrained thermodynamic equilibrium approach as compared to 0.37-0.6 when using GTE approach. Concerning the separation of H_2S and CO_2 mixture stream (stream 14, refer Figure 5.1), we found the highest H_2S/CO_2 selectivity of 30 (approx.) with hollow fiber-membrane contracts. However, other methods including PSA and ionic liquid membrane separation also demonstrates a good H_2S/CO_2 selectivity and furthermore, could be potentially explored and integrated into the design.

6 | CONCLUDING REMARKS

This chapter summarizes the conclusions drawn which are based on the scope of this study. Lastly, recommendations are provided for potential future research.

6.1 CONCLUSIONS

In line with the scope of this study, the following conclusions can be drawn.

1. The use of Factsage^{TM} software for multiphase thermodynamic equilibrium modelling of wet biomass waste provided reasonable results for the product gas compositions. The model was separately adjusted and defined for both subcritical and supercritical conditions. The GTE model gave an insight into the SCWG process showcasing the potential gas behavior for different reactor conditions. It is expected that with increasing reactor temperature the total gas yield would increase along with H_2, CO_2, and CO while the yield would decrease for CH_4. Furthermore, the model was used in understanding and analyzing the elemental compositions of the selected feedstocks which could pave a way in better understanding and handling the generated impurities in the form of slag and tars.

2. The GTE model has its limitations in predicting the gas compositions at global minima. The use of advanced thermodynamic modelling techniques portrayed more sophisticated prediction results. Under the constrained thermodynamic equilibrium approach, CGE efficiency was found to be one of the most important additional constraints and we observed an improved accuracy with the use of more additional constraints such as constant molar amounts of specific compounds. The best predictions using this approach were found to have a product gas concentration error of 6.9% for SCWG of fruit/vegetable waste at 560 °C, 240 bar, and 11wt% feed concentration. Furthermore, to our knowledge, we introduced a novel approach for predicting the product gas compositions at equilibrium which uses the concept of "approach temperature". The model showed even better predictive capabilities with a maximum error of 0.001%, compared to constrained equilibrium modelling for a typical case study.

3. To get a comprehensive overview of the entire process of SCWG, we modelled a conceptual biorefinery using ASPEN modelling software which was aimed at producing treated biogas having maximum lower heating value. We introduced the gas concentration results from global and constrained thermodynamic modelling into the process model to study both chemical and thermal behavior. Using the inputs from GTE approach, the highest process efficiency for fruit/vegetable waste feedstock was computed as 56.7% at 550 °C, 240 bar, and 20wt% feed concentration. The comparison between global and constrained equilibrium gas compositions results for ASPEN simulations highlighted the deficiency of using GTE approach for process modelling. Remarkably, we observed a very high split fraction of 0.95 using more realistic constrained thermodynamic modelling gas composition results, whilst the GTE modelling gas composition results displayed a split fraction of 0.37 at 438 °C, 235 bar and 11wt% fruit/vegetable waste feed concentration.

6.2 RECOMMENDATIONS

6.2.1 General recommendations

1. Modelling analysis for supercritical water gasification of biomass waste presented in this study is is benchmarked against the experimental results obtained from autoclave experiments. While in general, continuous fluidized and/or fixed bed reactors with a limited a residence time is employed. Thus, it is recommended to use a continuous flow reactor for experiments which enables more accurate validation.

2. This study is only limited to three types of wet waste streams such as cattle manure, fruit/vegetable waste, and cheese whey. It is therefore recommended to cover a wider range of biomass wastes including real feedstocks such as (sewage sludge, waste paper sludge, sawdust, wheat straw, microalgae, corncobs, etc.), liquid-type feedstocks (such as methanol, glycerol, ethanol, petroleum-based hydrocarbons, etc.), and model compounds (such as lignin, glucose, and others) and investigate the influence of LHV of different biomass wastes on full process performance.

3. The current effort is based on non-catalytic supercritical water gasification of wet biomass waste. The scope of the study could be extended to cover the use of catalytic media which could potentially reduce the severity of the process such as operation in a lower temperature and pressure environment.

4. Processing of biomass slurry across reactors and heat exchangers is likely to cause plugging and/or fouling problems associated with the tars produced. Further research is needed to address and resolve the associated challenges.

5. To commercialize the technology, an economic evaluation of the bio-refinery design at different operating conditions with multiple feedstock is needed. The assessment could possibly include evaluation of the following parameters; equipment sizing, capital costs, operational costs, revenues, profitability, etc.

6.2.2 Modelling recommendations

Global thermodynamic equilibrium modelling: PR equation of state was used for modelling the gasification system. Although use of PR EoS provides good predictions when compared to the experimental results, still other EoS such as RKS and PC-SAFT or other packages such as ASPEN OLI can be explored and compared.

Constrained thermodynamic equilibrium modelling: For this study, only three additional constraints were used which assisted a better prediction of the equilibrium product compositions. However, new additional constraints such as hydrogen gasification efficiency, tar formation efficiency, and use of constant amount of compounds in the form of inequalities can be tested.

Quasi-thermal equilibrium modelling: We introduced the concept of approach temperature in this study which has capabilities of predicting equilibrium product compositions with an accuracy of 0.001%. However, due to the limited availability of experimental data and time, we were not able to examine the concept thoroughly. Therefore, it will be worthwhile to explore the concept further as it has the potential to make the modelling predictions even more accurate.

Process modelling: A simple process model defining the concept of an SCWG based biorefinery was developed which helped us enabled a better understanding of the technical feasibility of the full process. However, further improvements on the current design are possible with the effective use of high-pressure and temperature streams, and individual process systems. For example, the use of waste internal energy from the streams for the slurry thickening unit. Furthermore, explore and integrate more gas separation techniques such as the use of pressure swing absorption and ionic liquids separation instead of simple membrane separation. The later idea can be further explored in LCA analysis.

BIBLIOGRAPHY

Acelas, N. Y., López, D. P., Brilman, D. W., Kersten, S. R., and Kootstra, A. M. J. (2014). Supercritical water gasification of sewage sludge: gas production and phosphorus recovery. *Bioresource technology*, 174:167–175.

Ahmad, A. L., Adewole, J. K., Leo, C. P., Sultan, A. S., and Ismail, S. (2014). Preparation and gas transport properties of dual-layer polysulfone membranes for high pressure co2 removal from natural gas. *Journal of Applied Polymer Science*, 131(20).

Amrullah, A. and Matsumura, Y. (2018). Supercritical water gasification of sewage sludge in continuous reactor. *Bioresource technology*, 249:276–283.

Antal Jr, M. J., Allen, S. G., Schulman, D., Xu, X., and Divilio, R. J. (2000). Biomass gasification in supercritical water. *Industrial & Engineering Chemistry Research*, 39(11):4040–4053.

Basu, P. (2010). *Biomass gasification and pyrolysis: practical design and theory*. Academic press.

Basu, P., Mettanant, V., and Leon, A. (2009). Gasification of rice husk in supercritical water. In *Proceedings of the 8th World Conference on Chemical Engineering*, page 520.

Bates, E. D., Mayton, R. D., Ntai, I., and Davis, J. H. (2002). Co2 capture by a task-specific ionic liquid. *Journal of the American Chemical Society*, 124(6):926–927.

Behnia, I., Yuan, Z., Charpentier, P., and Xu, C. (2016). Supercritical water gasification of aqueous fraction of pyrolysis oil in the presence of a ni-ru catalyst. *AIChE Journal*, 62(8):2786–2793.

Berendes, D. M., Yang, P. J., Lai, A., Hu, D., and Brown, J. (2018). Estimation of global recoverable human and animal faecal biomass. *Nature Sustainability*, 1(11):679–685.

Bermejo, M. and Cocero, M. (2006). Supercritical water oxidation: a technical review. *AIChE Journal*, 52(11):3933–3951.

Byrd, A. J., Pant, K., and Gupta, R. B. (2007). Hydrogen production from glucose using ru/al2o3 catalyst in supercritical water. *Industrial & engineering chemistry research*, 46(11):3574–3579.

Calzavara, Y., Joussot-Dubien, C., Boissonnet, G., and Sarrade, S. (2005). Evaluation of biomass gasification in supercritical water process for hydrogen production. *Energy conversion and management*, 46(4):615–631.

Cao, W., Cao, C., Guo, L., Jin, H., Dargusch, M., Bernhardt, D., and Yao, X. (2016). Hydrogen production from supercritical water gasification of chicken manure. *International Journal of Hydrogen Energy*, 41(48):22722–22731.

Chainey, R. (2015). Which countries waste the most food. In *World Economic Forum*, pages 1–3.

Chen, Y., Guo, L., Cao, W., Jin, H., Guo, S., and Zhang, X. (2013). Hydrogen production by sewage sludge gasification in supercritical water with a fluidized bed reactor. *International journal of hydrogen energy*, 38(29):12991–12999.

Cosoli, P., Ferrone, M., Pricl, S., and Fermeglia, M. (2008). Hydrogen sulphide removal from biogas by zeolite adsorption: Part i. gcmc molecular simulations. *Chemical Engineering Journal*, 145(1):86–92.

Davis, G. (2001). Process for converting sewage sludge and municipal solid wastes to clean fuels.

Elliott, D. C. (2008). Catalytic hydrothermal gasification of biomass. *Biofuels, Bioproducts and Biorefining*, 2(3):254–265.

Eriksson, G., Hack, K., and Petersen, S. (1997). Chemapp—a programmable thermodynamic calculation interface. *Werkstoff Woche*, 96:47–51.

Faiz, R. and Al-Marzouqi, M. (2009). Mathematical modeling for the simultaneous absorption of co2 and h2s using mea in hollow fiber membrane contactors. *Journal of Membrane Science*, 342(1-2):269–278.

FAO (2014). Full-cost accounting. *Final Report, FAO Food Waste*.

FAO (2015). Food waste footprint and climate change, retrieved 21 january 2020, from. http://www.fao.org/3/a-bb144e.pdf.

Feng, W., Van Der Kooi, H. J., and de Swaan Arons, J. (2004). Biomass conversions in subcritical and supercritical water: driving force, phase equilibria, and thermodynamic analysis. *Chemical Engineering and Processing: Process Intensification*, 43(12):1459–1467.

Fiori, L., Valbusa, M., and Castello, D. (2012). Supercritical water gasification of biomass for h2 production: process design. *Bioresource technology*, 121:139–147.

Font-Palma, C. (2019). Methods for the treatment of cattle manure—a review. *C—Journal of Carbon Research*, 5(2):27.

Furusawa, T., Sato, T., Sugito, H., Miura, Y., Ishiyama, Y., Sato, M., Itoh, N., and Suzuki, N. (2007). Hydrogen production from the gasification of lignin with nickel catalysts in supercritical water. *International Journal of Hydrogen Energy*, 32(6):699–704.

Gumz, W. (1950). *Gas producers and blast furnaces: theory and methods of calculation*. Wiley.

Guo, L., Lu, Y., Zhang, X., Ji, C., Guan, Y., and Pei, A. (2007). Hydrogen production by biomass gasification in supercritical water: a systematic experimental and analytical study. *Catalysis Today*, 129(3-4):275–286.

Guo, Y., Wang, S., Xu, D., Gong, Y., Ma, H., and Tang, X. (2010). Review of catalytic supercritical water gasification for hydrogen production from biomass. *Renewable and Sustainable Energy Reviews*, 14(1):334–343.

Gurkan, B. E., de la Fuente, J. C., Mindrup, E. M., Ficke, L. E., Goodrich, B. F., Price, E. A., Schneider, W. F., and Brennecke, J. F. (2010). Equimolar co2 absorption by anion-functionalized ionic liquids. *Journal of the American Chemical Society*, 132(7):2116–2117.

Gustavsson, J., Cederberg, C., Sonesson, U., Van Otterdijk, R., and Meybeck, A. (2011). Global food losses and food waste.

Handy, H., Santoso, A., Widodo, A., Palgunadi, J., Soerawidjaja, T. H., and Indarto, A. (2014). H2s–co2 separation using room temperature ionic liquid [bmim][br]. *Separation Science and Technology*, 49(13):2079–2084.

He, X., Kim, T.-J., and Hägg, M.-B. (2014). Hybrid fixed-site-carrier membranes for co2 removal from high pressure natural gas: Membrane optimization and process condition investigation. *Journal of Membrane Science*, 470:266–274.

Hernández-Maldonado, A. J., Yang, R. T., Chinn, D., and Munson, C. L. (2003). Partially calcined gismondine type silicoaluminophosphate sapo-43: isopropylamine elimination and separation of carbon dioxide, hydrogen sulfide, and water. *Langmuir*, 19(6):2193–2200.

Hodes, M., Marrone, P. A., Hong, G. T., Smith, K. A., and Tester, J. W. (2004). Salt precipitation and scale control in supercritical water oxidation—part a: fundamentals and research. *The Journal of Supercritical Fluids*, 29(3):265–288.

IEA, I. (2019). World energy outlook.

Kabyemela, B. M., Adschiri, T., Malaluan, R. M., and Arai, K. (1999). Glucose and fructose decomposition in subcritical and supercritical water: detailed reaction pathway, mechanisms, and kinetics. *Industrial & Engineering Chemistry Research*, 38(8):2888–2895.

Klingler, D., Berg, J., and Vogel, H. (2007). Hydrothermal reactions of alanine and glycine in sub-and supercritical water. *The Journal of Supercritical Fluids*, 43(1):112–119.

Kritzer, P. (2004). Corrosion in high-temperature and supercritical water and aqueous solutions: a review. *The Journal of Supercritical Fluids*, 29(1-2):1–29.

Kruse, A. (2008). Supercritical water gasification. *Biofuels, Bioproducts and Biorefining: Innovation for a sustainable economy*, 2(5):415–437.

Kulvaranon, S., Findley, M. E., and Liapis, A. I. (1990). Increased separation by variable-temperature stepwise desorption in multicomponent adsorption processes. *Industrial & engineering chemistry research*, 29(1):106–115.

Lappa, I. K., Papadaki, A., Kachrimanidou, V., Terpou, A., Koulougliotis, D., Eriotou, E., and Kopsahelis, N. (2019). Cheese whey processing: Integrated biorefinery concepts and emerging food applications. *Foods*, 8(8):347.

Lee, I.-G., Kim, M.-S., and Ihm, S.-K. (2002). Gasification of glucose in supercritical water. *Industrial & engineering chemistry research*, 41(5):1182–1188.

Li, X., Grace, J., Watkinson, A., Lim, C., and Ergüdenler, A. (2001). Equilibrium modeling of gasification: a free energy minimization approach and its application to a circulating fluidized bed coal gasifier. *Fuel*, 80(2):195–207.

Lopes, A. C. A., Eda, S. H., Andrade, R. P., Amorim, J. C., and Duarte, W. F. (2019). New alcoholic fermented beverages—potentials and challenges. In *Fermented Beverages*, pages 577–603. Elsevier.

Louw, J., Schwarz, C. E., Knoetze, J. H., and Burger, A. J. (2014). Thermodynamic modelling of supercritical water gasification: Investigating the effect of biomass composition to aid in the selection of appropriate feedstock material. *Bioresource technology*, 174:11–23.

Lu, Y., Guo, L., Ji, C., Zhang, X., Hao, X., and Yan, Q. (2006). Hydrogen production by biomass gasification in supercritical water: a parametric study. *International Journal of Hydrogen Energy*, 31(7):822–831.

Lu, Y., Guo, L., Zhang, X., and Ji, C. (2012). Hydrogen production by supercritical water gasification of biomass: explore the way to maximum hydrogen yield and high carbon gasification efficiency. *International Journal of Hydrogen Energy*, 37(4):3177–3185.

Luis, P., Van Gerven, T., and Van der Bruggen, B. (2012). Recent developments in membrane-based technologies for co2 capture. *Progress in Energy and Combustion Science*, 38(3):419–448.

Ma, C. and Koros, W. J. (2013). Ester-cross-linkable composite hollow fiber membranes for co2 removal from natural gas. *Industrial & Engineering Chemistry Research*, 52(31):10495–10505.

Marzouk, S. A., Al-Marzouqi, M. H., Abdullatif, N., and Ismail, Z. M. (2010). Removal of percentile level of h2s from pressurized h2s–ch4 gas mixture using hollow fiber membrane contactors and absorption solvents. *Journal of Membrane Science*, 360(1-2):436–441.

Matsumura, Y. and Minowa, T. (2004). Fundamental design of a continuous biomass gasification process using a supercritical water fluidized bed. *International Journal of Hydrogen Energy*, 29(7):701–707.

Matsumura, Y., Minowa, T., Xu, X., Nuessle, F., Adschiri, T., and Antal, M. (1997). High-pressure carbon dioxide removal in supercritical water gasification of biomass. In *Developments in thermochemical biomass conversion*, pages 864–877. Springer.

Minowa, T., Zhen, F., and Ogi, T. (1998). Cellulose decomposition in hot-compressed water with alkali or nickel catalyst. *The Journal of supercritical fluids*, 13(1-3):253–259.

Mirfendereski, S. M., Niazi, Z., and Mohammadi, T. (2019). Selective removal of h2s from gas streams with high co2 concentration using hollow-fiber membrane contractors. *Chemical Engineering & Technology*, 42(1):196–208.

Mizuno, T., Goto, M., Kodama, A., and Hirose, T. (2000). Supercritical water oxidation of a model municipal solid waste. *Industrial & engineering chemistry research*, 39(8):2807–2810.

Modell, M. (1982). Processing methods for the oxidation of organics in supercritical water. US Patent 4,338,199.

Modell, M., Reid, R., and Amin, S. (1978). Gasification process us patent 4 (113), 446.

Molino, A., Migliori, M., Blasi, A., Davoli, M., Marino, T., Chianese, S., Catizzone, E., and Giordano, G. (2017). Municipal waste leachate conversion via catalytic supercritical water gasification process. *Fuel*, 206:155–161.

Nanda, S., Isen, J., Dalai, A. K., and Kozinski, J. A. (2016). Gasification of fruit wastes and agro-food residues in supercritical water. *Energy Conversion and Management*, 110:296–306.

Nanda, S., Reddy, S. N., Hunter, H. N., Dalai, A. K., and Kozinski, J. A. (2015). Supercritical water gasification of fructose as a model compound for waste fruits and vegetables. *The Journal of Supercritical Fluids*, 104:112–121.

Ortiz, F. G., Ollero, P., Serrera, A., and Galera, S. (2012). An energy and exergy analysis of the supercritical water reforming of glycerol for power production. *International journal of hydrogen energy*, 37(1):209–226.

Pomelli, C. S., Chiappe, C., Vidis, A., Laurenczy, G., and Dyson, P. J. (2007). Influence of the interaction between hydrogen sulfide and ionic liquids on solubility: experimental and theoretical investigation. *The Journal of Physical Chemistry B*, 111(45):13014–13019.

Prins, W., Kersten, S. R., van de Beld, L., and Penninger, J. (2005). Gasification of wet biomass in supercritical water. In *Handbook Biomass Gasification*, pages 231–247. BTG Biomass technology Group.

Promdej, C., Chuntanapum, A., and Matsumura, Y. (2010). Effect of temperature on tarry material production of glucose in supercritical water gasification. *Journal of the Japan Institute of Energy*, 89(12):1179–1184.

Puig Arnavat, M. et al. (2011). *Performance modelling and validation of biomass gasifiers for trigeneration plants*. PhD thesis, Universitat Rovirai Virgili.

Rahbari, A., Venkataraman, M. B., and Pye, J. (2018). Energy and exergy analysis of concentrated solar supercritical water gasification of algal biomass. *Applied Energy*, 228:1669–1682.

Reddy, S. N., Nanda, S., Dalai, A. K., and Kozinski, J. A. (2014). Supercritical water gasification of biomass for hydrogen production. *International Journal of Hydrogen Energy*, 39(13):6912–6926.

Rezakazemi, M., Niazi, Z., Mirfendereski, M., Shirazian, S., Mohammadi, T., and Pak, A. (2011). Cfd simulation of natural gas sweetening in a gas–liquid hollow-fiber membrane contactor. *Chemical Engineering Journal*, 168(3):1217–1226.

Rongwong, W., Boributh, S., Assabumrungrat, S., Laosiripojana, N., and Jiraratananon, R. (2012). Simultaneous absorption of co2 and h2s from biogas by capillary membrane contactor. *Journal of membrane science*, 392:38–47.

Ruya, P. M., Purwadi, R., and Lim, S. S. (2020). Supercritical water gasification of sewage sludge for power generation–thermodynamic study on auto-thermal operation using aspen plus. *Energy Conversion and Management*, 206:112458.

Schmieder, H., Abeln, J., Boukis, N., Dinjus, E., Kruse, A., Kluth, M., Petrich, G., Sadri, E., and Schacht, M. (2000). Hydrothermal gasification of biomass and organic wastes. *The Journal of Supercritical Fluids*, 17(2):145–153.

Tanai, Y. S. (2017). Food waste energy analysis: Characterizing energy content as a function of proximate analysis factors, retrieved 22 december 2019, from. http://ccnyeec.org/wp-content/uploads/2016/11/FINAL20Regeneron20FWTE.pdf.

Tang, H. and Kitagawa, K. (2005). Supercritical water gasification of biomass: thermodynamic analysis with direct gibbs free energy minimization. *Chemical Engineering Journal*, 106(3):261–267.

Tomadakis, M. M., Heck, H. H., Jubran, M. E., and Al-Harthi, K. (2011). Pressure-swing adsorption separation of h2s from co2 with molecular sieves 4a, 5a, and 13x. *Separation Science and Technology*, 46(3):428–433.

Truong, L.-A. and Abatzoglou, N. (2005). A h2s reactive adsorption process for the purification of biogas prior to its use as a bioenergy vector. *Biomass and Bioenergy*, 29(2):142–151.

Van Swaaij, W. P., Matsumura, Y., Prins, W., Minowa, T., and Antal Jr, M. J. (2003). Technical feasibility of biomass gasofocation in a fluidised bed with supercritical water. *University of Twente, Enschede, The Netherlands*.

Wang, C., Luo, H., Li, H., Zhu, X., Yu, B., and Dai, S. (2012). Tuning the physicochemical properties of diverse phenolic ionic liquids for equimolar co2 capture by the substituent on the anion. *Chemistry–A European Journal*, 18(7):2153–2160.

Wang, C., Luo, X., Luo, H., Jiang, D.-e., Li, H., and Dai, S. (2011). Tuning the basicity of ionic liquids for equimolar co2 capture. *Angewandte Chemie*, 123(21):5020–5024.

WBA (2018). Wba global bioenergy statistics; 2017. *World Bioenergy Association: Stockholm, Sweden*.

Wilkinson, N., Wickramathilaka, M., Hendry, D., Miller, A., Espanani, R., and Jacoby, W. (2012). Rate determination of supercritical water gasification of primary sewage sludge as a replacement for anaerobic digestion. *Bioresource technology*, 124:269–275.

Withag, J. A., Smeets, J. R., Bramer, E. A., and Brem, G. (2012). System model for gasification of biomass model compounds in supercritical water–a thermodynamic analysis. *The Journal of supercritical fluids*, 61:157–166.

Xu, X., Matsumura, Y., Stenberg, J., and Antal, M. J. (1996). Carbon-catalyzed gasification of organic feedstocks in supercritical water. *Industrial & Engineering Chemistry Research*, 35(8):2522–2530.

Yakaboylu, O. (2016). Supercritical water gasification of wet biomass: Modeling and experiments.

Yakaboylu, O., Albrecht, I., Harinck, J., Smit, K., Tsalidis, G.-A., Di Marcello, M., Anastasakis, K., and de Jong, W. (2018). Supercritical water gasification of biomass in fluidized bed: First results and experiences obtained from tu delft/gensos semi-pilot scale setup. *Biomass and Bioenergy*, 111:330–342.

Yakaboylu, O., Harinck, J., Smit, K., and de Jong, W. (2014). Supercritical water gasification of biomass: A thermodynamic model for the prediction of product compounds at equilibrium state. *Energy & fuels*, 28(4):2506–2522.

Yakaboylu, O., Harinck, J., Smit, K., and De Jong, W. (2015a). Supercritical water gasification of biomass: a literature and technology overview. *Energies*, 8(2):859–894.

Yakaboylu, O., Harinck, J., Smit, K., and De Jong, W. (2015b). Testing the constrained equilibrium method for the modeling of supercritical water gasification of biomass. *Fuel Processing Technology*, 138:74–85.

Yakaboylu, O., Harinck, J., Smit, K. G., and de Jong, W. (2013). Supercritical water gasification of manure: A thermodynamic equilibrium modeling approach. *Biomass and bioenergy*, 59:253–263.

Yan, Q., Guo, L., and Lu, Y. (2006). Thermodynamic analysis of hydrogen production from biomass gasification in supercritical water. *Energy conversion and management*, 47(11-12):1515–1528.

Yanagida, T., Minowa, T., Nakamura, A., MATSUMURA, Y., and NODA, Y. (2008). Behavior of inorganic elements in poultry manure during supercritical water gasification. *Journal of the Japan Institute of Energy*, 87(9):731–736.

Yoshida, Y., Dowaki, K., Matsumura, Y., Matsuhashi, R., Li, D., Ishitani, H., and Komiyama, H. (2003). Comprehensive comparison of efficiency and co2 emissions between biomass energy conversion technologies—position of supercritical water gasification in biomass technologies. *Biomass and Bioenergy*, 25(3):257–272.

Zhang, X., Tu, Z., Li, H., Huang, K., Hu, X., Wu, Y., and MacFarlane, D. R. (2017). Selective separation of h2s and co2 from ch4 by supported ionic liquid membranes. *Journal of Membrane Science*, 543:282–287.

Zhang, X.-M., Huang, K., Xia, S., Chen, Y.-L., Wu, Y.-T., and Hu, X.-B. (2015). Low-viscous fluorine-substituted phenolic ionic liquids with high performance for capture of co2. *Chemical Engineering Journal*, 274:30–38.

A | ELEMENTAL PARTITIONING BEHAVIOR

Manure

The elemental partitioning behavior for manure feedstock is presented and discussed below. These results are based on the SCWG for the biomass wastes at 240 bar and a temperature range of 100-700°C. For this purpose, FactSage^{TM} simulations were performed under subcritical conditions for a temperature range of 100-375°C whilst the range of 400-700°C was considered for supercritical conditions.

Partitioning behavior of manure is shown in Figure A.1. As shown, the first region which lies between 100-325°C is dominated by solid carbon in the form of graphite along with small amounts of Mg(butanoate)$_2$ and $CaCO_3$. While the second region in the range of 350–700°C shows the dominance of gas products such as CO2, CH4, CO followed by the appearance of compounds such as Na_2CO_3, $K_2Ca_2(CO_3)_3$, K_2CO_3, HCO_3^- in small quantities. At temperatures exceeding 350°C solid carbon decomposes to form CO_2 and CH_4. CH_4 further starts decomposing around 400°C and gets converted into CO_2, CO and H_2.

Partitioning behavior of sulfur is shown in Figure A.2. At temperatures lower than 225°C, mainly FeS_2 is present in the fraction along with smaller quantities of FeS(s2) and HS$^-$. At temperatures higher than 225°C, sulfur further decomposes to compounds like FeS(s3), aqueous H_2S, and HS$^-$. In the supercritical region, sulfur is only present in the gaseous form of H_2S.

As shown in A.3 phosphorus compounds are only present in solid form in the entire gasification temperature range. At temperatures lower than 375°C, phosphorus is present only in two forms of $Ca_5HO_13P_3$ and $Na_2CaP_2O_7$ with an average of 45% and 54% respectively. Between 400°C and 52°C, the region is dominated by $NaMgPO_4$ along with smaller quantities of $Ca_5HO_13P_3$. At temperatures exceeding 550°C, $Ca_5HO_13P_3$ is the only stable form of phosphorous.

The partitioning behavior of nitrogen is shown in Figure A.4. As illustrated in this figure, nitrogen in the form of N_2 gas is the most stable compound present at temperatures below 375°C along with smaller quantities of aqueous N_2 and NH_3. At temperatures exceeding 400°C, the only compound present is $NH_3(g)$.

Figure A.3 exhibits the partitioning behavior of potassium. The results show that KOH in its dissolved aqueous form is mainly formed along with small quantities of K$^+$ ions in the subcritical region. The supercritical region only consists of solid compounds of potassium in the form of $K_2Ca_2(CO_3)_3$ mainly present at temperatures below 52°C and $K_2Ca(CO_3)_2$ dominating beyond 550°C along with smaller quantities of K_2CO_3.

Figure A.6 illustrates the partitioning behavior of calcium. The results reveal that calcium is only present in solid compound forms within the entire temperature range of 100-700°C. Moreover, $CaCO_3$ is mainly present in the subcritical region along with smaller quantities of $Na_2CaP_2O_7$. In the supercritical region between 400-52°C, $K_2Ca_2(CO_3)_3$ is mainly present while $K_2Ca(CO_3)_2$ appears in small quantities at temperatures higher than 550°C. Furthermore, $Ca_5HO_13P_3$ is present in the entire considered temperature range. However, it is mainly formed in the supercritical region beyond 550°C.

The partitioning behavior of magnesium is shown in Figure A.7. The figure shows that the only stable form of magnesium is Mg(butanoate)$_2$ in the subcritical region, wherein it is presented in its dissolved aqueous form. Only solid forms of magnesium compounds are present in the supercritical region

with the compound form of $NaMgPO_4$, MgO, $Mg_5Al_2Si_3O_{10}(OH)_8$, $KMg_3AlSi_3O_{10}(OH)_2$, Mg_2SiO_4, and $MgCO_3$. Furthermore, $MgCO_3$ and MgO are mainly present in the temperature range of 400-500°C and beyond 550°C, respectively.

Partitioning behavior of sodium is shown in Figure A.8. the results demonstrate that at temperatures lower than 375°C, four compounds of sodium are present including solid $Na_2CaP_2O_7$, Na^+ ion, solid $NaAlSiO_4$, and aqueous $NaHCO_2$. The subcritical region is dominated by solid $Na_2CaP_2O_7$ with an average mole fraction of 64%. Between 400-525°C and at temperatures exceeding 550°C, the most stable forms present are $NaMgPO_4$, and Na_2CO_3 respectively in their solid forms. Solid $Na_2Ca_3Al_{16}O_{28}$ is present in very small quantities in the supercritical range.

As shown in Figure A.9, only solid forms of iron compounds are present in the entire evaluated temperature range. At temperatures below 200°C, the only stable compound present is FeS_2. In between 225°C and 375°C, FeS_2, $FeS(s2)$, Fe_3O_4, and $FeS(s3)$ are present in different quantities. In the higher temperature supercritical region, the only stable form of iron is Fe_2O_3.

Figure A.1: Partitioning behavior of carbon compounds during supercritical water gasification of manure for a temperature range of 100-700°C at 240bar having a concentration of 17wt%.

Figure A.2: Partitioning behavior of sulphur compounds during supercritical water gasification of manure for a temperature range of 100-700°C at 240bar having a concentration of 17wt%.
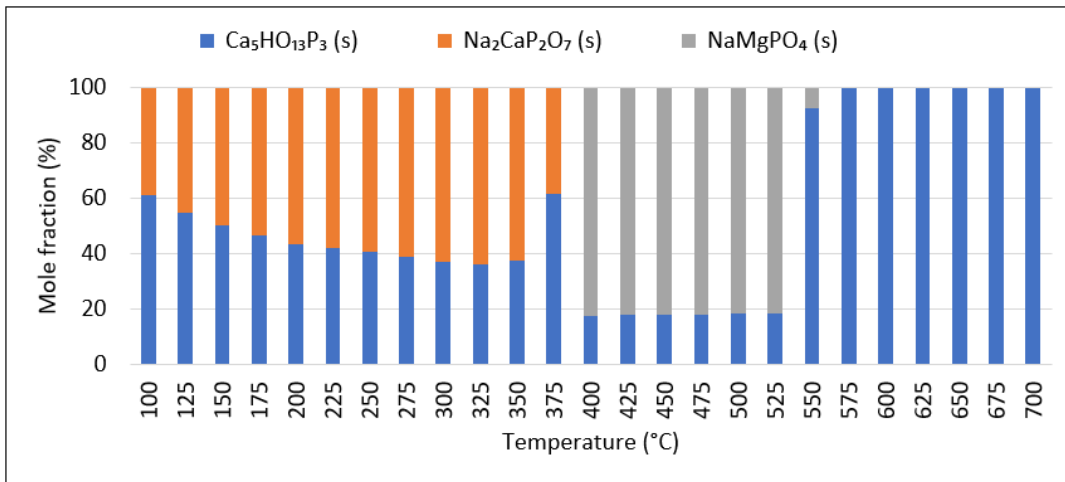
Figure A.3: Partitioning behavior of phosphorous compounds during supercritical water gasification of manure for a temperature range of 100-700°C at 240bar having a concentration of 17wt%.
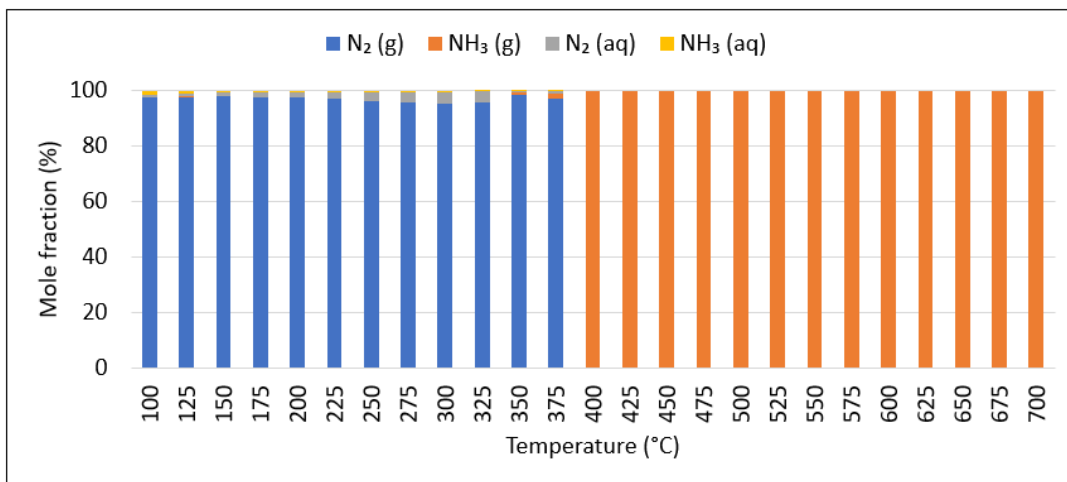
Figure A.4: Partitioning behavior of nitrogen compounds during supercritical water gasification of manure for a temperature range of 100-700°C at 240bar having a concentration of 17wt%.
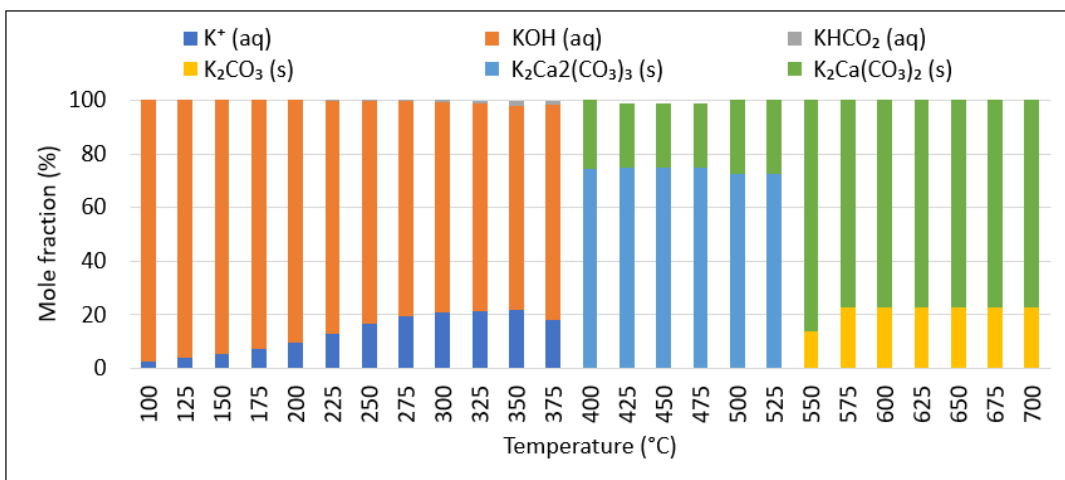
Figure A.5: Partitioning behavior of potassium compounds during supercritical water gasification of manure for a temperature range of 100-700°C at 240bar having a concentration of 17wt%.
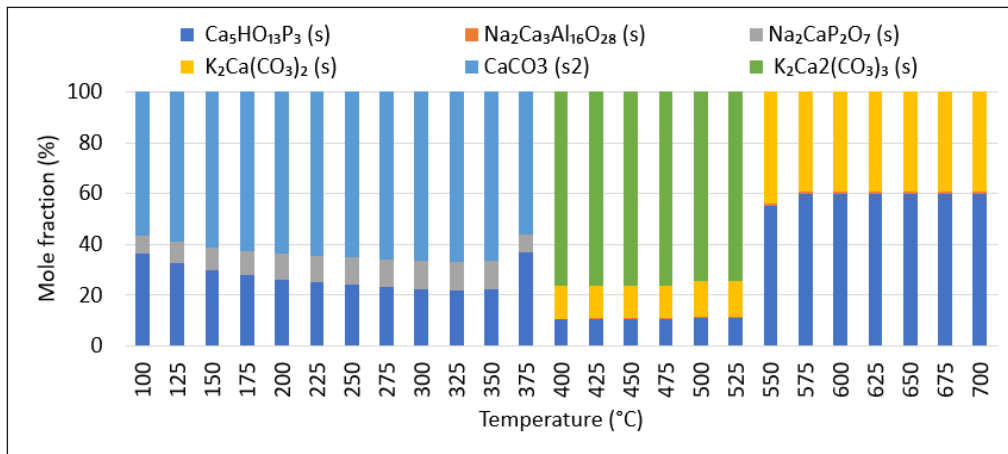
Figure A.6: Partitioning behavior of calcium compounds during supercritical water gasification of manure for a temperature range of 100-700°C at 240bar having a concentration of 17wt%.
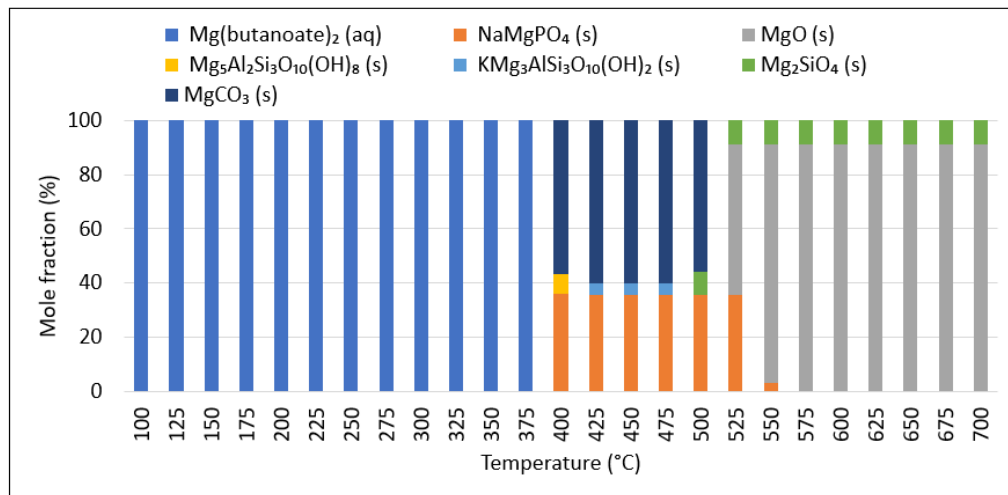
Figure A.7: Partitioning behavior of magnesium compounds during supercritical water gasification of manure for a temperature range of 100-700°C at 240bar having a concentration of 17wt%.
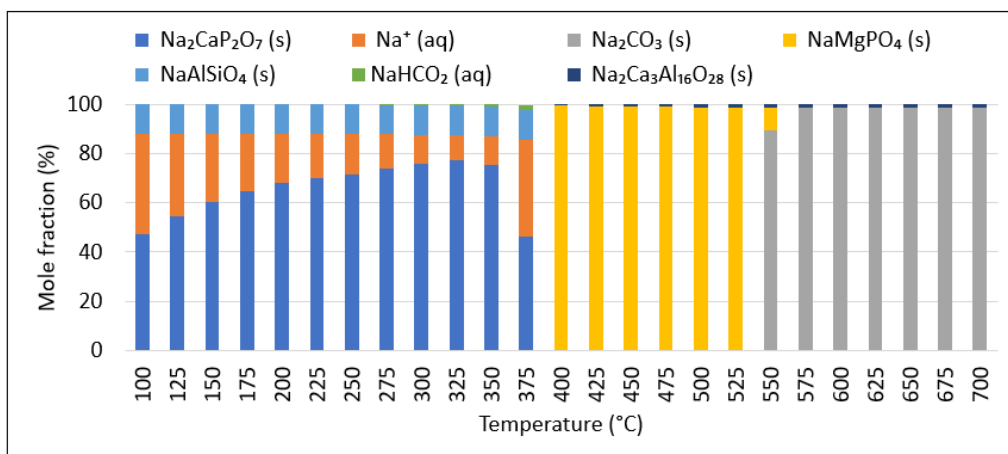
Figure A.8: Partitioning behavior of sodium compounds during supercritical water gasification of manure for a temperature range of 100-700°C at 240bar having a concentration of 17wt%.
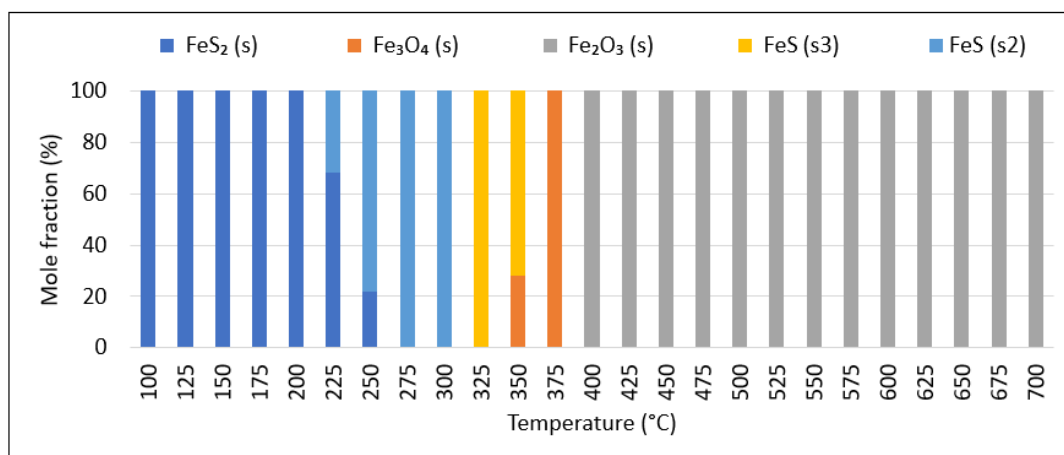
Figure A.9: Partitioning behavior of iron compounds during supercritical water gasification of manure for a temperature range of 100-700°C at 240bar having a concentration of 17wt%.

Cheese whey

The elemental partitioning behavior results for cheese whey are discussed below. The results are based on the SCWG for cheese whey at 240 bar and a temperature range of 100-700 °C. For this, Factsage^{TM} simulations were under subcritical conditions for a temperature range of 100-375 °C while 400-700 °C was considered under supercritical conditions.

Partitioning behavior of carbon is shown in Figure A.10. As shown, the first region which lies between 100-325°C is dominated by solid carbon in the form of graphite along with small amounts of $Mg(butanoate)_2$ and CaCO3(s2) and CH4(aq). While the second region lying beyond 350 °C shows the dominance of gas products such as CO2, CH4, CO followed by appearances of other compounds like KCaCO3(s2), K_2CO_3, HCO_3^- present in smaller quantities. The trend can be explained as at temperatures exceeding 350 °C, solid carbon decomposes to form CO2 and CH4. CH4 further starts decomposing around 400 °C and gets converted into CO_2, CO and H_2.

Partitioning behavior of sulfur is shown in Figure A.11. Between 100-325 °C, the region is mainly HS^- followed by aqueous H_2S and ZNS(s) present in smaller quantities. At temperatures higher than 350 °C, H_2S is the most stable form with smaller quantities of ZNS present in its solid form.

Partitioning behavior of phosphorous is shown in Figure A.12 which suggests that the phosphorus compounds are only present in their solid forms in the entire gasification temperature range. At temperatures lower than 400 °C, phosphorus is present majorly in the form of $Na_2CaP_2O_7$ while $Ca_5HO_13P_3$ and $NaMgPO_4$ present in small quantities. At temperatures exceeding 400°C, the region mainly consists of $Ca_5HO_13P_3$ with small quantities of $NaMgPO_4$ and Na_3PO_4.

Partitioning behavior of potassium is shown in Figure A.13. KOH in its aqueous form is majorly formed with small quantities of K^+ ions and $KHCO_2$ present in the subcritical region with temperatures below 375 °C. Around 400 °C, $K_2Ca(CO_3)_2$ gets formed with a molar fraction of 95%. Between425°C and 700 °C, K_2CO_3 is the most stable compound present with small quantities of $K_2Ca(CO_3)_2$ at temperatures lower than 500 °C.

Partitioning behavior of calcium is shown in Figure A.14. The results depict that calcium compounds are only present in their solid forms in the entire gasification temperature range of 100-700 °C. The subcritical region consists of three calcium compounds $Ca_5HO_13P_3$, CaCO3(s2), and $Na_2CaP_2O_7$. Around 400°C, $K_2Ca(CO_3)_2$ appears with a molar fraction of 70% along with $Na_2CaP_2O_7$ and $Ca_5HO_13P_3$. Between 425 °C and 700 °C, $Ca_5HO_13P_3$ gets majorly formed with smaller quantities of $K_2Ca(CO_3)_2$

present at temperatures lower than 500 °C.

Partitioning behavior of magnesium is shown in Figure A.15. The results show that the only stable form of magnesium is $Mg(butanoate)_2$ in the subcritical region with temperatures lower than 375 °C, wherein it is present in its aqueous form. Only solid forms of magnesium compounds are present in the supercritical region with $NaMgPO_4$ decreasing while MgO increasing in the supercritical temperature range.

Partitioning behavior of sodium is shown in Figure A.16. The results show that at temperatures below 400°C, $Na_2CaP_2O_7$ is the most stable form present with Na^+ ions found in small quantities and $NaMgPO_4(s)$ appears at 400°C. Between 400°C and 600°C, the region is dominated by $Na_2CO_3(s)$ along with small quantities of $NaMgPO_4(s)$. At temperatures exceeding 600°C, $Na_2CO_3(s)$ starts decreasing while $Na_3PO_4(s)$ starts increasing.
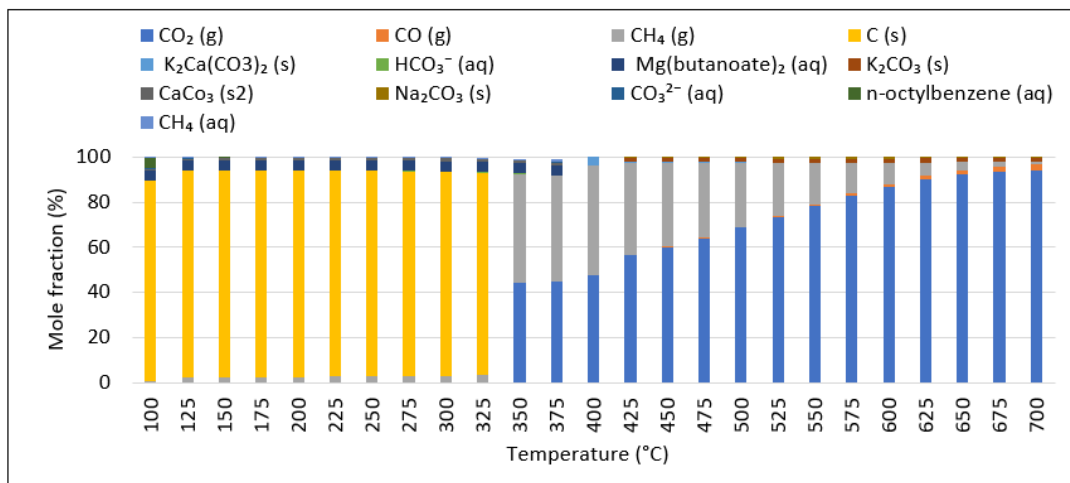
Figure A.10: Partitioning behavior of carbon compounds during supercritical water gasification of cheese whey for a temperature range of 100-700°C at 240bar having a concentration of 3wt%.
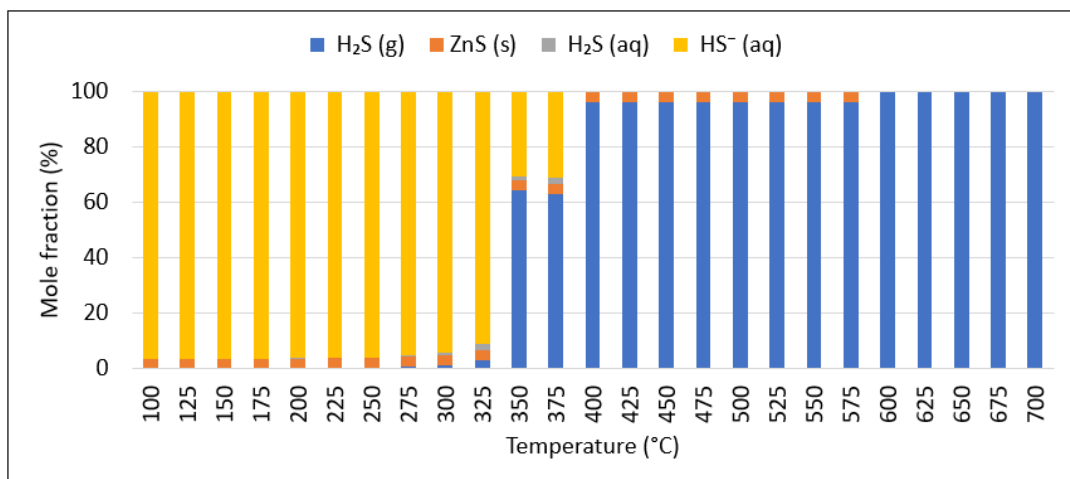
Figure A.11: Partitioning behavior of sulphur compounds during supercritical water gasification of cheese whey for a temperature range of 100-700°C at 240bar having a concentration of 3wt%.
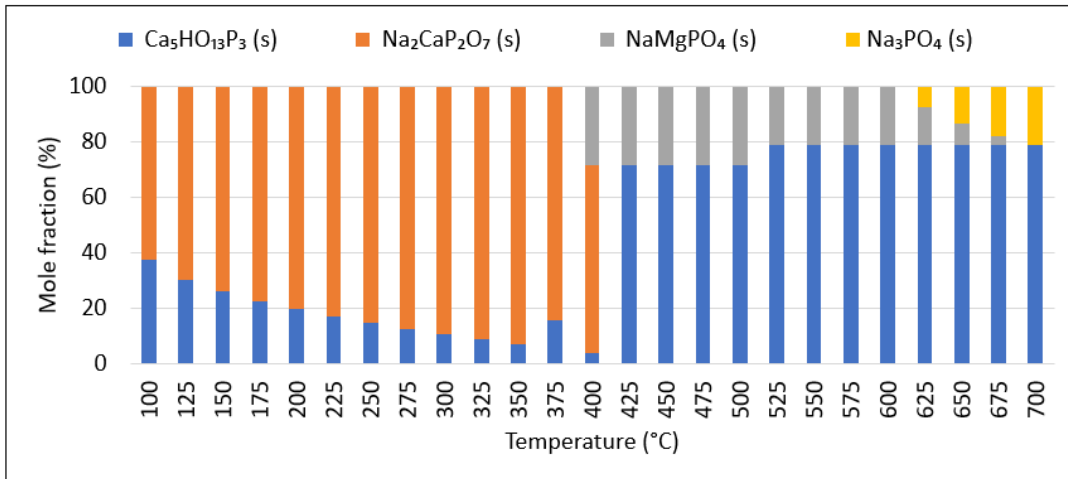
Figure A.12: Partitioning behavior of phosphorous compounds during supercritical water gasification of cheese whey for a temperature range of 100-700°C at 240bar having a concentration of 3wt%.
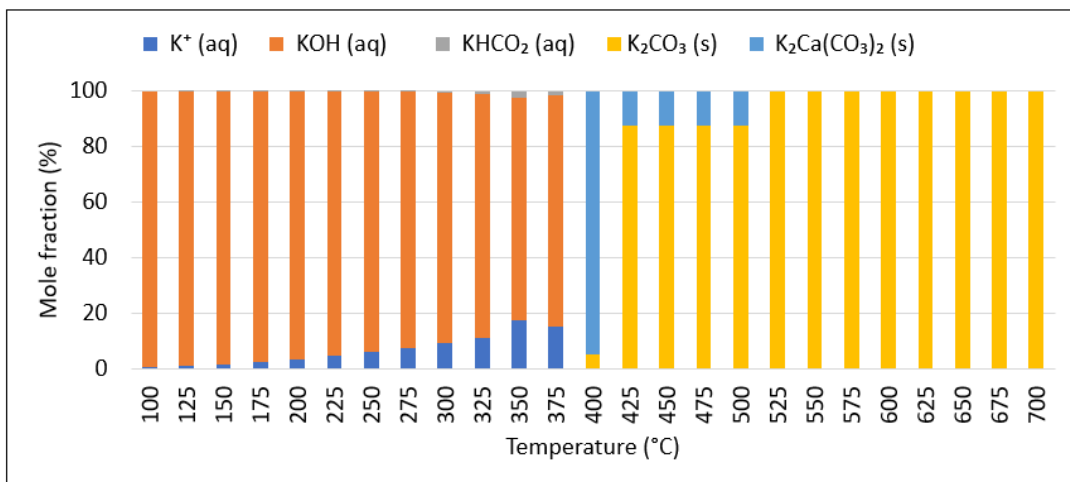
Figure A.13: Partitioning behavior of potassium compounds during supercritical water gasification of cheese whey for a temperature range of 100-700°C at 240bar having a concentration of 3wt%.
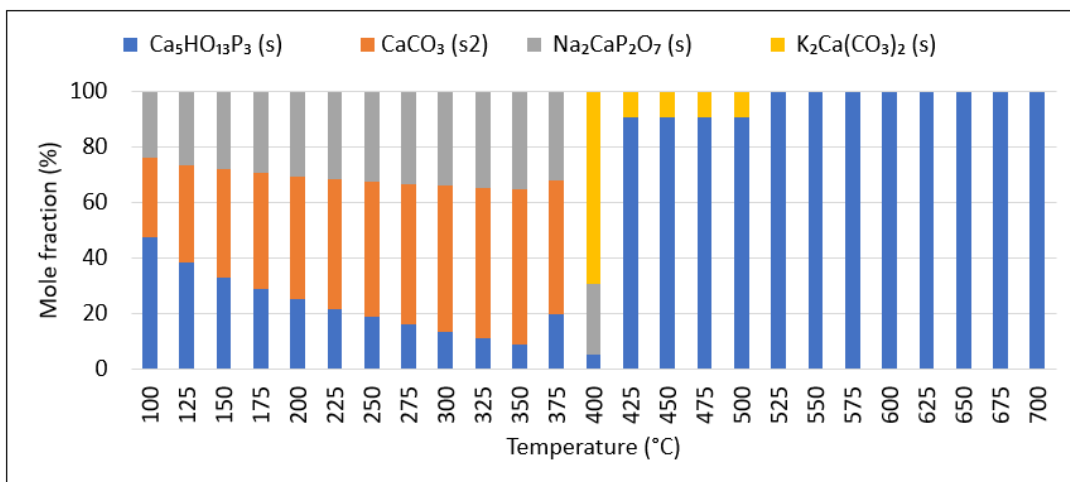
Figure A.14: Partitioning behavior of calcium compounds during supercritical water gasification of cheese whey for a temperature range of 100-700°C at 240bar having a concentration of 3wt%.
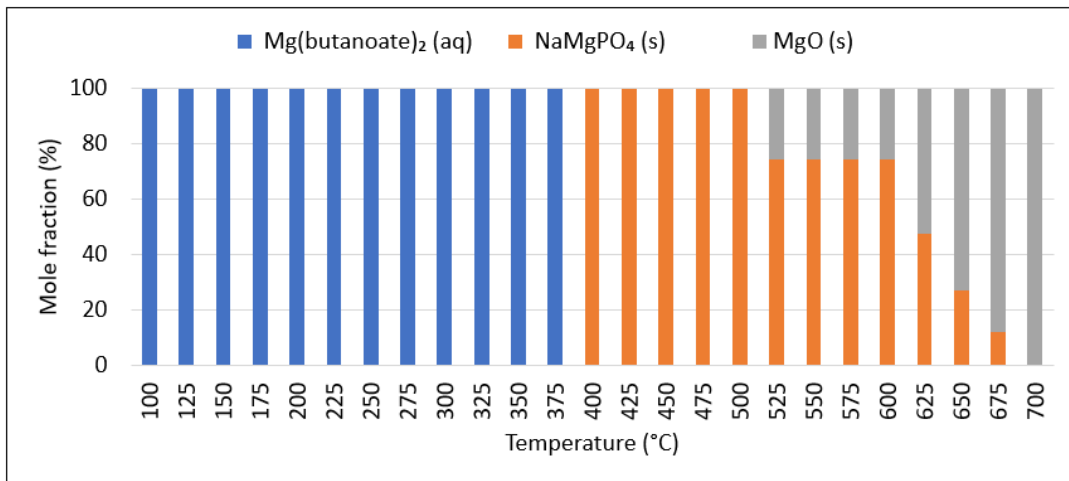
Figure A.15: Partitioning behavior of magnesium compounds during supercritical water gasification of cheese whey for a temperature range of 100-700°C at 240bar having a concentration of 3wt%.
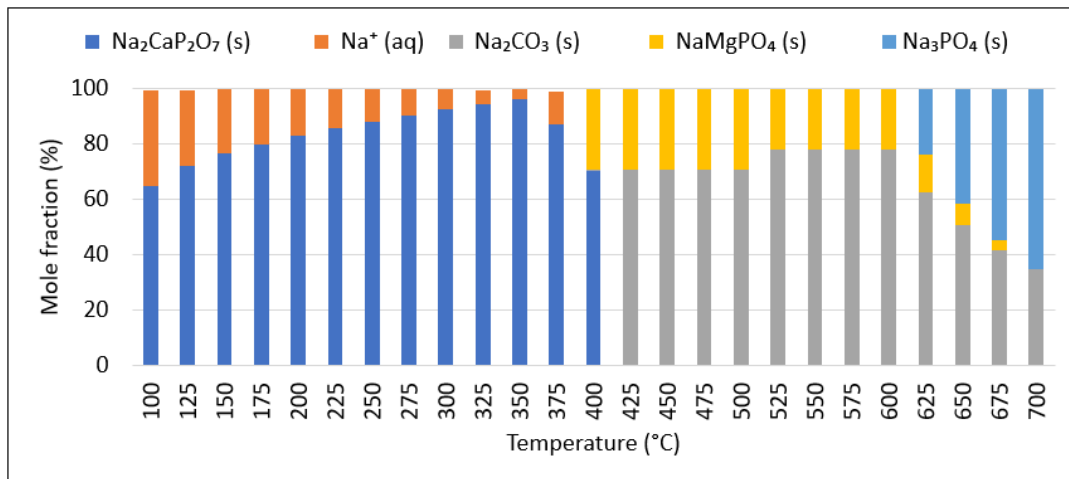
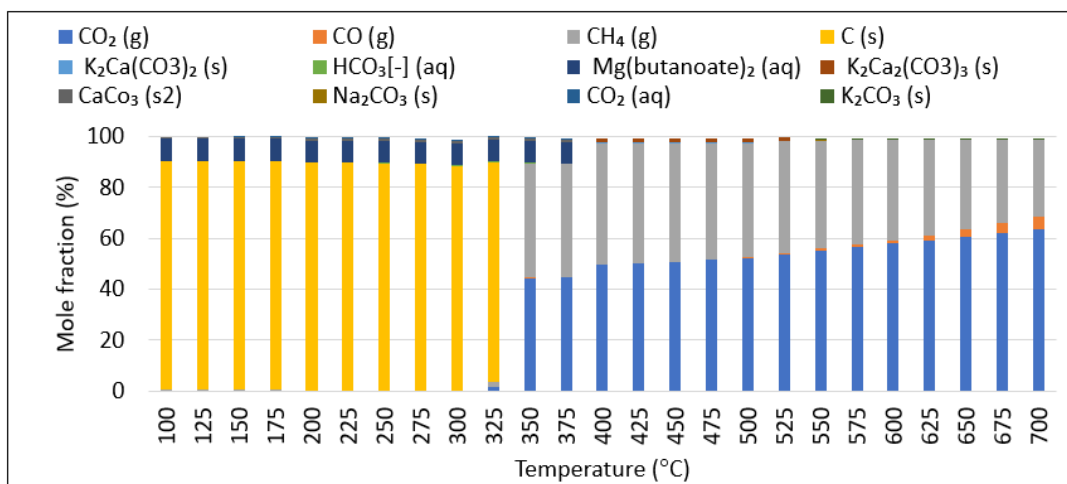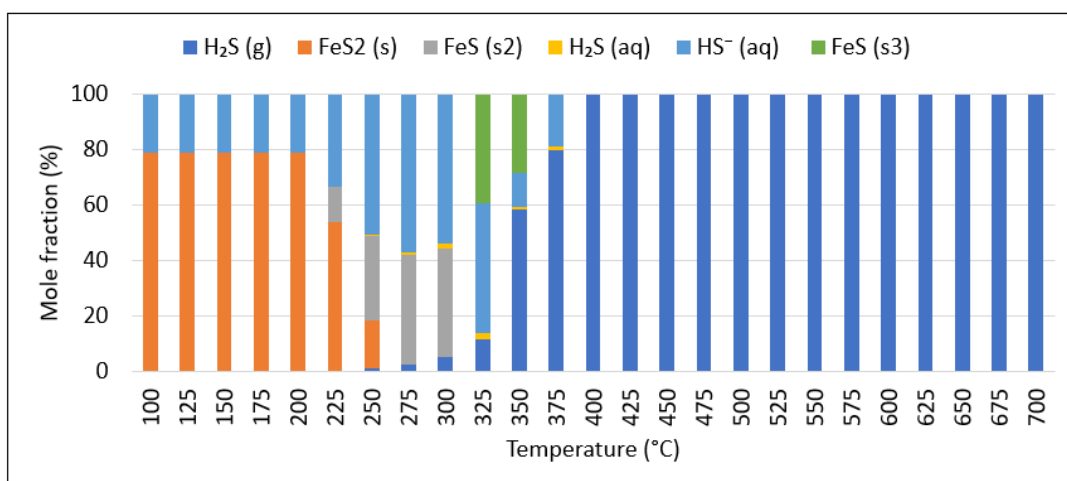**Figure A.16:** Partitioning behavior of sodium compounds during supercritical water gasification of cheese whey for a temperature range of 100-700 °C at 240bar having a concentration of 3wt%.

B | GAS BEHAVIOR USING CONSTRAINED EQUILIBRIUM THERMODYNAMIC MODEL

Figures B.1, B.2, B.3, B.4, and B.5 show comparison results for the main gaseous products predicted by unconstrained (Factsage^{TM} simulation) and constrained models and experimental data for all the three different biomass wastes. A comparison study for each biomass type has been conducted at specific temperatures and pressures. The analysis includes case studies for each biomass Case A involves no additional constraints and gas compositions are based on the GTE approach. Case B uses carbon gasification efficiency as the only additional constraint. Case C uses carbon gasification efficiency along with a specific amount of CH4 obtained from experiments as additional constraints. Case D employs carbon gasification efficiency together with specific amounts of CH4 and H2 obtained from experiments as additional constraints. It is worth noting that carbon gasification efficiencies have been determined using experimental data. The overall view of the data used for constrained equilibrium analysis is listed in Table B.1.

As evident in Figures B.1, B.2, B.3, B.4, and B.5, Case A which shows the results of GTE approach does not hold a satisfactory agreement with gas compositions obtained from experiments. Similarly, Cases B and C do not show good agreement with the experimental product gas compositions. However, Case D, where three additional constraints are used reveals good agreement with experimental data. The results of Case D demonstrate that integration of CGE value and experimental values of CH4 and H2 into the model shall result in better accuracy.

Table B.1: Additional constraint values used for modelling.

Biomass feed	Experimental cond. (T (°C) / P (bar))	Carbon gasification efficiency (%)	CH4 amount (mol/kg of d.b.)	H2 amount (mol/kg of d.b.)
Manure	539 / 270	72.0	7.9	4.9
Fruit/vegetable waste	545 / 230	73.0	6.8	6.9
Fruit/vegetable waste	483 / 235	64.0	5.4	5.5
Cheese whey	543 / 230	82.8	7.2	7.3
Cheese whey	498 / 240	53.2	3.6	6.9
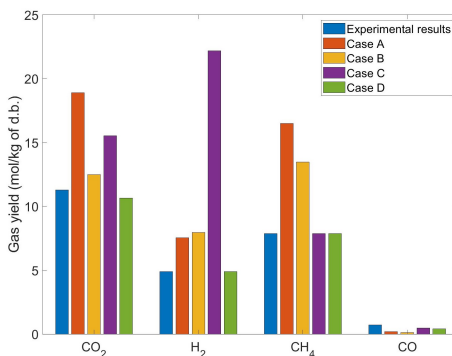
Figure B.1: Comparison between different modelling approaches and experimental values for manure at 539 °C and 270 bar with a feed concentration of 17 wt%. Case A includes only GTE values, Case B includes CGE as constraint, Case C includes CGE + constant amount of CH4 as constraints, Case D includes CGE + constant amount of CH4 and H2 as constraints.
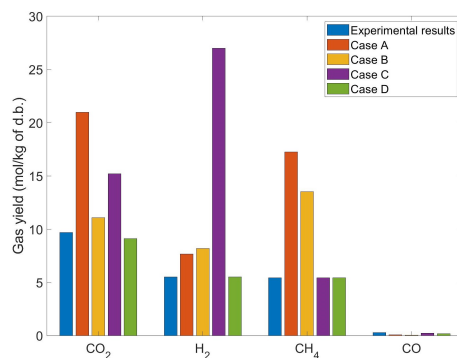
Figure B.2: Comparison between different modelling approaches and experimental values for fruit/vegetable waste at 483 °C and 235 bar with a feed concentration of 11 wt%. Case A includes only GTE values, Case B includes CGE as constraint, Case C includes CGE + constant amount of CH4 as constraints, Case D includes CGE + constant amount of CH4 and H2 as constraints.
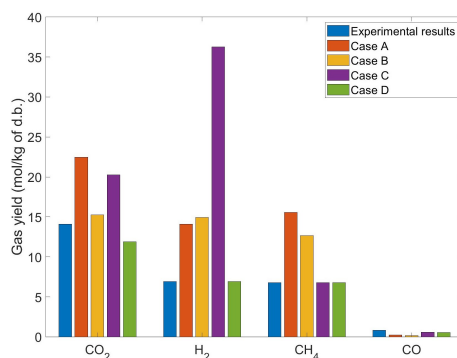
Figure B.3: Comparison between different modelling approaches and experimental values for fruit/vegetable waste at 545 °C and 230 bar with a feed concentration of 11 wt%. Case A includes only GTE values, Case B includes CGE as constraint, Case C includes CGE + constant amount of CH4 as constraints, Case D includes CGE + constant amount of CH4 and H2 as constraints.
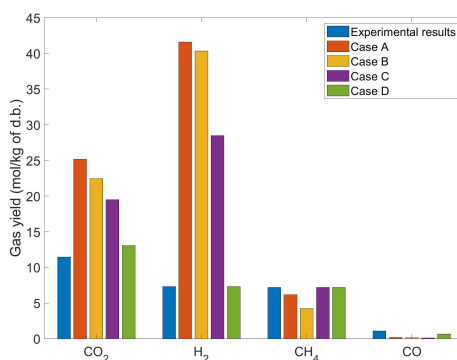
Figure B.4: Comparison between different modelling approaches and experimental values for cheese whey at 543 °C and 230 bar with a feed concentration of 3 wt%. Case A includes only GTE values, Case B includes CGE as constraint, Case C includes CGE + constant amount of CH4 as constraints, Case D includes CGE + constant amount of CH4 and H2 as constraints.
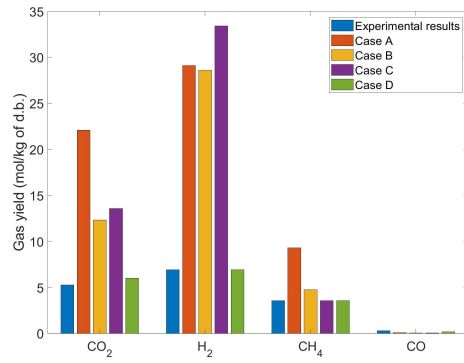
Figure B.5: Comparison between different modelling approaches and experimental values for cheese whey at 498 °C and 240 bar with a feed concentration of 3 wt%. Case A includes only GTE values, Case B includes CGE as constraint, Case C includes CGE + constant amount of CH4 as constraints, Case D includes CGE + constant amount of CH4 and H2 as constraints.

C | ASPEN SIMULATION DATA

Fruit/vegetable waste

ASPEN simulation data for all process streams is presented for SCWG of fruit/vegetable waste at different process conditions (mentioned along with the Figures).

Table C.1: Feed type: Fruit/vegetable waste, Reactor temperature 550 °C, Pressure: 240 bar, Feed concentration: 20wt%

Particular/Streams	ST1	ST2	ST3	ST4	ST5	ST6	ST7	ST8	ST9	ST10	ST11	ST12	ST13	ST14	ST15	ST16	ST17	ST18	ST19	ST20	ST21	ST22	ST23	ST24	ST25	ST26
Temperature (°C)	550,0	517,0	130,0	20,0	20,0	20,0	20,0	20,0	80,0	39,9	63,0	30,0	65,0	26,8	26,8	26,8	25,2	25,2	130,0	34,9	200,0	34,0	20,0	33,9	25,0	989,7
Pressure (bar)	240,0	238,0	238,0	238,0	238,0	2,0	2,0	238,0	238,0	130,0	130,0	80,0	80,0	49,0	49,0	49,0	49,0	49,0	49,0	15,0	15,0	2,0	2,0	2,0	1,0	2,0
Total mole flow rate (mol/hr)	25395,6	25395,6	25395,6	25395,6	20804,6	20804,6	20797,7	4591,1	4591,1	4591,1	4591,1	4591,1	4591,1	4591,1	2512,8	2078,2	1733,8	779,0	779,0	779,0	779,0	779,0	6,9	785,8	6818,7	7482,5
Mole flow rate (mol/hr)																										
H_2	759,7	759,7	759,7	759,7	0,2	0,2	<0.001	759,5	759,5	759,5	759,5	759,5	759,5	759,5	759,5		524,1	235,4	235,4	235,4	235,4	235,4	0,2	235,6		<0.001
CH_4	1721,0	1721,0	1721,0	1721,0	0,7	0,7	0,0	1720,3	1720,3	1720,3	1720,3	1720,3	1720,3	1720,3	1720,3		1187,0	533,3	533,3	533,3	533,3	533,3	<0.001	534,0		trace
NH_3	3,0	3,0	3,0	3,0	3,0	3,0	3,0	0,0	0,0	0,0	0,0	0,0	0,0	0,0	0,0		0,0	0,0	0,0	0,0	0,0	0,0	<0.001	0,0		trace
H_2O	20800,0	20800,0	20800,0	20800,0	20794,3	20794,3	20794,2	5,7	5,7	5,7	5,7	5,7	5,7	5,7	5,7		4,0	1,8	1,8	1,8	1,8	1,8	0,1	1,8		1305,5
CO	27,3	27,3	27,3	27,3	0,0	0,0	trace	27,3	27,3	27,3	27,3	27,3	27,3	27,3	27,3		18,8	8,5	8,5	8,5	8,5	8,5	0,0	8,5		<0.001
CO_2	2082,0	2082,0	2082,0	2082,0	6,2	6,2	0,4	2075,8	2075,8	2075,8	2075,8	2075,8	2075,8	2075,8		2075,8							5,8	5,8		548,3
HCOOH	0,0	0,0	0,0	0,0	<0.001	<0.001	<0.001	0,0	0,0	0,0	0,0	0,0	0,0	0,0	0,0		0,0	0,0	0,0	0,0	0,0	0,0	<0.001	0,0		trace
H_2S	2,7	2,7	2,7	2,7	0,2	0,2	0,1	2,5	2,5	2,5	2,5	2,5	2,5	2,5		2,5							0,1	0,1		0,1

Table C.2: Feed type: Fruit/vegetable waste, Reactor temperature 600 °C, Pressure: 240 bar, Feed concentration: 20wt%.

Particular/Streams	ST1	ST2	ST3	ST4	ST5	ST6	ST7	ST8	ST9	ST10	ST11	ST12	ST13	ST14	ST15	ST16	ST17	ST18	ST19	ST20	ST21	ST22	ST23	ST24	ST25	ST26
Temperature (°C)	600,0	561,1	155,0	20,0	20,0	20,0	20,0	20,0	80,0	39,8	63,0	30,3	65,0	26,7	26,7	26,7	25,6	25,6	130,0	32,9	200,0	29,4	20,0	29,4	25,0	1003,1
Pressure (bar)	240,0	238,0	238,0	238,0	238,0	2,0	2,0	238,0	238,0	130,0	130,0	80,0	80,0	49,0	49,0	49,0	49,0	49,0	49,0	15,0	15,0	2,0	2,0	2,0	1,0	2,0
Total mole flow rate (mol/hr)	25584,6	25584,6	25584,6	25584,6	20605,4	20605,4	20598,5	4979,2	4979,2	4979,2	4979,2	4979,2	4979,2	4979,2	2825,0	2154,2	1610,3	1214,8	1214,8	1214,8	1214,8	1214,8	6,9	1221,6	9419,8	10382,5
Mole flow rate (mol/hr)																										
H_2	1148,0	1148,0	1148,0	1148,0	0,2	0,2	<0,001	1147,8	1147,8	1147,8	1147,8	1147,8	1147,8	1147,8	1147,8		654,2	493,5	493,5	493,5	493,5	493,5	0,2	493,8		0,0
CH_4	1617,0	1617,0	1617,0	1617,0	0,6	0,6	0,0	1616,4	1616,4	1616,4	1616,4	1616,4	1616,4	1616,4	1616,4		921,3	695,0	695,0	695,0	695,0	695,0	0,6	695,7		trace
NH_3	3,0	3,0	3,0	3,0	3,0	3,0	3,0	0,0	0,0	0,0	0,0	0,0	0,0	0,0	0,0		0,0	0,0	0,0	0,0	0,0	0,0	<0,001	0,0		trace
H_2O	20600,0	20600,0	20600,0	20600,0	20595,1	20595,1	20595,0	4,9	4,9	4,9	4,9	4,9	4,9	4,9	4,9		2,8	2,1	2,1	2,1	2,1	2,1	0,1	2,2		1887,3
CO	55,9	55,9	55,9	55,9	0,0	0,0	trace	55,9	55,9	55,9	55,9	55,9	55,9	55,9	55,9		31,9	24,1	24,1	24,1	24,1	24,1	0,0	24,1		<0,001
CO_2	2158,0	2158,0	2158,0	2158,0	6,2	6,2	0,4	2151,8	2151,8	2151,8	2151,8	2151,8	2151,8	2151,8		2151,8							5,9	5,9		725,6
HCOOH	0,0	0,0	0,0	0,0	<0,001	<0,001	<0,001	0,0	0,0	0,0	0,0	0,0	0,0	0,0	0,0		0,0	0,0	0,0	0,0	0,0	0,0	<0,001	0,0		trace
H_2S	2,7	2,7	2,7	2,7	0,2	0,2	0,1	2,5	2,5	2,5	2,5	2,5	2,5	2,5		2,5							0,1	0,1		0,1

Table C.3: Feed type: Fruit/vegetable waste, Reactor temperature 650 °C, Pressure: 240 bar, Feed concentration: 20wt%.

Particular/Streams	ST1	ST2	ST3	ST4	ST5	ST6	ST7	ST8	ST9	ST10	ST11	ST12	ST13	ST14	ST15	ST16	ST17	ST18	ST19	ST20	ST21	ST22	ST23	ST24	ST25	ST26
Temperature (° C)	650,0	604,2	177,9	20,0	20,0	20,0	20,0	20,0	80,0	39,9	63,0	30,7	65,0	26,6	26,6	26,6	25,9	25,9	130,0	30,7	200,0	24,6	20,0	24,6	25,0	993,9
Pressure (bar)	240,0	238,0	238,0	238,0	238,0	2,0	2,0	238,0	238,0	130,0	130,0	80,0	80,0	49,0	49,0	49,0	49,0	49,0	49,0	15,0	15,0	2,0	2,0	2,0	1,0	2,0
Total mole flow rate (mol/hr)	25879,7	25879,7	25879,7	25879,7	20406,0	20406,0	20399,2	5473,7	5473,7	5473,7	5473,7	5473,7	5473,7	5473,7	3232,5	2241,2	1551,6	1680,9	1680,9	1680,9	1680,9	1680,9	6,8	1687,7	11314,4	12547,6
Mole flow rate (mol/hr)																										
H_2	1642,0	1642,0	1642,0	1642,0	0,3	0,3	<0.001	1641,7	1641,7	1641,7	1641,7	1641,7	1641,7	1641,7	1641,7		788,0	853,7	853,7	853,7	853,7	853,7	0,3	854,0		0,0
CH_4	1481,0	1481,0	1481,0	1481,0	0,5	0,5	0,0	1480,5	1480,5	1480,5	1480,5	1480,5	1480,5	1480,5	1480,5		710,6	769,8	769,8	769,8	769,8	769,8	0,5	770,4		trace
NH_3	3,0	3,0	3,0	3,0	3,0	3,0	3,0	0,0	0,0	0,0	0,0	0,0	0,0	0,0	0,0		0,0	0,0	0,0	0,0	0,0	0,0	<0.001	0,0		trace
H_2O	20400,0	20400,0	20400,0	20400,0	20395,7	20395,7	20395,7	4,3	4,3	4,3	4,3	4,3	4,3	4,3	4,3		2,1	2,2	2,2	2,2	2,2	2,2	0,1	2,3		2397,0
CO	106,0	106,0	106,0	106,0	106,0	106,0	trace	106,0	106,0	106,0	106,0	106,0	106,0	106,0	106,0		50,9	55,1	55,1	55,1	55,1	55,1	0,0	55,1		<0.001
CO_2	2245,0	2245,0	2245,0	2245,0	6,3	6,3	0,4	2238,7	2238,7	2238,7	2238,7	2238,7	2238,7	2238,7		2238,7	0,0	0,0	0,0	0,0	0,0	0,0	5,9	5,9		831,4
HCOOH	0,0	0,0	0,0	0,0	0,0	0,0	0,0	0,0	0,0	0,0	0,0	0,0	0,0	0,0	0,0		0,0	0,0	0,0	0,0	0,0	0,0	<0.001	0,0		trace
H_2S	2,7	2,7	2,7	2,7	0,2	0,2	0,1	2,4	2,4	2,4	2,4	2,4	2,4	2,4		2,4							0,1	0,1		0,1

Table C.4: Feed type: Fruit/vegetable waste, Reactor temperature 700 °C, Pressure: 240 bar, Feed concentration: 20wt%.

Particular/Streams	ST1	ST2	ST3	ST4	ST5	ST6	ST7	ST8	ST9	ST10	ST11	ST12	ST13	ST14	ST15	ST16	ST17	ST18	ST19	ST20	ST21	ST22	ST23	ST24	ST25	ST26
Temperature (° C)	700,0	660,0	203,2	20,0	20,0	20,0	20,0	20,0	80,0	40,1	63,0	31,1	65,0	26,4	26,4	26,4	26,1	26,1	130,0	28,4	200,0	19,8	20,0	19,8	25,0	997,1
Pressure (bar)	240,0	238,0	238,0	238,0	238,0	2,0	2,0	238,0	238,0	130,0	130,0	80,0	80,0	49,0	49,0	49,0	49,0	49,0	49,0	15,0	15,0	2,0	2,0	2,0	1,0	2,0
Total mole flow rate (mol/hr)	26172,7	26172,7	26172,7	26172,7	20106,4	20106,4	20099,6	6066,3	6066,3	6066,3	6066,3	6066,3	6066,3	6066,3	3738,1	2328,2	1383,1	2355,0	2355,0	2355,0	2355,0	2355,0	6,7	2361,7	13557,5	15155,9
Mole flow rate (mol/hr)																										
H_2	2236,0	2236,0	2236,0	2236,0	0,3	0,3	<0.001	2235,7	2235,7	2235,7	2235,7	2235,7	2235,7	2235,7	2235,7		827,2	1408,5	1408,5	1408,5	1408,5	1408,5	0,3	1408,8		0,0
CH_4	1312,0	1312,0	1312,0	1312,0	0,4	0,4	0,0	1311,6	1311,6	1311,6	1311,6	1311,6	1311,6	1311,6	1311,6		485,3	826,3	826,3	826,3	826,3	826,3	0,4	826,7		trace
NH_3	3,0	3,0	3,0	3,0	3,0	3,0	3,0	0,0	0,0	0,0	0,0	0,0	0,0	0,0	0,0		0,0	0,0	0,0	0,0	0,0	0,0	<0.001	0,0		trace
H_2O	20100,0	20100,0	20100,0	20100,0	20096,2	20096,2	20096,1	3,8	3,8	3,8	3,8	3,8	3,8	3,8	3,8		1,4	2,4	2,4	2,4	2,4	2,4	0,1	2,5		3064,7
CO	187,0	187,0	187,0	187,0	0,0	0,0	trace	187,0	187,0	187,0	187,0	187,0	187,0	187,0	187,0		69,2	117,8	117,8	117,8	117,8	117,8	0,0	117,8		<0.001
CO_2	2332,0	2332,0	2332,0	2332,0	6,3	6,3	0,4	2325,7	2325,7	2325,7	2325,7	2325,7	2325,7	2325,7		2325,7	0,0	0,0	0,0	0,0	0,0	0,0	5,9	5,9		950,4
HCOOH	0,0	0,0	0,0	0,0	0,0	0,0	0,0	0,0	0,0	0,0	0,0	0,0	0,0	0,0	0,0		0,0	0,0	0,0	0,0	0,0	0,0	<0.001	0,0		trace
H_2S	2,7	2,7	2,7	2,7	0,2	0,2	0,1	2,4	2,4	2,4	2,4	2,4	2,4	2,4		2,4							0,1	0,1		0,1

Table C.5: Feed type: Fruit/vegetable waste, Reactor temperature 500 °C, Pressure: 240 bar, Feed concentration: 11wt%.

Particular/Streams	ST1	ST2	ST3	ST4	ST5	ST6	ST7	ST8	ST9	ST10	ST11	ST12	ST13	ST14	ST15	ST16	ST17	ST18	ST19	ST20	ST21	ST22	ST23	ST24	ST25	ST26
Temperature (° C)	500,0	484,4	105,8	20,0	20,0	20,0	20,0	20,0	80,0	39,9	63,0	30,1	65,0	26,8	26,8	26,8	25,4	25,4	130,0	34,3	200,0	32,6	20,0	32,4	25,0	996,9
Pressure (bar)	240,0	238,0	238,0	238,0	238,0	2,0	2,0	238,0	238,0	130,0	130,0	80,0	80,0	49,0	49,0	49,0	49,0	49,0	49,0	15,0	15,0	2,0	2,0	2,0	1,0	2,0
Total mole flow rate (mol/hr)	48174,0	48174,0	48174,0	48174,0	43452,9	43452,9	43438,5	4721,0	4721,0	4721,0	4721,0	4721,0	4721,0	4721,0	2603,9	2117,2	1484,2	1119,7	1119,7	1119,7	1119,7	1119,7	14,4	1134,1	9481,8	10420,2
Mole flow rate (mol/hr)																										
H_2	897,4	897,4	897,4	897,4	0,5	0,5	<0.001	896,9	896,9	896,9	896,9	896,9	896,9	896,9	896,9		511,3	385,7	385,7	385,7	385,7	385,7	0,5	386,1		<0.001
CH_4	1691,0	1691,0	1691,0	1691,0	1,5	1,5	0,0	1689,5	1689,5	1689,5	1689,5	1689,5	1689,5	1689,5	1689,5		963,0	726,5	726,5	726,5	726,5	726,5	0,0	728,0		trace
NH_3	3,0	3,0	3,0	3,0	3,0	3,0	3,0	0,0	0,0	0,0	0,0	0,0	0,0	0,0	0,0		0,0	0,0	0,0	0,0	0,0	0,0	<0.001	0,0		trace
H_2O	43440,0	43440,0	43440,0	43440,0	43434,5	43434,5	43434,4	5,5	5,5	5,5	5,5	5,5	5,5	5,5	5,5		3,1	2,3	2,3	2,3	2,3	2,3	0,1	2,5		1844,6
CO	11,9	11,9	11,9	11,9	0,0	0,0	trace	11,9	11,9	11,9	11,9	11,9	11,9	11,9	11,9		6,8	5,1	5,1	5,1	5,1	5,1	0,0	5,1		<0.001
CO_2	2128,0	2128,0	2128,0	2128,0	13,1	13,1	0,8	2114,9	2114,9	2114,9	2114,9	2114,9	2114,9	2114,9		2114,9	0,0	0,0	0,0	0,0	0,0	0,0	12,3	12,3		745,3
HCOOH	0,0	0,0	0,0	0,0	<0.001	<0.001	<0.001	0,0	0,0	0,0	0,0	0,0	0,0	0,0	0,0		0,0	0,0	0,0	0,0	0,0	0,0	<0.001	0,0		trace
H_2S	2,7	2,7	2,7	2,7	0,4	0,4	0,3	2,3	2,3	2,3	2,3	2,3	2,3	2,3		2,3							0,1	0,1		0,1

Table C.6: Feed type: Fruit/vegetable waste, Reactor temperature 550 °C, Pressure: 240 bar, Feed concentration: 11wt%.

Particular/Streams	ST1	ST2	ST3	ST4	ST5	ST6	ST7	ST8	ST9	ST10	ST11	ST12	ST13	ST14	ST15	ST16	ST17	ST18	ST19	ST20	ST21	ST22	ST23	ST24	ST25	ST26
Temperature (° C)	550,0	529,1	134,9	20,0	20,0	20,0	20,0	20,0	80,0	39,8	63,0	30,5	65,0	26,7	26,7	26,7	25,8	25,8	130,0	31,8	200,0	27,1	20,0	27,0	25,0	998,2
Pressure (bar)	240,0	238,0	238,0	238,0	238,0	2,0	2,0	238,0	238,0	130,0	130,0	80,0	80,0	49,0	49,0	49,0	49,0	49,0	49,0	15,0	15,0	2,0	2,0	2,0	1,0	2,0
Total mole flow rate (mol/hr)	48449,6	48449,6	48449,6	48449,6	43198,9	43198,9	43184,3	5250,7	5250,7	5250,7	5250,7	5250,7	5250,7	5250,7	3011,8	2238,9	1415,5	1596,3	1596,3	1596,3	1596,3	1596,3	14,5	1610,8	11659,4	12884,7
Mole flow rate (mol/hr)																										
H_2	1427,0	1427,0	1427,0	1427,0	0,6	0,6	<0,001	1426,4	1426,4	1426,4	1426,4	1426,4	1426,4	1426,4	1426,4		670,4	756,0	756,0	756,0	756,0	756,0	0,6	756,6		0,0
CH_4	1555,0	1555,0	1555,0	1555,0	1,2	1,2	0,0	1553,8	1553,8	1553,8	1553,8	1553,8	1553,8	1553,8	1553,8		730,3	823,5	823,5	823,5	823,5	823,5	1,2	824,7		trace
NH_3	3,0	3,0	3,0	3,0	3,0	3,0	3,0	0,0	0,0	0,0	0,0	0,0	0,0	0,0	0,0		0,0	0,0	0,0	0,0	0,0	0,0	<0,001	0,0		trace
H_2O	43185,0	43185,0	43185,0	43185,0	43180,4	43180,4	43180,2	4,6	4,6	4,6	4,6	4,6	4,6	4,6	4,6		2,2	2,4	2,4	2,4	2,4	2,4	0,1	2,6		2408,6
CO	26,9	26,9	26,9	26,9	0,0	0,0	trace	26,9	26,9	26,9	26,9	26,9	26,9	26,9	26,9		12,7	14,3	14,3	14,3	14,3	14,3	0,0	14,3		<0,001
CO_2	2250,0	2250,0	2250,0	2250,0	13,3	13,3	0,8	2236,7	2236,7	2236,7	2236,7	2236,7	2236,7	2236,7		2236,7							12,5	12,5		851,5
$HCOOH$	0,0	0,0	0,0	0,0	0,0	0,0	<0,001	0,0	0,0	0,0	0,0	0,0	0,0	0,0	0,0		0,0	0,0	0,0	0,0	0,0	0,0	<0,001	0,0		trace
H_2S	2,7	2,7	2,7	2,7	0,4	0,4	0,3	2,3	2,3	2,3	2,3	2,3	2,3	2,3		2,3							0,1	0,1		0,1

Table C.7: Feed type: Fruit/vegetable waste, Reactor temperature 600 °C, Pressure: 240 bar, Feed concentration: 11wt%.

Particular/Streams	ST1	ST2	ST3	ST4	ST5	ST6	ST7	ST8	ST9	ST10	ST11	ST12	ST13	ST14	ST15	ST16	ST17	ST18	ST19	ST20	ST21	ST22	ST23	ST24	ST25	ST26
Temperature (° C)	600,0	574,3	161,2	20,0	20,0	20,0	20,0	20,0	80,0	40,0	63,0	31,0	65,0	26,5	26,5	26,5	26,1	26,1	130,0	29,2	200,0	21,5	20,0	21,5	25,0	997,9
Pressure (bar)	240,0	238,0	238,0	238,0	238,0	2,0	2,0	238,0	238,0	130,0	130,0	80,0	80,0	49,0	49,0	49,0	49,0	49,0	49,0	15,0	15,0	2,0	2,0	2,0	1,0	2,0
Total mole flow rate (mol/hr)	48807,2	48807,2	48807,2	48807,2	42869,5	42869,5	42854,9	5937,7	5937,7	5937,7	5937,7	5937,7	5937,7	5937,7	3548,0	2389,7	1028,9	2519,1	2519,1	2519,1	2519,1	2519,1	14,6	2533,7	15553,9	17317,3
Mole flow rate (mol/hr)																										
H_2	2114,0	2114,0	2114,0	2114,0	0,7	0,7	0,0	2113,4	2113,4	2113,4	2113,4	2113,4	2113,4	2113,4	2113,4		612,9	1500,5	1500,5	1500,5	1500,5	1500,5	0,7	1501,1		0,0
CH_4	1376,0	1376,0	1376,0	1376,0	0,9	0,9	0,0	1375,1	1375,1	1375,1	1375,1	1375,1	1375,1	1375,1	1375,1		398,8	976,3	976,3	976,3	976,3	976,3	0,9	977,2		trace
NH_3	3,0	3,0	3,0	3,0	3,0	3,0	3,0	0,0	0,0	0,0	0,0	0,0	0,0	0,0	0,0		0,0	0,0	0,0	0,0	0,0	0,0	<0,001	0,0		trace
H_2O	42855,0	42855,0	42855,0	42855,0	42851,0	42851,0	42850,8	4,0	4,0	4,0	4,0	4,0	4,0	4,0	4,0		1,2	2,9	2,9	2,9	2,9	2,9	0,1	3,0		3458,6
CO	55,6	55,6	55,6	55,6	0,0	0,0	trace	55,6	55,6	55,6	55,6	55,6	55,6	55,6	55,6		16,1	39,4	39,4	39,4	39,4	39,4	0,0	39,4		<0,001
CO_2	2401,0	2401,0	2401,0	2401,0	13,6	13,6	0,8	2387,4	2387,4	2387,4	2387,4	2387,4	2387,4	2387,4		2387,4							12,7	12,7		1029,4
$HCOOH$	0,0	0,0	0,0	0,0	0,0	0,0	0,0	0,0	0,0	0,0	0,0	0,0	0,0	0,0	0,0		0,0	0,0	0,0	0,0	0,0	0,0	<0,001	0,0		trace
H_2S	2,7	2,7	2,7	2,7	0,4	0,4	0,3	2,3	2,3	2,3	2,3	2,3	2,3	2,3		2,3							0,1	0,1		0,1

Table C.8: Feed type: Fruit/vegetable waste, Reactor temperature 650 °C, Pressure: 240 bar, Feed concentration: 11wt%.

Particular/Streams	ST1	ST2	ST3	ST4	ST5	ST6	ST7	ST8	ST9	ST10	ST11	ST12	ST13	ST14	ST15	ST16	ST17	ST18	ST19	ST20	ST21	ST22	ST23	ST24	ST25	ST26
Temperature (° C)	650,0	624,2	187,4	20,0	20,0	20,0	20,0	20,0	80,0	40,3	63,0	31,3	65,0	26,3	26,3	26,3	26,1	26,1	130,0	26,7	200,0	16,4	20,0	16,4	25,0	997,9
Pressure (bar)	240,0	238,0	238,0	238,0	238,0	2,0	2,0	238,0	238,0	130,0	130,0	80,0	80,0	49,0	49,0	49,0	49,0	49,0	49,0	15,0	15,0	2,0	2,0	2,0	1,0	2,0
Total mole flow rate (mol/hr)	49245,9	49245,9	49245,9	49245,9	42481,9	42481,9	42467,3	6764,0	6764,0	6764,0	6764,0	6764,0	6764,0	6764,0	4205,4	2558,6	504,7	3700,8	3700,8	3700,8	3700,8	3700,8	14,5	3715,3	19150,8	21525,7
Mole flow rate (mol/hr)																										
H_2	2941,0	2941,0	2941,0	2941,0	0,7	0,7	0,0	2940,3	2940,3	2940,3	2940,3	2940,3	2940,3	2940,3	2940,3		352,8	2587,4	2587,4	2587,4	2587,4	2587,4	0,7	2588,2		0,0
CH_4	1157,0	1157,0	1157,0	1157,0	0,7	0,7	0,0	1156,3	1156,3	1156,3	1156,3	1156,3	1156,3	1156,3	1156,3		138,8	1017,5	1017,5	1017,5	1017,5	1017,5	0,7	1018,2		trace
NH_3	3,0	3,0	3,0	3,0	3,0	3,0	3,0	0,0	0,0	0,0	0,0	0,0	0,0	0,0	0,0		0,0	0,0	0,0	0,0	0,0	0,0	<0,001	0,0		trace
H_2O	42467,0	42467,0	42467,0	42467,0	42463,4	42463,4	42463,2	3,6	3,6	3,6	3,6	3,6	3,6	3,6	3,6		0,4	3,2	3,2	3,2	3,2	3,2	0,1	3,3		4628,0
CO	105,2	105,2	105,2	105,2	0,0	0,0	trace	105,2	105,2	105,2	105,2	105,2	105,2	105,2	105,2		12,6	92,6	92,6	92,6	92,6	92,6	0,0	92,6		<0,001
CO_2	2570,0	2570,0	2570,0	2570,0	13,7	13,7	0,8	2556,3	2556,3	2556,3	2556,3	2556,3	2556,3	2556,3		2556,3							12,9	12,9		1123,7
$HCOOH$	0,0	0,0	0,0	0,0	0,0	0,0	0,0	0,0	0,0	0,0	0,0	0,0	0,0	0,0	0,0		0,0	0,0	0,0	0,0	0,0	0,0	<0,001	0,0		trace
H_2S	2,7	2,7	2,7	2,7	0,4	0,4	0,3	2,3	2,3	2,3	2,3	2,3	2,3	2,3		2,3							0,1	0,1		0,1

Cattle manure

ASPEN simulation data for all process streams is presented for SCWG of cattle manure for different process conditions (mentioned along with the Figures).

Table C.9: An overview of the ASPEN simulation results for cattle manure with a feed concentration of 17wt% at different reactor conditions.

Particular/ S.no	Gasifier temperature (°C)	Gasifier pressure (bar)	Temperature at preheater outlet (°C)	Required energy for preheater (MJ/h)	Required energy for furnace (MJ/h)	Split fraction (recycle/to-grid)	Multistage pressure recovery units (kW)	Pump Duty (kW)
1	500	240	390	1355,61	205,02	0,29	4,38	13,29
2	550	240	390	1355,61	280,33	0,39	5,46	13,29
3	600	240	390	1355,61	380,74	0,51	6,96	13,29

Table C.10: Feed type: Cattle manure, Reactor temperature: 500 °C, Pressure: 240 bar, Feed concentration: 17wt%.

Particular/Streams	ST1	ST2	ST3	ST4	ST5	ST6	ST7	ST8	ST9	ST10	ST11	ST12	ST13	ST14	ST15	ST16	ST17	ST18	ST19	ST20	ST21	ST22	ST23	ST24	ST25	ST26
Temperature	500,0	476,6	102,6	20,0	20,0	20,0	20,0	20,0	80,0	40,0	63,0	29,8	65,0	26,8	26,8	26,8	24,9	24,9	130,0	35,8	200,0	36,2	20,0	35,9	25,0	1001,9
Pressure (bar)	240,0	238,0	238,0	238,0	238,0	2,0	2,0	238,0	238,0	130,0	130,0	80,0	80,0	49,0	49,0	49,0	49,0	49,0	49,0	15,0	15,0	2,0	2,0	2,0	1,0	2,0
Total mole flow rate (mol/hr)	29901,7	29901,7	29901,7	29901,7	25798,9	25798,9	25789,9	4102,8	4102,8	4102,8	4102,8	4102,8	4102,8	4102,8	2206,7	1896,9	1566,8	640,0	640,0	640,0	640,0	640,0	9,0	648,9	5914,5	6480,7
Mole flow rate (mol/hr)																										
H_2	559,3	559,3	559,3	559,3	0,2	0,2	<0,001	559,1	559,1	559,1	559,1	559,1	559,1	559,1	559,1		396,9	162,1	162,1	162,1	162,1	162,1	0,2	162,4		<0,001
CH_4	1631,0	1631,0	1631,0	1631,0	1,0	1,0	0,0	1630,0	1630,0	1630,0	1630,0	1630,0	1630,0	1630,0	1630,0		1157,3	472,7	472,7	472,7	472,7	472,7	1,0	473,7		trace
NH_3	195,5	195,5	195,5	195,5	194,7	194,7	194,6	0,8	0,8	0,8	0,8	0,8	0,8	0,8	0,8		0,6	0,2	0,2	0,2	0,2	0,2	0,0	0,3		trace
H_2O	25600,0	25600,0	25600,0	25600,0	25594,3	25594,3	25594,2	5,7	5,7	5,7	5,7	5,7	5,7	5,7	5,7		4,0	1,7	1,7	1,7	1,7	1,7	0,1	1,7		1111,9
CO	11,1	11,1	11,1	11,1	0,0	0,0	trace	11,1	11,1	11,1	11,1	11,1	11,1	11,1	11,1		7,9	3,2	3,2	3,2	3,2	3,2	0,0	3,2		<0,001
CO_2	1897,0	1897,0	1897,0	1897,0	7,9	7,9	0,5	1889,1	1889,1	1889,1	1889,1	1889,1	1889,1	1889,1		1889,1							7,4	7,4		484,4
HCOOH	0,0	0,0	0,0	0,0	<0,001	<0,001	<0,001	0,0	0,0	0,0	0,0	0,0	0,0	0,0	0,0		0,0	0,0	0,0	0,0	0,0	0,0	trace	0,0		trace
H_2S	7,7	7,7	7,7	7,7	0,8	0,8	0,5	6,9	6,9	6,9	6,9	6,9	6,9	6,9		6,9							0,2	0,2		0,2

Table C.11: Feed type: Cattle manure, Reactor temperature: 550 °C, Pressure: 240 bar, Feed concentration: 17wt%.

Particular/Streams	ST1	ST2	ST3	ST4	ST5	ST6	ST7	ST8	ST9	ST10	ST11	ST12	ST13	ST14	ST15	ST16	ST17	ST18	ST19	ST20	ST21	ST22	ST23	ST24	ST25	ST26
Temperature	550,0	524,4	135,0	20,0	20,0	20,0	20,0	20,0	80,0	39,8	63,0	30,1	65,0	26,8	26,8	26,8	25,4	25,4	130,0	33,9	200,0	31,6	20,0	31,5	25,0	1003,4
Pressure (bar)	240,0	238,0	238,0	238,0	238,0	2,0	2,0	238,0	238,0	130,0	130,0	80,0	80,0	49,0	49,0	49,0	49,0	49,0	49,0	15,0	15,0	2,0	2,0	2,0	1,0	2,0
Total mole flow rate (mol/hr)	30172,4	30172,4	30172,4	30172,4	25699,7	25699,7	25690,7	4472,7	4472,7	4472,7	4472,7	4472,7	4472,7	4472,7	2467,8	2004,9	1505,4	962,4	962,4	962,4	962,4	962,4	9,1	971,5	7930,2	8722,3
Mole flow rate (mol/hr)																										
H_2	894,8	894,8	894,8	894,8	0,3	0,3	<0,001	894,5	894,5	894,5	894,5	894,5	894,5	894,5	894,5		545,7	348,9	348,9	348,9	348,9	348,9	0,3	349,1		<0,001
CH_4	1543,0	1543,0	1543,0	1543,0	0,9	0,9	0,0	1542,1	1542,1	1542,1	1542,1	1542,1	1542,1	1542,1	1542,1		940,7	601,4	601,4	601,4	601,4	601,4	0,9	602,3		trace
NH_3	195,5	195,5	195,5	195,5	194,7	194,7	194,7	0,8	0,8	0,8	0,8	0,8	0,8	0,8	0,8		0,5	0,3	0,3	0,3	0,3	0,3	0,0	0,3		trace
H_2O	25500,0	25500,0	25500,0	25500,0	25495,0	25495,0	25494,9	5,0	5,0	5,0	5,0	5,0	5,0	5,0	5,0		3,0	1,9	1,9	1,9	1,9	1,9	0,1	2,0		1556,3
CO	25,4	25,4	25,4	25,4	0,0	0,0	trace	25,4	25,4	25,4	25,4	25,4	25,4	25,4	25,4		15,5	9,9	9,9	9,9	9,9	9,9	0,0	9,9		<0,001
CO_2	2006,0	2006,0	2006,0	2006,0	8,1	8,1	0,5	1997,9	1997,9	1997,9	1997,9	1997,9	1997,9	1997,9		1997,9							7,6	7,6		619,8
HCOOH	0,0	0,0	0,0	0,0	<0,001	<0,001	<0,001	0,0	0,0	0,0	0,0	0,0	0,0	0,0	0,0		0,0	<0,001	<0,001	<0,001	<0,001	<0,001	trace	<0,001		trace
H_2S	7,7	7,7	7,7	7,7	0,8	0,8	0,6	6,9	6,9	6,9	6,9	6,9	6,9	6,9		6,9							0,2	0,2		0,2

Table C.12: Feed type: Cattle manure, Reactor temperature: 600 °C, Pressure: 240 bar, Feed concentration: 17wt%.

Particular/Streams	ST1	ST2	ST3	ST4	ST5	ST6	ST7	ST8	ST9	ST10	ST11	ST12	ST13	ST14	ST15	ST16	ST17	ST18	ST19	ST20	ST21	ST22	ST23	ST24	ST25	ST26
Temperature	600,0	573,9	163,6	20,0	20,0	20,0	20,0	20,0	80,0	39,8	63,0	30,5	65,0	26,7	26,7	26,7	25,8	25,8	130,0	31,6	200,0	26,6	20,0	26,5	25,0	993,2
Pressure (bar)	240,0	238,0	238,0	238,0	238,0	2,0	2,0	238,0	238,0	130,0	130,0	80,0	80,0	49,0	49,0	49,0	49,0	49,0	49,0	15,0	15,0	2,0	2,0	2,0	1,0	2,0
Total mole flow rate (mol/hr)	30423,4	30423,4	30423,4	30423,4	25500,5	25500,5	25491,4	4922,9	4922,9	4922,9	4922,9	4922,9	4922,9	4922,9	2824,2	2098,8	1383,8	1440,3	1440,3	1440,3	1440,3	1440,3	9,1	1449,4	10326,9	11420,3
Mole flow rate (mol/hr)																										
H_2	1344,0	1344,0	1344,0	1344,0	0,3	0,3	<0,001	1343,7	1343,7	1343,7	1343,7	1343,7	1343,7	1343,7	1343,7		658,4	685,3	685,3	685,3	685,3	685,3	0,3	685,6		<0,001
CH_4	1424,0	1424,0	1424,0	1424,0	0,7	0,7	0,0	1423,3	1423,3	1423,3	1423,3	1423,3	1423,3	1423,3	1423,3		697,4	725,9	725,9	725,9	725,9	725,9	0,7	726,6		trace
NH_3	195,5	195,5	195,5	195,5	194,7	194,7	194,7	0,8	0,8	0,8	0,8	0,8	0,8	0,8	0,8		0,4	0,4	0,4	0,4	0,4	0,4	0,0	0,4		trace
H_2O	25300,0	25300,0	25300,0	25300,0	25295,7	25295,7	25295,7	4,3	4,3	4,3	4,3	4,3	4,3	4,3	4,3		2,1	2,2	2,2	2,2	2,2	2,2	0,1	2,3		2141,7
CO	52,2	52,2	52,2	52,2	0,0	0,0	trace	52,2	52,2	52,2	52,2	52,2	52,2	52,2	52,2		25,6	26,6	26,6	26,6	26,6	26,6	0,0	26,6		<0,001
CO_2	2100,0	2100,0	2100,0	2100,0	8,2	8,2	0,5	2091,8	2091,8	2091,8	2091,8	2091,8	2091,8	2091,8		2091,8							7,7	7,7		760,9
HCOOH	0,0	0,0	0,0	0,0	<0,001	<0,001	<0,001	0,0	0,0	0,0	0,0	0,0	0,0	0,0	0,0		0,0	0,0	0,0	0,0	0,0	0,0	<0,001	0,0		trace
H_2S	7,7	7,7	7,7	7,7	0,8	0,8	0,6	6,9	6,9	6,9	6,9	6,9	6,9	6,9		6,9							0,2	0,2		0,2

Cheese Whey

Table C.13: An overview of the ASPEN simulation results for cheese whey with a feed concentration of 3wt% at different reactor conditions.

Particular/ S.no	Gasifier temperature (°C)	Gasifier pressure (bar)	Temperature at preheater outlet (°C)	Required energy for preheater (MJ/h)	Required energy for furnace (MJ/h)	Inference
1	500	240	390	8669,25	1548,08	Design failed due to very high energy requirement for furnace
2	550	240	390	8669,25	2058,53	Design failed due to very high energy requirement for furnace
3	600	240	390	8669,25	2535,50	Design failed due to very high energy requirement for furnace

LHV of different biomass waste feedstock

The LHV of considered biomass waste feedstock at different temperatures and feed concentrations having a pressure of 240 bar are presented in Table C.14. The results indicate that the highest LHV for the considered temperature range was calculated as 58.33 MJ/kg for fruit/vegetable waste feed. Furthermore, the considered feedstock have different lower heating values as the feedstock have different feed compositions and concentrations. For the case of cheese whey, the ASPEN simulation results showed errors due to very low whey concentration of 3wt% present in the feed.

Table C.14: LHV of considered biomass waste feedstock at different reactor temperatures and feed concentrations having a pressure of 240 bar

Feedstock type	Feed concentration (wt%)	LHV values (MJ/kg) at different reactor temperatures		
		500 °C	550 °C	600 °C
Fruit/vegetable waste	11	53.72	55.85	58.33
Cattle manure	17	52.20	53.42	54.70
Cheese whey	3	Design fail	Design fail	Design fail

CURRICULUM VITAE

Avishek Goel was born on 25th January 1992 in Uttar Pradesh, India. He completed his bachelor's in Mechanical Engineering from Birla Institute of Technology, Pilani-Dubai, UAE. During his bachelor's, his specialization was centered on the Designing and Optimization of Gas-Fired Furnaces.

He has over 3 years of comprehensive R&D and project management experience as a Research Associate with The Energy and Resources Institute (TERI), India. He has researched, designed, and developed decentralized 2-stage biomass gasification (developed in partnership with DTU), fixed bed thermal gasification, torrefaction, pyrolysis, and agricultural waste management technologies. At TERI, he has worked with a multitude of real-life projects which focused on empowering rural communities using local biomass resources. During his tenure with TERI, he has published numerous technical reports and publications.

In September 2018, he started his M.Sc. at the Process and Energy Department in Delft University of Technology Netherlands. During his masters, he joined the Large Scale Energy Storage group to work on his thesis in the domain of Supercritical Water Gasification under the supervision of Prof.dr.ir. W. de Jong. During his masters, he has been awarded certifications and acknowledgments. In 2019, he got selected as one of the 33 young clean energy researchers from around the world and participated at the 'International Clean Energy Challenge: 33 under 33'. He was also acknowledged as the Best Young Biomass Researcher in 2020 for his contribution towards the performance evaluation of traditional and improved biomass cookstoves in rural Guatemala.